Fiammetta Cerreti

# Some topics in bio-mathematical modeling

*Dottorato in Matematica*, Roma «La Sapienza» (2009).

<http://www.bdim.eu/item?id=tesi_2009_CerretiFiammetta_1>

# Some topics in bio-mathematical modeling

Ph.D. Thesis

of

Fiammetta Cerreti

Department of Mathematics, "G. Castelnuovo"

University of Rome, "Sapienza"

Ph. D. in Applied Mathematics (XXI Ciclo)

Advisor: Paolo Buttà

**Acknowledgements.**

I would like to thank and express my gratitude to all those who have supported and encouraged me in the realization of this thesis.

*Paolo Buttà*, per avermi voluto seguire fin dalla mia tesi di laurea, con attenzione, curiosità e competenza, mostrandomi come realmente debba essere il lavoro di ricerca. Per avermi dato ottimi suggerimenti e tantissime spiegazioni.

*Livio Triolo*, per il supporto che mi ha dato a partire dalla mia tesi di laurea, suggerendomi argomenti così come scuole o convegni. Per esserci sempre stato quando gli ho voluto chiedere un consiglio.

*Vito D. P. Servedio*, per l'imprescindibile aiuto e collaborazione con la programmazione in C e con le simulazioni del modello di dinamica molecolare, per non parlare dell'assistenza nel debugging.

*Errico Presutti*, per avermi suggerito il problema descritto nella prima parte della mia tesi e per i preziosi consigli che mi ha dato nel corso dello svolgimento del lavoro.

*Benoit Perthame*, je le remercie de me donner l'occasion de travailler avec lui et son groupe de recherche multidisciplinaire à Paris et pour le sujet de recherche intéressant et les explications qui l'accompagnent.

*Nicolas Vauchelet et Min Tang*, je les remercie de leur collaboration et des conversations utiles sur le modèle proposé par Perthame et de l'assistance dans sa simulation.

*Stefania Melillo*, per avermi aiutato in una parte del programma sull'elongazione delle cellule e per aver diviso con me interminabili ore davanti al computer.

*Valentina Masi*, con cui ho diviso intere giornate a fare conti.

*Castelnuovo and Friends*, perché avete un po' colorato le bianche mura del Castelnuovo e mi avete sopportato per tanti anni. Grazie.

# Contents

CHAPTER 1

# Introduction

Since the days of my master degree I have developed a great interest in biology and medicine and therefore in mathematical modeling related to this field. During my Phd I have worked on deepen my knowledge about this matter through seminars, workshops and congresses, keeping a link, more or less direct, between my mathematical work and biomedical subjects. Through the years my study faced three main problems, one of which has come out during my latest working period in Paris.

## 1.1. Interface fluctuations for the $D = 1$ stochastic Ginzburg-Landau equation with an asymmetric, periodic, mean-zero, *on-off* external potential

Modern biology has shown that an important number of biological processes is governed by the action of molecular complexes reminiscent in some way of macroscopic machines, the "molecular motors". The word "motor" is used for proteins or protein complexes that transduce at a molecular scale chemical energy into mechanical work. Extensive studies have shown that a significant part of eukaryotic cellular traffic relies on motor proteins that move in a deterministic way along filaments similar in function to railway tracks; these filaments are periodic, fairly rigid structures and, moreover, polar. A given motor always moves in the same direction (towards plus or minus extremity of the

filaments). There are many chemical reactions involved during individual molecular transitions. As long as these reactions occur there are several local fluctuations, which are present also at the equilibrium.

Nonequilibrium fluctuations, brought about by an energy releasing process, can be "absorbed" and used to do chemical or mechanical work by an energy requiring process. In the study of molecular motor, it was shown that zero-average oscillation or fluctuation of a chemical potential causes net flux as long as the period of the oscillation is not much shorter than the relaxation time of the reaction.

Theory shows that the direction of flow is governed by a combination of local spatial anisotropy of the applied potential, the diffusion coefficient of the motor, and the specific details of how the external modulation of the force is carried out (also stochastically). Here it's shown that the above mechanism also appears in a completely different context, the dynamic of interface in phase transition theory. To this end, it's introduced a model in the framework of stochastically perturbed Ginzburg-Landau (G-L) equations for phase transitions.

We study the Ginzburg-Landau equation perturbed by an additive white noise $\alpha$, of strength $\sqrt{\varepsilon}$, and by an external field of strength $\varepsilon$

$$\frac{\partial}{\partial t}m = \frac{1}{2}\frac{\partial^2 m}{\partial x^2} - V'(m) + \varepsilon\, h(x)G(\varepsilon t) + \sqrt{\varepsilon}\alpha \tag{1.1}$$

where $\varepsilon > 0$ is a small parameter that eventually goes to 0 and $V(m)$, $m \in \mathbb{R}$, is the paradigmatic double well potential $V(m) = m^4/4 - m^2/2$, with minima at $m = \pm 1$. Finally, $G(t)$ is a periodic function alternatively equal to 1, during the *day time* $T_D$, or to 0, during the *night time* $T_N$. We say that it *switches On-Off* the potential $h(x)$, which is a periodic, asymmetric and mean zero step function. We consider the above equation in the interval $\mathcal{T}_\varepsilon = [-\varepsilon^{-1}, \varepsilon^{-1}]$, with Neumann boundary conditions (N.b.c.).

We call pure phases the two constant functions $m(x) = \pm 1$, $x \in \mathcal{T}_\varepsilon$, and we study the interface dynamics, that is the evolution of profiles that are close to the two pure phases to the left and to the right of some point, say $x_0$.

Equation (1.1), setting $\varepsilon = 0$ and considering it in the whole space $\mathbb{R}$, is the deterministic Ginzburg-Landau equation, that arises as the gradient flow associated to the Ginzburg-Landau free energy functional. In this contest $m$ represents the order parameter of the system, e.g. the magnetization. It has a stationary solution $\bar{m}(x) = \tanh x$, $x \in \mathbb{R}$ that we call *instanton*. The solution $\bar{m}$ is a wavefront with speed 0, that connects the two pure phases. The set of all the translates of $\bar{m}$ is locally attractive, that is if the initial datum is close to $\bar{m}(x - x_0)$, for some "center" $x_0$, then the solution of the deterministic Ginzburg-Landau converges to an instanton with center $x_0'$ close to $x_0$.

Fusco and Hale, [**15**], and Carr and Pego, [**10**], have studied the deterministic Ginzburg-Landau equation in the finite interval $\mathcal{T}_\varepsilon = [-\varepsilon^{-1}, \varepsilon^{-1}]$ with N.b.c. and with initial datum close to the two pure phases to the right and to the left of some point $x_0$ respectively. They prove that the solution relaxes in a short time to an almost stationary state which represents a front connecting the two stable phases, $m = \pm 1$. This front is very close to the instanton $\bar{m}_{x_0} = \bar{m}(x - x_0)$ restricted to the finite interval. The front which has been formed in $\mathcal{T}_\varepsilon$ is not truly stationary, in fact it moves but extremely slowly, with speed $\approx e^{c\ell}$, $c$ a positive "slowly varying" factor, $\ell$ the distance of the center from the boundary of $\mathcal{T}_\varepsilon$. During this motion the front keeps almost the same shape.

If we take into account the stochastic term, the picture initially does not change much: except for small deviations we still have a short relaxation time and the formation of a profile very close to a

front. However, under the action of the noise, the front moves in a dramatically shorter time than in the deterministic case. At times $t_\varepsilon \equiv t\varepsilon^{-1}$, $t > 0$, the displacement is finite and the motion of the center converges as $\varepsilon \to 0^+$ to a brownian motion $b_t$, as shown in [**9**].

At much longer times the picture may in principle change, for instance the system could pick some drift, as it happens when the potential $V$ is not symmetric, as shown in [**7**]. In [**8**] it is shown that, for symmetric potentials $V$, in $\mathcal{T}_\varepsilon = [-\varepsilon^{-k}, \varepsilon^{-k}]$, $k \geq 1$, with N.b.c., there is no drift for times of order $t_\varepsilon \equiv t\varepsilon^{-h}$, $t$, $h > 0$. Roughly speaking, the process, for $k \geq 1$, is in some sense close to $\bar{m}_{x_0+\sqrt{\varepsilon}b_t}$ with $b_t$ a Brownian motion with diffusion $\sigma = 3/4$.

Here we prove a stability result for (1.1), showing that its solution with the initial condition close to the restriction of some instanton to $\mathcal{T}_\varepsilon$, remains close to the set of translates of $\bar{m}(x-x_0)$, for times of order $t \approx \varepsilon^{-1}\log\varepsilon^{-1}$, and that its center, suitable normalized, for times of order $t \approx \varepsilon^{-1}$, converges, as $\varepsilon \to 0^+$ to a brownian motion with a deterministic positive drift.

Let our initial condition to equation (1.1) be a continuous function $m_{0,\varepsilon} \in \mathcal{C}(\mathbb{R})$ satisfying N.b.c. in $\mathcal{T}_\epsilon$, such that for any $\eta > 0$

$$\lim_{\varepsilon\to 0} \varepsilon^{-\frac{1}{2}+\eta} \sup_{x\in\mathcal{T}_\epsilon} |m_{0,\varepsilon}(x) - \bar{m}_0(x)| = 0.$$

Then, calling $m_t$ the solution to (1.1) with this initial data, we have a first result stating the closeness of the solution to an instanton centered in some $\mathcal{F}_t$-adapted process $X_\varepsilon$.

THEOREM 1.1. *Let $\lambda = \log\varepsilon^{-1}$ and $x_0 = x_0(m_{0,\varepsilon}) \in \mathbb{R}$. There exists a $\mathcal{F}_t$-adapted process $X_\varepsilon$ such that, for each $\tau, \eta > 0$*

$$\lim_{\varepsilon\to 0^+} \mathbb{P}\Big( \sup_{t\in[0,\lambda\varepsilon^{-1}\tau]} \sup_{x\in\mathcal{T}_\varepsilon} |m_t - \bar{m}_{X_\varepsilon(t)}| > \varepsilon^{\frac{1}{2}-\eta}\Big) = 0 \tag{1.2}$$

*where $\mathbb{P} = \mathbb{P}^\varepsilon$ is the probability on the basic space, where the noise $\alpha$ and the process $m_t$ are constructed.*

In the first section of Chapter 2 there are more details about the construction of the initial data and of the solution $m_t$ and the previous Theorem is rewritten in a more precise way.

As already mentioned, our motivation for studying such a problem, with this choice of the external potential $h$, arises from the study of molecular motors. The connection between our work and the molecular motors becomes clear once we study the limit equation, as $\varepsilon \to 0^+$, satisfied by the center $X_\varepsilon$, suitable normalized, for times of order $t \approx \varepsilon^{-1}$. Actually, using the same notations of the previous Theorem, we have the following statement that characterizes this limit equation.

THEOREM 1.2. *The real process $Y_\varepsilon(\theta) = X_\varepsilon(\varepsilon^{-1}\theta) - x_0$, $\theta \in \mathbb{R}_+$, converges weakly in $\mathcal{C}(\mathbb{R}_+)$ as $\varepsilon \to 0^+$, to the unique strong solution $Y$ of the stochastic equation*

$$\begin{cases} dY(\theta) = D(Y,\theta)d\theta + db(\theta) \\ Y(0) = 0 \end{cases}$$

*where $b$ is a Brownian motion with diffusion coefficient $3/4$ and the drift is given by*

$$D(Y,\theta) \doteq -G(\theta)\langle \bar{m}'_Y, h\rangle.$$

*The function $D$ is periodic asymmetric and mean-zero .*

Following the definition of [**18**] this stochastic equation on $Y$ describes an On-Off molecular motor, once chosen in the correct way the constants $T_D$ and $T_N$ in the definition of $h(x,t)$. Quantitatively, the asymptotic average particle current $\langle \dot{Y} \rangle$ reaches a finite positive or negative value. For our choice of $H(x)$ we have that this net current is positive, as it is shown, in the contest of an asymptotic analysis for fast oscillations, in the Section 2.6.

For a more detailed introduction and for the proof, see Chapter 2. I presented this work in a poster during the thematical trimester on "Statistical Mechanics" at the Institute Henri Poincaré in Paris, on December 2008.

## 1.2. Modeling of biological pattern formation

The past decade has seen growing interest in the dynamical properties of interacting, self-propelled organisms, such as bacteria, sperm cells, fish, marching locust, etc. This many body problem was motivated by phenomena in biology but is now recognized to encompass nonequilibrium statistical mechanics and nonlinear dynamics. A fundamental issue is the nature of possible transitions to collective motion and the relation based on local interactions between elements, and the phenomenon of collective swimming in which nonlocal hydrodynamic interactions are obviously important. Two key questions involving collective dynamics can be identified. How do spatiotemporal correlations depend on the concentration of microorganisms? How can their concentration be managed as a control parameter?

One of the most studied mechanism that causes collective motion and pattern formation in a group of organisms is the *chemotaxis*, i.e. the movement of living organisms under the effect of the gradient of the concentration of a chemical substance. This substance, which is in case secreted by the organisms themselves, is considered a key factor in morphogenesis, in the regulation of life cycle of some protozoan species, in bacteria diffusion, in angiogenesis and in vascularization of tumours, as in the seasonal migration of some animals.

It is not the aim of the present thesis to review on chemotaxis mathematical modeling, therefore I just remember here that on the theoretical side, the first partial differential equation based models of

chemotaxis appeared in the early '70s [**23**], and were soon followed by hyperbolic and kinetic models.

During my Phd I faced two different problems modeling biological pattern formations, both including chemotaxis even if in two different ways.

**1.2.1. Molecular dynamics simulation of vascular network formation.** In collaboration with professors Paolo Buttà, Livio Triolo and Vito D. P. Servedio I went on the study of a discrete model simulating the process of vascular network formation, which I proposed on my degree thesis. We refined this model and performed numerical simulations. Finally I presented the work in the poster session of the international congress StatPhys23 in Genova, in July 2007, and we published an article in 2009 [**21**].

Vascular networks are complex structures resulting from the interaction and self organization of endothelial cells (ECs). Their formation is a fundamental process occurring in embryonic development and in tumor vascularization. In order to optimize the function of providing oxygen to tissues, vascular network topological structure has to involve a characteristic length practically dictated by the diffusion coefficient of oxygen [**22**]. In fact, observation of these networks reveals that they consist of a collection of nodes connected by thin chords with approximately the same length.

We study the process of formation of vascular networks by means of two-dimensional off-lattice molecular dynamics simulations involving a finite number $N$ of interacting simple units, modeling endothelial cells. The interaction among cells is due to the presence of a chemical signal, in turn produced by the cells themselves. This mechanism of motion is what we called *chemotaxis*, a mechanism still object of intensive experimental and theoretical research. As already mentioned, the

relevance of chemotaxis reflects its important role in many situations of biomedical interest such as wound healing, embryonic development, vascularization, angiogenesis, cell aggregation, to cite a few.

We explicitely refer to in vitro experiments of Gamba et al.[**29**] and shall use the same numerical values of parameters therein introduced. Our models refers to the first 2 hours of experiments in which the $ECs$ self-organize into a network structure. The gradient of the chemical signal dictates the direction of individual cell motion. Cells migrate untill collision with other cells, while keeping approximately a round shape. The final capillary-like network can be represented as a collection of nodes connected by thin chords of characteristic length, whose experimentally measured average stays around $200\mu m$ for values of the cell density between 100 to $200 cells/mm^2$.

The peculiar advantage of mocular dynamics methods is the extreme ease with which one can introduce forces acting in individual particles. Therefore we developed our model with increasing complexity, refining it by gradually adding features that would allow a closer resemblance with experiments. Here I just mention the main steps of our work presenting the final model, addressing the reader to Chapter 1 for more details.

Particles, which we shall also refer to as "cells" in the following, are constrained inside a square box of given edge $L$ with periodic boundary conditions and their number is kept constant during the simulations, i.e. we will consider neither cell creation nor cell destruction. At first, we consider cells as adimensional point-like particles moving only under the effect of the concentration gradient of the chemoattractant substance $\nabla c$. The chemical substance is released by the particles themselves, diffuses according to a difusive coefficient $D$ and degrades

within finite time $\tau$. The combination of these two processes introduces a characteristic length $l$. In a second time we introduced in the system a dynamical friction $\mathbf{F}_{\mathrm{F}}$ in order to simulate the dragging force between the substrate and the cells. To further refine the simulation, we introduced an anelastic hardcore repulsion mechanism $\mathbf{F}_{\mathrm{IR}}$ between cells, avoiding compenetration between cells. Every cell is no more adimensional but possesses its own radius $r$. The introduction of a cell radius changes sensibly the simulation. Above all we could use the experimental number of cells. Our last refinement faces the problem of the "cell persistence" of motion, i.e. the observed large inertia of cells in changing the direction of their motion. For each $i$-cell, we add the force $\mathbf{F}_{\mathrm{T}}$, which simply reduces the component of the gradient of the chemical field along the direction of cell motion by a factor depending on $|\mathbf{v}_i|$ and $|\nabla c(\mathbf{x}_i, t)|$.

All together, the dynamical system of equations we solve with $i = 1 \dots N$ is

$$\begin{cases} \dot{\mathbf{x}}_i(t) = \mathbf{v}_i(t) \\ \dot{\mathbf{v}}_i(t) = \mu \nabla c(\mathbf{x}_i(t), t) + \mathbf{F}_{\mathrm{IR}} + \mathbf{F}_{\mathrm{T}} + \mathbf{F}_{\mathrm{F}} \\ \partial_t c(\mathbf{x}, t) = D \Delta c(\mathbf{x}, t) - \frac{c(\mathbf{x},t)}{\tau} + \alpha \sum_{j=1}^{N} J(\mathbf{x} - \mathbf{x}_j(t)), \end{cases}$$

where $\mu$ measures the strength of the cell response to the chemical factor. Here $c(\mathbf{x}, t)$ is the total chemical field acting on the position $\mathbf{x}$ at time $t$ and it is set to zero at time $t = 0$, as the initial velocities, while cell initial positions were extracted at random. The function $J(\mathbf{x})$ is responsible of chemoattractant production.

Without both the repulsion and persistence terms, the simulations, far from be realistic, are although interesting since they deliver a picture of the capillary with a characteristic chord size $\ell$. Nevertheless the organized capillary network structure arises as a brief transient, after which cells collapse all together. The dynamical friction term helps to

lengthen the duration of the transient. At this stage, we confirm that the bare process of chemotaxis is capable of organizing cells in a non trivial functional displacement.

With the addition of the cell anelastic repulsion we are able to reproduce experiments qualitatively. However, the capillary network still appears during a short transient and the overall visual contrast of the filaments is not as satisfactory as it was in the bare chemotaxis simulations with much higher densities. This lack of visual contrast of chord structures may reflect the experimental fact that cells elongate their shape in the act of moving, a process intimately bound to the phenomenon of cell persistence of motion. This is the main reason that led us to introduce the persistence force $\mathbf{F}_{\mathrm{T}}$. With this term the transient phase gets longer and the network visual impact becomes more clear.

I address the reader to the first Chapter 3 for the discussion and conclusions on the results of the simulation.

As a consequence of the Congress in Genova I had fruitfull conversations with professor A. Gamba (Department of Mathematics, Politecnico di Torino) and doctor G. Serini (Institute for Cancer Research and Treatment, Torino). Thanks to these discussions I found out the most important changes and additions we have to do to our model. Therefore, in the last year I worked to introduce these new features in the simulations.

Actually cells elongate during the motion. They have an approximately rounded shape while standing, but, as soon as they start to move, they change their shape into an ellipse, with the long axe oriented along the direction of the gradient of $c$ (in some sense they polarize themselves). They continually update their "head" and "tail". In the last year we produced a new model representing cells like rectangules

and introducing a new hardcore force proportional to the overlapping area. We deal with the updating polarization by means of our *persistence* force. This feature would also be usefull to stabilize the network. At this stage, this work is still in progress.

**1.2.2. A model to reproduce the physical elongation of dendrites during swarming migration and branching.** In the last eight months I had the opportunity to work in Paris with professor Benoit Perthame and one of his research groups. I worked in a project of the network DEASE, the European Doctoral School "Differential Equations with Applications in Science and Engineering". We worked joint with biologists and physicists on modeling the formation of bacterial dendrites, i.e. digital pattern formation in bacterial colonies.

During the cours of evolution, bacteria have developed sophisticated cooperative behaviour and intricate communication capabilities. These include: direct cell-cell physical interaction via extra-membrane polymers, collective production of extracellular "wetting" fluid for movement on hard surface, long range chemical signaling, such as quorum sensing and chemotactic signaling, collective activation and deactivation of genes and an even exchange of genetic material. Utilizing these capabilities, bacterial colonies develop complex spatio-temporal patterns in response to adverse growth conditions.

In our specific case we are dealing with a problem proposed by the biologists Simone Seror and Barry Holland, on the subject of *Bacillus Subtilis* swarming, [**65, 56**]. This is a process involving mass movement over a surface of a synthetic agar medium. This process has the great advantage that the key stages in development occur entirely as a monolayer.

The dendritic swarming appears to be a multistage developmental-like process that is likely to be controlled by extracellular signaling

mechanisms that should be amenable to genetic analysis. Bacteria are capable of surface translocation using variety of mechanisms, and in our case we follow the idea that the term swarming has to be reserved for rapid cooperative movement, requiring *flagella* over an agar with *low-concentration of nutrient*.

Swarming of *B.subtilis* is absolutely depending upon flagella and, under most conditions, the production and secretion of *surfactin*. The surfactin is a *surfactant* (which stands for *surface active agent*), i.e. a cyclic lipopeptide which spreads just ahead of the migrating bacteria throughout the swarming process. It presumably reduces surface tension, friction or viscosity, or modifies the great agar surface to maintain a depth of fluid that is sufficient to swarming.

Summing up, the experiment we should reproduce mathematically is the following. On an agar surface is put a drop of bacterial culture, which, from now, we call Mother Colony ($MC$), after more or less $10\,h$ from the edge of the $MC$ a part of the bacterial population (a fraction that we call the *Swarmers*) starts to swarm, thanks to flagella and with the emergence of surfactin zone spreading from the edge of $MC$. At $t \sim 11\,h$, $10-14$ buds appear at the edge of $MC$. At about $14\,h$, when dendrites are approximately $2\,mm$ long, $MC$ could be excised with no significant effect on swarming.

At this stage the swarm migration is restricted to $1.5\,cm$ and the dendrites are monolayer with minimal branching. Population density along dendrites, up to $1.4\,cm$, is constant, even if not completely uniform. And this density increases sharply, up to two folds, in the extreme terminal from 1 to $1.2\,mm$ at the tip. The swarm migration speed is linear with a constant rate of about $3.5\,mm/h$.

Swarming is dependent on, at least, two distinguishable cell types, *hyper-motile swarmers* (24 flagella), present in the multi-folder tips of

the dendrites, and *largely immobile supporters* (12 flagella), composing the 1−folder queues. Dead cells in the swarm are extremely rare.

The concentration of *nutrients* provided in a swarm plate can be reduced drastically, without affecting swarming. Under the experimental conditions therefore, nutrients do not appear to be limiting. From this observation, it follows the request of the biologists not to include any nutrient density term in the model. This is a complete new feature in the field of bacterial pattern formation modeling and makes our model really different from the pre-existing ones (see [**54, 69**] and references therein).

This is the experimental setting. There are many questions that biologists addressed to us. They would understand if both supporters and swarmers may divide or if just the supporters do, as they suspect; which is, in case, the time of divisions of both; if the supporters also produce surfactin or if it is sufficient the one produced at the edge of $MC$. They have experimental double time for cells only in liquid culture, but not on agar, and they expect us to find it in this case.

Here I have just summarized the most important clues they gave us, but the questions to answer are more than these. We are actually working on the following model partially inspired by the ones explained in [**51, 49, 50, 53**].

We consider the following features. The density population of active cells $n$ obeys a conservation equation. The swarmers move under the chemotactic effect of the surfactin $S$ and of a short range chemical substance $c$ which has the aim to hold together the cells forming the dendrites and to cooperate with $S$ in the splitting mechanism.
The surfactin density is $S$ and it is released by both supporters and mother colony, with rates $\alpha_f$ and $\alpha_s$ respectively; it diffuses with a coefficient $D_s$ and it is degraded with a rate $\tau_s$.

The chemical concentration of the short range attractant is given by $c$, which is itself produced by the swarmers, with a rate $\alpha_c$. It diffuses with a coefficient $D_c$ and decreases by a factor $\tau_c$.
The trace left by the swarmers, $D_m$, is released by $n$ with a rate $d_m$; $m_{col}$ is the population density of the mother colony of bacteria.
Finally we consider the supporters density $f$, that diffuses according to $D_m$ and is produced by $n$, with a birth rate $B_n$, and by $f$, with a rate $B_f$.

Therefore we have a system composed by five pde which we simulate in one and two dimensions looking for the branching phenomenon and the stable states. The whole system has the following form

$$\begin{cases} \partial_t n + div\big(n(1-n)\nabla c - n\nabla S\big) = 0, \\ -D_c\Delta c + \tau_c c = \alpha_c n, \\ \partial_t S - D_s\Delta S + \tau_s S = \alpha_s m_{col} + \alpha_f f, \\ \partial_t D_m = d_m n, \\ \partial_t f - div(D_m\nabla f) = B_f f(1-f) + B_n n, \end{cases}$$

where all the quantities are adimensionalized. This system is considered in a bounded domain $\Omega \subset \mathbb{R}^2$ and it is completed with N.b.c. for $c$ and $S$, with no-flux boundary condition for the swarmer concentration $n$.

OBSERVATION 1.1. *It is important to underline here that in our contest, avoiding the presence of any nutrient, actually there is no substance generating a chemotactic movement of the bacteria which had been identified experimentally. Biologists do not consider precisely surfactants as chemotactic factors. Nevertheless the structure of the digital patterns and the ability of the dendrites to avoid each other suggest that there should be some mechanism similar to a repulsive chemical signal. This consideration and the main features of the phenomenon and of*

*the characteristics of the surfactin lead us to model $S$ like a chemorepellent. This is not wrong, but it is a mathematical representation, in some sense it is a "mathematical chemotaxis".*

Up to now we performed numerical simulations of this model with a resulting good picture of the first two subsequent branching from the $MC$. We also studied some reduced models to work out the main features of each term of the system. The existence and stability of branching solutions such as the main theorems are asserted by numerical results.

I address the reader to Chapter 4 for an overview of this *in fieri* work.

CHAPTER 2

# Interface fluctuations for the $D = 1$ stochastic Ginzburg-Landau equation with an asymmetric, periodic, mean-zero, *on-off* external potential

## 2.1. Definitions and main results

Let us consider the family of processes given as solutions of the initial value problem for the following stochastic one-dimensional Ginzburg-Landau equation perturbed by an external field, $\forall t \geq 0$, $x \in \mathcal{T}_\varepsilon = [-\varepsilon^{-1}, \varepsilon^{-1}]$

$$\begin{cases} \frac{\partial}{\partial t} m = \frac{1}{2}\frac{\partial^2 m}{\partial x^2} - V'(m) + \varepsilon h(x) G(\varepsilon t) + \sqrt{\varepsilon}\alpha, \\ m(x,0) = m_0(x), \end{cases} \tag{2.1}$$

with Neumann boundary conditions in $\mathcal{T}_\varepsilon = [-\varepsilon^{-1}, \varepsilon^{-1}]$. Here $V(m) = m^4/4 - m^2/2$ is the paradigmatic double well potential, $\varepsilon$ is a small positive parameter which eventually goes to zero while $\alpha = \alpha(t,x)$ is a standard space-time white noise on a standard filtered probability space $(\Omega, \mathcal{F}, \mathcal{F}_t, \mathbb{P})$. The external field $h(x)G(t)$ is defined as follows. Let $L > 3$, $h_0 > 0$ be constants,

$$h(x) = \begin{cases} Lh_0 & \text{if } k(L+1) < x \leq k(L+1)+1 \quad k \in \mathbb{Z}, \\ -h_0 & \text{if } \; k(L+1)+1 < x \leq (k+1)(L+1) \quad k \in \mathbb{Z}, \end{cases} \tag{2.2}$$

therefore $h(x)$ is an asymmetric periodic step function with mean zero. By the way, for technical reason, we will call $h(x) = h_\delta(x) = (h * \phi_\delta)(x)$, with $\phi_\delta \in \mathcal{C}_c^\infty(-\delta, \delta)$ ($\delta$ small enough), its mollified version $h \in \mathcal{C}^\infty(\mathbb{R})$ and consider its restriction to $\mathcal{T}_\varepsilon$. The function $G$ is a periodic function which has the aim to switch off, during the *night time* $T_N$, the potential

$h$ and to switch it on during the *day time* $T_D$ ($T_N$ and $T_D$ positive constant)

$$G(t) = \begin{cases} 0 & \text{if } \ k(T_D+T_N) < t \le k(T_D+T_N)+T_N \quad k \in \mathbb{Z}, \\ 1 & \text{if } \ k(T_D+T_N)+T_N < t \le (k+1)(T_D+T_N) \quad k \in \mathbb{Z}. \end{cases} \tag{2.3}$$

Here again we consider a mollified version of $G(t)$.

Let us denote by $H_t^{(\varepsilon)}$ the Green operator for the heat equation with N.b.c. in $\mathcal{T}_\varepsilon$ and by $H_t^{(\varepsilon)}(x,y)$ the corresponding kernel. We say that $m_t$ is a solution to equation (2.1) with initial condition $m_0 \in \mathcal{C}(\mathcal{T}_\varepsilon)$ if it satisfies the integral equation, with $t \ge 0$ and $x \in \mathcal{T}_\varepsilon$

$$m_t = H_t^{(\varepsilon)} m_0 - \int_0^t ds\, H_{t-s}^{(\varepsilon)}(m_s^2 - m_s) + \int_0^t ds\, H_{t-s}^{(\varepsilon)} h(\cdot) G(\varepsilon s) + \sqrt{\varepsilon} Z_t^{(\varepsilon)} \tag{2.4}$$

where $Z_t^{(\varepsilon)}$ is the Gaussian process defined by the stochastic integral in the sense of [**20**]

$$Z_t^{(\varepsilon)}(x) = \int_0^t ds \int_{\mathcal{T}_\varepsilon} dy\, \alpha(s,y) H_{t-s}^{(\varepsilon)}(x,y). \tag{2.5}$$

$Z_t^{(\varepsilon)}$ is continuous in both variables and, by following the same arguments of [**13**], there exists a unique $\mathcal{F}_t$-adapted process $m \in \mathcal{C}(\mathbb{R}, \mathcal{C}(\mathcal{T}_\varepsilon))$ which solves (2.4).

As it is explained in [**9, 8**] the function $\bar{m}(x) \doteq \tanh(x)$, which we call *instanton* with *center* 0, is a stationary solution for the deterministic Ginzburg-Landau on the whole line $\mathbb{R}$,

$$\frac{1}{2}\frac{\partial^2 \bar{m}}{\partial x^2} = V'(\bar{m}) \ \text{ with } \ \bar{m}(\pm\infty) = \pm 1 \ \text{ and } \ \bar{m}(0) = 0, \tag{2.6}$$

and its translates,

$$\bar{m}_{x_0}(x) \doteq \bar{m}(x - x_0), \qquad x,\, x_0 \in \mathbb{R},$$

are also stationary solutions, called *instanton centered in* $x_0$. Fife and McLeod ([**14**]) have proved that the set

$$\mathcal{M} = \{\bar{m}_{x_0}, x_0 \in \mathbb{R}\} \subset \mathcal{C}^0(\mathbb{R})$$

is locally attractive under the flow $m_t = T_t(m_0)$, $t \geq 0$, associated to equation (2.1) with $\varepsilon = 0$ in the whole line. More precisely, let $\|\cdot\|$ denote the sup norm in $\mathbb{R}$ and, for $\delta \geq 0$, define

$$\mathcal{M}_\delta \doteq \{m \in \mathcal{C}^0(\mathbb{R}) : \text{dist}(m, \mathcal{M}) \doteq \inf_{x_0 \in \mathbb{R}} \|m - \bar{m}_{x_0}\| \leq \delta\}$$

then, there exists $\delta_* > 0$ and a real valued function $x(m)$ defined on $\mathcal{M}_{\delta_*}$, called the (linear) center, such that

$$\lim_{t\to\infty} T_t(m) = \bar{m}_{x(m)} \qquad \forall m \in \mathcal{M}_{\delta_*}$$

in sup norm and exponentially fast.

When we restrict to $\mathcal{T}_\varepsilon$, we evidentely loose the notion of instanton and one may ask why to consider $\mathcal{T}_\varepsilon$ instead of $\mathbb{R}$. Actually, by this way we avoid to deal with unbounded processes, furthermore, by the choice of N.b.c in $\mathcal{T}_\varepsilon$ we have the advantage of recovering to some extent the instanton structure present in $\mathbb{R}$ as proved in [**15, 10**] and explained in [**9, 8**]. Since we are interested in studying the evolution of $m_t$ when the initial datum is close to an instanton, and to use the stability under the dynamics of the instanton on the whole line, it will be convenient, in the sequel, to consider the problem in $\mathbb{R}$ instead of in $\mathcal{T}_\varepsilon$, as in [**9**]. To this end, given a continuous function $f$ on $\mathcal{T}_\varepsilon$, we denote by $\hat{f}$ its extension to $\mathbb{R}$ obtained by successive reflections around the points $(2n+1)\varepsilon^{-1}$, $n \in \mathbb{Z}$, and define the space of functions so obtained

$$\mathcal{C}_\varepsilon(\mathbb{R}) \doteq \{f : f \in \mathcal{C}^0(\mathbb{R}), f \text{ is invariant by reflections around the point } (2n+1)\varepsilon^{-1}, n \in \mathbb{Z}\}.$$

We define

$$Z_t = \hat{Z}_t^{(\varepsilon)}$$

and refer to $Z_t$ as the free process. We denote by $H_t$ the Green operator for the heat equation on the whole line, so that for any $m \in \mathcal{C}(\mathcal{T}_\varepsilon)$,

$$H_t^{(\varepsilon)} m(x) = H_t \hat{m}(x).$$

As proved in Proposition 2.3 of [**9**], as it follows for instance from [**12**], for any $\varepsilon > 0$, given $m_0 \in \mathcal{C}^0(\mathbb{R})$ and satisfying N.b.c. in $\mathcal{T}_\varepsilon$, and for any $Z_t$ continuous in both variables and satysfying N.b.c., there is a unique continuous solution $m_t$ of the integral equation

$$m_t = H_t m_0 - \int_0^t ds\, H_{t-s}(m_s^2 - m_s) + \varepsilon \int_0^t ds\, H_{t-s} \hat{h}(\cdot) G(\varepsilon s) + \sqrt{\varepsilon} Z_t, \tag{2.7}$$

with $(t, x) \in \mathbb{R}^+ \times \mathbb{R}$. Where $\hat{h}$ is the extension, by reflection on the whole space, of $h$, once restricted to $\mathcal{T}_\varepsilon$. We set

$$m_t \doteq T_t(m_0, \varepsilon)$$

for the solution of equation (2.7) with $\varepsilon \neq 0$. Moreover $m_t = \hat{m}_t^{(\varepsilon)}$ where $\hat{m}_t^{(\varepsilon)}$ solves (2.4) with $Z_t^{(\varepsilon)}$ and $m_0^{(\varepsilon)}$ obtained by restricting $Z_t$ and $m_0$ to $\mathcal{T}_\varepsilon$. In case $m_0 \in \mathcal{C}_\varepsilon(\mathbb{R})$, by an abuse of notation, we will also refer to $T_t(m_0, \varepsilon)$ as the Ginzburg-Landau process in $\mathcal{T}_\varepsilon$ with N.b.c.

With the aim of using extensively the stability properties of the instantons we will take great advantage of the representation (2.7) where the only memory of the boudary conditions is in the "small perturbation" $\sqrt{\varepsilon} Z_t$, in $\hat{h}$ and in the initial data. The equation (2.7) is thus well suited for a perturbative analysis of data close to instantons.

However, even if $m \in \mathcal{C}_\varepsilon(\mathbb{R})$ is very close to an instanton in $\mathcal{T}_\varepsilon$, it is not close to an instanton in the sup norm on the whole line. We overcome this problem by using barrier lemmas that allow us to modify the function away from $\mathcal{T}_\varepsilon$ without changing too much its evolution in $\mathcal{T}_\varepsilon$. The modified function can be taken in a neighborhood of $\mathcal{M}$ and we can adopt the results of Fife and McLeod about convergence to an instanton. The noise works against this trend by preventing the

orbit from getting too close to $\bar{m}$ and forces the solution to live in a small neighborhood of $\mathcal{M}$, whose size depends on the strength of the noise and vanishes as $\varepsilon \to 0^+$. Nevertheless these small 'kicks' given by the noise have the effect of changing the linear center of the deterministic evolution. Their cumulative effect causes the Brownian motion on $\mathcal{M}$ that describes the stochastic part of the limit process. It means that there exists a stochastic process $X_\varepsilon(t)$ such that $m_t$ is in some sense close to $\bar{m}_{X_\varepsilon(t)}$, as $\varepsilon \to 0^+$. This stochastic process, opportunately rescaled, in the limit, performs a Brownian motion. On the other hand the presence of the asymmetric periodic on-off potential $h$, causes a deterministic periodic asymmetric and mean-zero drift in the limit process. The motion of this rescaled center, as $\varepsilon \to 0$, is given by an equation that describes a typical on-off molecular motor (see [**18**]).

Let us now give some notation and the main results. As explained above, the first step is to change the functions in $\mathcal{C}_\varepsilon(\mathbb{R})$, outside $\mathcal{T}_\varepsilon$, in such a way that they are in a small neighborhood of an instanton on the whole line. Given $m \in \mathcal{C}^0(\mathbb{R})$, we define $m^\varepsilon \equiv m$ if $m \notin \mathcal{C}_\varepsilon(\mathbb{R})$, setting in the other case

$$m^\varepsilon(x) = \begin{cases} m(x), & x \in \mathcal{T}_\varepsilon \\ m(\pm\varepsilon^{-1}) & x \geq \varepsilon^{-1}, \text{ respectively, } x \leq -\varepsilon^{-1} \end{cases} \tag{2.8}$$

Before stating the main result, we need to introduce the kernel $g_{t,x_0}(x,y)$ which is the fundamental solution of the linearized deterministic Ginzburg-Landau equation in $\mathbb{R}$ around the instanton $\bar{m}_{x_0}$ (see [**8**] for more details). Its generator $L_{x_0}$ acts on $f \in \mathcal{C}^2(\mathbb{R})$ as

$$L_{x_0} f(x) = \frac{1}{2}\frac{\partial^2 f}{\partial x^2} f(x) + [1 - 3\bar{m}_{x_0}^2(x)] f(x)$$

Denote by $\bar{m}'_{x_0}$ the derivative w.r.t. $x$ of $\bar{m}_{x_0}$. By differentiating (2.6), we get $L_{x_0}\bar{m}'_{x_0} = 0$ for any $x_0 \in \mathbb{R}$. Denoting by $\langle \cdot, \cdot \rangle$ the scalar product

in $L^2(\mathbb{R})$ we set, for any $x_0 \in \mathbb{R}$,

$$\tilde{m}'_{x_0} = \frac{\sqrt{3}}{2}\bar{m}'_{x_0} \qquad \langle \tilde{m}'_{x_0}, \tilde{m}'_{x_0} \rangle = 1$$

Therefore 0 is an eigenvalue of $L_{x_0}$, and $\tilde{m}'_{x_0}$ is the corresponding unitary eigenvector in $L^2(\mathbb{R})$. The generator $L_{x_0}$ has a spectral gap:

LEMMA 2.1. *There are $a$ and $C$ positive so that $\forall f \in \mathcal{C}^0(\mathbb{R})$ and $x_0 \in \mathbb{R}$*

$$\|g_{t,x_0}[f - \langle \tilde{m}'_{x_0}, f\rangle \tilde{m}'_{x_0}]\| \leq Ce^{-at}\|f - \langle \tilde{m}'_{x_0}, f\rangle \tilde{m}'_{x_0}\| \tag{2.9}$$

For the proof see [**9**]. Observe that the solution $m(x,t) = (T_t m)(x)$ of the deterministic Ginzburg-Landau equation solves the equation

$$\frac{\partial}{\partial t}(m - \bar{m}_{x_0}) = L_{x_0}(m - \bar{m}_{x_0}) - 3\bar{m}_{x_0}(m - \bar{m}_{x_0})^2 - (m - \bar{m}_{x_0})^3$$

We introduce now the concept of *linear center*, called in the sequel simply center, for a function $f \in \mathcal{C}^0(\mathbb{R})$

DEFINITION 2.2. *The point $\xi(m) \in \mathbb{R}$ is a linear center of $m \in \mathcal{C}^0(\mathbb{R})$ if*

$$\langle \bar{m}'_{\xi(m)}, m - \bar{m}_{\xi(m)} \rangle = 0$$

Existence and uniqueness of the center are stated in the next lemma (i.e. Proposition 3.2 of [**8**])

LEMMA 2.3. *There is a $\delta_0 > 0$ so that any $m \in \mathcal{M}_{\delta_0}$ has a unique linear center $\xi(m)$. Moreover there is $c_0 > 0$ so that if $m \in \mathcal{C}^0(\mathbb{R})$, $y_0 \in \mathbb{R}$ and*

$$\|m - \bar{m}_{y_0}\| = \delta \leq \delta_0$$

*then the linear center $\xi(m)$ is such that*

$$|\xi(m) - y_0| \leq c_0\delta, \tag{2.10}$$

$$\xi(m) - y_0 = -\Big[\frac{3}{4}\langle \bar{m}'_{y_0}, m - \bar{m}_{y_0}\rangle + \frac{9}{16}\langle \bar{m}'_{y_0}, m - \bar{m}_{y_0}\rangle\langle \bar{m}''_{y_0}, m - \bar{m}_{y_0}\rangle\Big]$$

$$+R(m-\bar m_{y_0})$$

*with*

$$|R(m-\bar m_{y_0})|\le C\|m-\bar m_{y_0}\|^3. \tag{2.11}$$

*Let $m$ and $\tilde m$ in $\mathcal{M}_{\delta_0}$, $\xi_0$, and $\tilde\xi_0$ their respective linear centers and $\|m-\tilde m\|\le\delta_0$. Then*

$$|\xi_0-\tilde\xi_0|\le\frac{c_0}{2}|\langle\bar m'_{\xi_0},m-\tilde m\rangle|\le\frac{c_0}{2}\int dx\,\bar m'_{\xi_0}\,|m-\tilde m| \tag{2.12}$$

Let us state now our last definition

$$\xi^\varepsilon(m)\doteq\begin{cases}\xi(m^\varepsilon(x)), & \text{if } m^\varepsilon\in\mathcal{M}_{\delta_0}\\ 0 & \text{otherwise}\end{cases} \tag{2.13}$$

which exists uniquely thanks to Lemma 2.3. Given any $\ell\in(0,1)$, $\delta\in(0,\delta_0]$ ($\delta_0$ as in Lemma 2.3) define

$$\mathcal{M}^\varepsilon_{\delta,\ell}=\{m\in\mathcal{C}(\mathbb{R}):\,m^\varepsilon\in\mathcal{M}_\delta,\,|\xi(m^\varepsilon)|\le(1-\ell)\varepsilon^{-1}\}$$

We are ready now to state our main result:

THEOREM 2.4. *Let $m_0\in\mathcal{C}_\varepsilon(\mathbb{R})$ such that for any $\eta>0$*

$$\lim_{\varepsilon\to0}\varepsilon^{-\frac12+\eta}\|m_0^\varepsilon(x)-\bar m_0(x)\|=0 \tag{2.14}$$

*Let $\lambda=\log\varepsilon^{-1}$ and $x_0=\xi^\varepsilon(m_0)$. Then, calling $m_t=T_t(m_0,\varepsilon)$,*

(1) *There exists a $\mathcal{F}_t$-adapted process $X_\varepsilon$ such that, for each $\tau,\eta>0$*

$$\lim_{\varepsilon\to0^+}\mathbb{P}(\sup_{t\in[0,\lambda\varepsilon^{-1}\tau]}\sup_{x\in\mathcal{T}_\varepsilon}|m_t-\bar m_{X_\varepsilon(t)}|)>\varepsilon^{\frac12-\eta})=0$$

*where $\mathbb{P}=\mathbb{P}^\varepsilon$ is the probability on the basic space, where the noise $\alpha$ and the process $m_t$ are constructed.*

(2) *The real process* $Y_\varepsilon(\theta) = X_\varepsilon(\varepsilon^{-1}\theta) - x_0$, $\theta \in \mathbb{R}_+$, *converges weakly in* $\mathcal{C}(\mathbb{R}_+)$ *as* $\varepsilon \to 0^+$, *to the unique strong solution* $Y$ *of the stochastic equation*

$$\begin{cases} dY(\theta) = D(Y,\theta)d\theta + db(\theta) \\ Y(0) = 0 \end{cases} \tag{2.15}$$

*where* $b$ *is a Brownian motion with diffusion coefficient* $3/4$ *and the drift is given by*

$$D(Y,\theta) \doteq -G(\theta)\langle \bar{m}'_Y, h\rangle$$

*where* $h$ *is defined in* (2.2)*, on the whole line, and* $G$ *in* (2.3)*. The function* $D$ *is periodic asymmetric and mean-zero .*

The equation (2.15) describes an On-Off molecular motor, which is a sample of brownian ratchet, see [**18**] for the exact definition. It is generally appreciated that, in accordance with the second law of thermodynamics, usable work cannot be extracted from equilibrium fluctuations. In the presence of nonequilibrium forces the situation changes drastically. Then, directed transport of Brownian particles in asymmetric periodic potentials (ratchets) can be induced by the application of nonthermal forces or with the help of deterministic, periodic coherent forces. Strictly speaking, a ratched system is a system that is able to transport particles in a periodic structure with nonzero macroscopic velocity although on average no macroscopic force is acting. These nonequilibrium models recently gained much interest in view of their role in describing the physics of molecular motors [**18**].

In an On-Off ratchet, the asymmetry is pull in the system by means of the asymmetric and periodic potential $h(x)$ which is switched on-off by the periodic force $G(t)$. A particle distribution which is initially located in a minimum of the potential will spread symmetrically by the brownian motion while the potential is switched off. When the

potential is switched on again, a net part of the distribution will settle in the minimum located to the right, if the minima of the potential are closer to their neighboring maxima to the right than to the left, otherwise into the negative direction. Hence, on average, there is a particle current flows to the right (or to the left). The only request is that the time $T_D$ during which the potential is on, it is sufficient to let the particle fall down into a minima but not long enough to let it escape from the basin in which is trapped.

## 2.2. Iterative construction

In this section we prove the first part of Theorem 2.4 and some of the key estimates to prove the second point. Let $m_{t_0} \in \mathcal{C}^0(\mathbb{R})$, set $m_t = T_t(m_0, \varepsilon)$, then, for any $\xi \in \mathbb{R}$, $v_t = m_t - \bar{m}_\xi$ solves the following integral version of the Ginzburg-Landau stochastic equation (see [**9, 8**])

$$\begin{aligned} v(t) \;&= g_{t-t_0,\xi}u_0 - \textstyle\int_{t_0}^t ds\, g_{t-s,\xi}(3\bar{m}_\xi v(s)^2 + v(s)^3) + \varepsilon \int_{t_0}^t ds\, g_{t-s,\xi}\hat{h}(\cdot)G(\varepsilon s) \\ &\quad + \sqrt{\varepsilon}\hat{Z}_{t-t_0,\xi} \end{aligned} \tag{2.16}$$

where, $g_{t-t_0,\xi}$ was defined in Section 2.1 and

$$\hat{Z}_{t-t_0,\xi} \doteq Z_{t-t_0} - \int_{t_0}^t ds\, g_{t-s,\xi}\big[(3\bar{m}_\xi^2 - 1)Z_{s-t_0}\big].$$

Note that the process $\hat{Z}_{t-t_0,\xi}$ is also given (see [**9**]) by the stochastic integral:

$$\hat{Z}_{t-t_0,\xi} = \int_{t_0}^t ds \int_{\mathcal{T}_\varepsilon} dy\, g^\varepsilon_{t-s,\xi}(x,y)\alpha(s,y)$$

where

$$g^\varepsilon_{t-s,\xi}(x,y) = \sum_{j\in\mathbb{Z}} \Big(g_{t-s,\xi}(x, y + 4j\varepsilon^{-1}) + g_{t-s,\xi}(x, 4j\varepsilon^{-1} + 2\varepsilon^{-1} - y)\Big)$$

Our aim is to analize $m_t$ as long as it stays in $\mathcal{M}^\varepsilon_{\delta,\ell}$ for any suitable $\ell \in (0,1)$. To this end we introduce an iterative procedure in which we

linearize the equation around $\bar{m}_x$ for a suitable $x$ recursively defined. First of all let we introduce the stopping time

$$\mathcal{S}_{\delta,\ell} = \inf\{t \in \mathbb{R}_+ : m_t \notin \mathcal{M}^{\varepsilon}_{\delta,\ell}\}. \tag{2.17}$$

Let $t_0 \in \mathbb{R}_+$ and $m(t)$, $t \geq 0$, the solution to equation (2.7) with initial condition $m_{t_0} \in \mathcal{C}_\varepsilon(\mathbb{R})$, satisfying $\lim_{\varepsilon\to 0} \varepsilon^{-\frac{1}{2}+\eta}\|m^{\varepsilon}_{t_0}(x) - \bar{m}_0(x)\| = 0$. By writing $T_t(m^{\varepsilon}_{t_0}, \varepsilon) = \bar{m}_\xi + v(t)$, $v(t)$ satisfies (2.16).

Consider now the partition $\mathbb{R}_+ = \bigcup_{n\geq 0}[T_n, T_{n+1})$ where $T_n = nT$, $n \in \mathbb{N}$, $T = \varepsilon^{-\frac{1}{10}}$. We next define, by induction on $n \geq 0$, reals $x_n$ and functions $v_n(t) = \{v_n(t,x), x \in \mathbb{R}\}$ , $t \in [T_n, T_{n+1}]$, which have the property that for any $t \in [T_n, T_{n+1}]$

$$T_{t\wedge\mathcal{S}_{\delta,\ell}}(m^{\varepsilon}(T_n \wedge \mathcal{S}_{\delta,\ell}), \varepsilon) = \bar{m}_{x_n} + v_n(t) \tag{2.18}$$

where $m^{\varepsilon}(T_n \wedge \mathcal{S}_{\delta,\ell}) = (m_{T_n\wedge\mathcal{S}_{\delta,\ell}}(x))^{\varepsilon}$. Let $t_0 = 0$, $m^{\varepsilon}_0 = m^{\varepsilon}(0)$, $x_0 = \xi^{\varepsilon}(m_0)$ and let $v_0(t)$ be the solution to (2.16) with initial data $v_0(0) = m^{\varepsilon}_0 - \bar{m}_{x_0}$, stopped at $\mathcal{S}_{\delta,\ell}$. Suppose now, by induction, that we have defined $x_{n-1}$ and $v_{n-1}$. We then define $x_n$ as the center of $m^{\varepsilon}(T_n \wedge \mathcal{S}_{\delta,\ell})$ (which exists by the definition of the stopping time $\mathcal{S}_{\delta,\ell}$) and $v_n(t)$, $t \in [T_n, T_{n+1}]$, as the solution to (2.16) with initial data $t_0 = T_n$, $\xi = x_n$ and $v_n(T_n) = m^{\varepsilon}(T_n \wedge \mathcal{S}_{\delta,\ell}) - \bar{m}_{x_n}$. We emphasize that in this construction the initial condition $v_n(T_n)$ is orthogonal to $\bar{m}'_{x_n}$, i.e.

$$\langle v_n(T_n), \bar{m}'_{x_n}\rangle = 0$$

We will use the representation (2.16) to prove in Proposition 2.5 below some a priori bounds on $v_n(t)$ and other quantities. We need first some notation. Given $\tau \in \mathbb{R}_+$, we let $n_\varepsilon(\tau) = [\varepsilon^{-1}\tau/T]$, remembering that $\lambda = \log\varepsilon^{-1}$, we define

$$V_n \doteq \sup_{t\in[T_n,T_{n+1}]} \|v_n(t)\|, \quad V_{n,*} = \sup_{k\leq n} V_k, \quad V_*(\tau) \doteq V_{n_\varepsilon(\lambda\tau),*} \tag{2.19}$$

$$\delta_*(\tau) \doteq \sup_{k\le n_\varepsilon(\lambda\tau)} |x_n - x_{n-1}| \tag{2.20}$$

and, calling $\hat{Z}_n(t) = \hat{Z}_{t-T_n,x_n}$, for $t \in [T_n, T_{n+1}]$,

$$Z_n \doteq \sup_{t\in[T_n,T_{n+1}]} \|\hat{Z}_n(t)\|, \quad Z_{n,*} = \sup_{k\le n} Z_k, \quad Z_*(\tau) \doteq Z_{n_\varepsilon(\lambda\tau),*} \tag{2.21}$$

Given $\eta > 0, \tau \in \mathbb{R}$, we define the event

$$\mathcal{B}^1_{\varepsilon,\tau,\eta} \doteq \Big\{ Z_*(\tau) \le \varepsilon^{-\eta}\sqrt{T} \Big\}. \tag{2.22}$$

By standard Gaussian estimate ([**3**] Appendix B) we have that for each $\eta, \tau, q > 0$ there is a constant $C = C(\eta, \tau, q) > 0$ such that for any $\varepsilon > 0$

$$\mathcal{P}(\mathcal{B}^1_{\varepsilon,\tau,\eta}) \ge 1 - C\varepsilon^q. \tag{2.23}$$

The next proposition contains the most important estimates we need to demostrate Theorem 2.4. In this section $C$ will denote a generic constant whose numerical value may change from line to line.

PROPOSITION 2.5. *Let $m_0 \in \mathcal{C}_\varepsilon(\mathbb{R})$ and $T = \varepsilon^{-\frac{1}{10}}$. Let $m_0^\varepsilon$ such that for any $\eta > 0$*

$$\lim_{\varepsilon\to 0} \varepsilon^{-\frac{1}{2}+\eta} \|m_0^\varepsilon(x) - \bar{m}_0(x)\| = 0 \tag{2.24}$$

*then there exists $\eta_0 > 0$ such that, for any $\eta \in (0, \eta_0)$, there is a constant $C = C(\tau, \eta)$ such that, for any $\varepsilon > 0$, on the set $\mathcal{B}^1_{\varepsilon,\tau,\eta}$*

$$V_*(\tau) \le \sqrt{T}\varepsilon^{\frac{1}{2}-2\eta} \text{ and } \delta_*(\tau) \le C\sqrt{T}\varepsilon^{\frac{1}{2}-\eta} \tag{2.25}$$

PROOF. First of all let us observe that, from (2.24) and Lemma 2.3, there exist $C > 0$ and $\ell \in (0, 1)$, such that $|x_0| \doteq |\xi(m_0^\varepsilon)| < C\varepsilon^{\frac{1}{2}-\eta} < (1-\ell)\varepsilon^{-1}$. As it will be more clear later, for our purpose, it is sufficient that $\ell$ is small enough that $C\varepsilon^{\frac{1}{2}-\eta} + \log \varepsilon^{-1} T^{-1/2}\varepsilon^{-1/2-\eta}\tau < (1-\ell)\varepsilon^{-1}$.

Choosing $\delta > \varepsilon^{\frac{1}{2}-\eta}$ we can define $S_{\delta,\ell}$, as in (2.17). From (2.19), the first of (2.25) follows once we prove that

$$V_n \leq \sqrt{T}\varepsilon^{\frac{1}{2}-2\eta} \quad \forall n \leq n_\varepsilon(\lambda\tau) \tag{2.26}$$

in the set $\mathcal{B}^1_{\varepsilon,\tau,\eta}$. Let us prove (2.26) by induction on $n$. Observe that by definition, for $t \in (\varepsilon^{-1}\lambda\tau \wedge S_{\delta,\ell}, \varepsilon^{-1}\lambda\tau]$, $v_n(t) = v_{[S_{\delta,\ell}/T]}(S_{\delta,\ell})$. For $n = 0$, we have $x_0 = \xi(m_0^\varepsilon)$, $T_0 = 0$ and, from (2.16), for any $t \leq T$

$$\|v_0(t)\| \leq C\, e^{-at}\varepsilon^{\frac{1}{2}-\eta} + \int_0^t ds\,(3\|v_0(s)\|^2 + \|v_0(s)\|^3) + C(1+t)\varepsilon + \sqrt{T}\varepsilon^{\frac{1}{2}-\eta} \tag{2.27}$$

in the set $\mathcal{B}^1_{\varepsilon,\tau,\eta}$. For the first term we use (2.9) and that $m_0 \in \mathcal{M}^\varepsilon_{\varepsilon^{1/2-\eta},\ell}$, for the third term we decompose $\int g_{t-s,x_0}\hat{h}(\cdot)G(\varepsilon s)ds$ into its parallel and its orthogonal component to $\bar{m}'_{x_0}$ and use again (2.9) and that $\|\hat{h}(x)G(\varepsilon s)\| \leq C$ for each $s$. Consider now the stopping time:

$$\beta \doteq \inf\{t \geq 0 : \|v_0(t)\| = \sqrt{T}\varepsilon^{\frac{1}{2}-2\eta}\} \tag{2.28}$$

and suppose that $\beta \leq T$, then, for $t \leq \beta$, equation (2.27) gives:

$$\begin{aligned}\sqrt{T}\varepsilon^{\frac{1}{2}-2\eta} &\leq C\varepsilon^{\frac{1}{2}-\eta} + 3C\beta(\sqrt{T}\varepsilon^{\frac{1}{2}-2\eta})^2 + C\beta(\sqrt{T}\varepsilon^{\frac{1}{2}-2\eta})^3 + C(\beta+1)\varepsilon \\ &\quad + \sqrt{T}\varepsilon^{\frac{1}{2}-\eta} = (\sqrt{T}\varepsilon^{\frac{1}{2}-2\eta})\big[CT^{-1/2}\varepsilon^\eta + 3C\beta\sqrt{T}\varepsilon^{\frac{1}{2}-2\eta} + C\beta T\varepsilon^{1-4\eta} \\ &\quad + C(\beta+1)T^{-\frac{1}{2}}\varepsilon^{\frac{1}{2}+2\eta} + \varepsilon^\eta\big]\end{aligned}$$

Remembering the definition of $T = \varepsilon^{-\frac{1}{10}}$, for $\eta_0 < \frac{1}{10}$ and $\varepsilon$ small enough, the quantity inside the square parenthesis is smaller than 1 and this leads to a contradiction. It follows that $\beta > T$ for $\varepsilon$ small enough. We have proved that, in $\mathcal{B}^1_{\varepsilon,\tau,\eta}$, $\sup_{0\leq t\leq T}\|v_0(t)\| < \sqrt{T}\varepsilon^{\frac{1}{2}-2\eta}$. Let now $t = T$,

$$\|v_0(T)\| \leq C\varepsilon^{\frac{1}{2}-\eta} + 3CT^2\varepsilon^{1-4\eta} + CT^{\frac{5}{2}}\varepsilon^{\frac{3}{2}-6\eta} + CT\varepsilon + C\varepsilon + \sqrt{T}\varepsilon^{\frac{1}{2}-\eta} \leq 2\sqrt{T}\varepsilon^{\frac{1}{2}-\eta}$$

for sufficiently small $\varepsilon$. Then $T_t(m_0^\varepsilon, \varepsilon)$ is in $\mathcal{M}_{\sqrt{T}\varepsilon^{1/2-2\eta}}$ for all $t \leq T$ and in $\mathcal{M}_{2\sqrt{T}\varepsilon^{1/2-\eta}}$ for $t = T$.

From the last inequality, calling $x_1^\varepsilon \doteq \xi(T_T(m_0^\varepsilon, \varepsilon))$, $|x_1^\varepsilon - x_0| \leq 2C\sqrt{T}\varepsilon^{\frac{1}{2}-\eta}$, therefore $|x_1^\varepsilon| \leq C\varepsilon^{\frac{1}{2}-\eta} + 2C\sqrt{T}\varepsilon^{\frac{1}{2}-\eta} < (1-\ell)\varepsilon^{-1}$, with the previous choice for $\ell$.

Finally we need to controll the position of the center $x_1 = \xi(m_T^\varepsilon)$. The key ingredients to this aim are the Barrier Lemma (Proposition 5.3 [**9**]), that works also for our equation, and the stability of $m \equiv 1$ (see Lemma A.2 in the Appendix of [**8**] which works also in our case with little modifications). In the set $\mathcal{B}^1_{\varepsilon,\tau,\eta}$ there are two positive constants $C$ and $V$ so that setting $L_\varepsilon \doteq \varepsilon^{-1} - VT$, with $m_t = T_t(m_0, \varepsilon)$,

$$\sup_{0\leq t\leq T}\sup_{|x|\leq L_\varepsilon} |m_t - T_t(m_0^\varepsilon, \varepsilon)| \leq Ce^{-T}. \tag{2.29}$$

Let next $x \in [L_\varepsilon, \varepsilon^{-1}]$ (the proof for $x \in [-\varepsilon^{-1}, -L_\varepsilon]$ is similar). Since $m_0 \in \mathcal{M}^\varepsilon_{\varepsilon^{1/2-\eta},\ell}$, using Lemma 2.3 and recalling that $\bar{m} = \tanh(x)$, we have, for any $\varepsilon > 0$ small enough,

$$\sup_{|x-\varepsilon^{-1}|\leq 2VT} |m_0^\varepsilon - 1| \leq C\varepsilon^{\frac{1}{2}-\eta} + 2e^{-(\ell\varepsilon^{-1}-2VT)}$$

Then, since $m_0 = m_0^\varepsilon$ for any $x \in [\varepsilon^{-1} - 2VT, \varepsilon^{-1}]$ and $m_0 \in \mathcal{C}^\varepsilon(\mathbb{R})$ there is a constant $C$ such that, for any $\varepsilon > 0$ small enough

$$\sup_{|x-\varepsilon^{-1}|\leq 2VT} |m_0 - 1| \leq C \tag{2.30}$$

Recalling that $m_0 \in \mathcal{C}^\varepsilon(\mathbb{R})$, we define $\hat{m}_0 \in \mathcal{C}(\mathbb{R})$ as

$$\hat{m}_0(x) = \begin{cases} m_0(x), & \text{if } |x-\varepsilon^{-1}| \leq 2VT \\ m_0(\varepsilon^{-1} - 2VT), & \text{if } x \leq \varepsilon^{-1} - 2VT \\ m_0(\varepsilon^{-1} + 2VT), & \text{if } x \geq \varepsilon^{-1} + 2VT \end{cases} \tag{2.31}$$

Using again the Barrier Lemma there is a $C > 0$ so that in $\mathcal{B}^1_{\varepsilon,\tau,\eta}$

$$\sup_{0\leq t\leq T}\sup_{L_\varepsilon\leq x\leq\varepsilon^{-1}} |m_t - T_t(\hat{m}_0, \varepsilon)| \leq Ce^{-T}. \tag{2.32}$$

Since $m \equiv 1$ is stable there is a constant $C > 0$ so that in $\mathcal{B}^1_{\varepsilon,\tau,\eta}$ for any $t \in [0,T]$

$$\|T_t(\hat{m}_0,\varepsilon) - 1\| \leq C[e^{-t} + \sqrt{T}\varepsilon^{\frac{1}{2}-\eta} + C(1+T)\varepsilon]. \tag{2.33}$$

By (2.29), (2.32), (2.33) there is a $C > 0$ so that $m^\varepsilon_t = (m_t)^\varepsilon$ is in $\mathcal{M}_{C\sqrt{T}\varepsilon^{1/2-2\eta}}$ for all $t \leq T$ and in $\mathcal{M}_{2C\sqrt{T}\varepsilon^{1/2-\eta}}$ for $t = T$. From (2.29), (2.33) and Lemma 2.3 we have

$$\|m^\varepsilon_T - T_T(m^\varepsilon_0,\varepsilon)\| \leq 2C\sqrt{T}\varepsilon^{1/2-\eta}, \tag{2.34}$$

therefore, remembering that, in our definition, $x_1 \doteq \xi(m^\varepsilon_T)$ and $x^\varepsilon_1 \doteq \xi(T_T(m^\varepsilon_0,\varepsilon))$

$$|x_1 - x_0| \leq |x_1 - x^\varepsilon_1| + |x^\varepsilon_1 - x_0| \leq 2C\sqrt{T}\varepsilon^{1/2-\eta}, \tag{2.35}$$

it follows that $|x_1| < C\varepsilon^{1/2-\eta} + 2C\sqrt{T}\varepsilon^{1/2-\eta}$ and once again $|x_1| \leq (1-\ell)\varepsilon^{-1}$.

By this way we have finished the proof for $n = 0$. Let us then suppose that for inductive hypothesis it is valid for $n$, and prove that it holds for $n+1$. For $t \in [T_{n+1}, T_{n+2}]$

$$v_{n+1}(t) = g_{t-T_{n+1},x_{n+1}} v_{n+1}(T_{n+1}) + \int_{T_n}^t ds\, g_{t-s,x_{n+1}}(3v_{n+1}(s)^2 + v_{n+1}(s)^3) \tag{2.36}$$

$$+ \varepsilon \int_{T_n}^t ds\, g_{t-s,x_{n+1}} \hat{h}(\cdot) G(\varepsilon s) + \sqrt{\varepsilon}\hat{Z}_{n+1}(t)$$

We have to deal with the first term $g_{t-T_{n+1},x_{n+1}} v_{n+1}(T_{n+1})$. By definition, $v_{n+1}(T_{n+1}) \perp \bar{m}_{x_{n+1}}$, therefore we can use (2.9). To this aim we need an appropriate estimate for $\|v_{n+1}(T_{n+1})\|$, using the inductive hypotesis and working as in (2.34), (2.35),

$$\|v_{n+1}(T_{n+1})\| \leq \|m^\varepsilon_{T_{n+1}} - T_T(m^\varepsilon_{T_n},\varepsilon)\| + \|T_T(m^\varepsilon_{T_n},\varepsilon) - \bar{m}_{x_n}\| \tag{2.37}$$

$$+ \|\bar{m}_{x_n} - \bar{m}_{x_{n+1}}\| \leq C\sqrt{T}\varepsilon^{1/2-\eta}$$

taking into account (2.36),(2.37), a reason similar to that leading to the estimate for $n = 0$ yelds $V_{n+1} \leq \sqrt{T}\varepsilon^{1/2-2\eta}$. Having proved this, we have that from (2.36), on the set $\mathcal{B}^1_{\varepsilon,\tau,\eta}$

$$\|v_{n+1}(T_{n+2})\| \leq 2\sqrt{T}\varepsilon^{1/2-\eta}. \tag{2.38}$$

where we used (2.9). Working in the same way that for $n = 0$ we have $m^\varepsilon_t \in \mathcal{M}_{C\sqrt{T}\varepsilon^{1/2-2\eta}}$ for all $t \in [T_{n+1}, T_{n+2}]$ and $m^\varepsilon_{T_{n+2}} \in \mathcal{M}_{C\sqrt{T}\varepsilon^{1/2-\eta}}$, for an appropriate choice of $C$. So the first estimate of (2.25) is proved. Furthermore, similarly to (2.35) we can prove that $|x_{n+1} - x_n| \leq C\sqrt{T}\varepsilon^{1/2-\eta}$. For inductive hypothesis, $|x_{n+1}| \leq |x_0| + nC\sqrt{T}\varepsilon^{1/2-\eta}$. Observe that for any $n < n_\varepsilon(\lambda\tau)$, $nC\sqrt{T}\varepsilon^{1/2-\eta} < \log \varepsilon^{-1}T^{-1/2}\varepsilon^{-1/2-\eta}\tau << \varepsilon^{-1}$, therefore $|x_{n+1}| << \varepsilon^{-1}$, in particular $|x_{n+1}| \leq (1-\ell)\varepsilon^{-1}$. By this way it is proved also the second estimate of (2.25). □

We are going to prove that the component of $v_n(T_{n+1})$ orthogonal to $\bar m'_{x_n}$ is bounded by $C\varepsilon^{1/2-2\eta}$, thus considerably improving the bound on the full $v_n(T_{n+1})$ just obtained. Let

$$g^\perp_{t,n} \doteq g_{t,n}\big(1 - \frac{3}{4}|\bar m'_{x_n}\rangle\langle \bar m'_{x_n}|\big)$$

the operator whose kernel is

$$g^\perp_{t,n}(x,y) = g_{t,n}(x,y) - \frac{3}{4}\bar m'_{x_n}(x)\bar m'_{x_n}(y) \tag{2.39}$$

The superscribe $\perp$ recalls the $L_2$-orthogonality w.r.t. the eigenvector $\bar m'_{x_n}$ of $g_{t,n}$, i.e. $g_{t,n}\bar m'_{x_n} = \bar m'_{x_n}$. It follows from (2.9) that there are constants $a > 0$ and $C < \infty$ so that, for any $\phi \in \mathcal{C}^0(\mathbb{R})$

$$\|g^\perp_{t,n}\phi\| \leq Ce^{-at}\|\phi\| \tag{2.40}$$

Let also

$$\hat Z^\perp_n(t) \doteq \hat Z_n(t) - \frac{3}{4}\langle \bar m'_{x_n}, \hat Z_n(t)\rangle \bar m'_{x_n} \tag{2.41}$$

be the component of $\hat{Z}_n(t)$ orthogonal to $\bar{m}'_{x_n}$, and

$$\mathcal{B}^2_{\varepsilon,\tau,\eta} \doteq \Big\{ \sup_{0\le n\le n_\varepsilon(\lambda\tau)} \sup_{t\in[T_n,T_{n+1}]} \|\hat{Z}^\perp_n(t)\| \le \varepsilon^{-\eta} \Big\} \tag{2.42}$$

with standard Gaussian estimate (see Appendix B [**3**]) we have that for each $\eta,\tau,q>0$ there is a constant $C=C(\eta,\tau,q)>0$ such that for any $\varepsilon>0$

$$\mathcal{P}(\mathcal{B}^2_{\varepsilon,\tau,\eta}) \ge 1 - C\varepsilon^q. \tag{2.43}$$

Define now

$$v^\perp_n(T_{n+1}) \doteq v_n(T_{n+1}) - \frac{3}{4}\langle \bar{m}'_{x_n}, v_n(T_{n+1})\rangle \bar{m}'_{x_n}$$
$$V^\perp_*(\tau) \doteq \sup_{0\le n\le n_\varepsilon(\lambda\tau)} \|v^\perp_n(T_{n+1})\|. \tag{2.44}$$

Let $f\in\mathcal{C}(\mathbb{R})$, $\varepsilon>0$, $x$ and $y\in\mathbb{R}$, we set

$$\|f\|_{\varepsilon,n} \doteq \sup_{|x-x_n|<\varepsilon^{-\frac{1}{10}}} |f(x)|. \tag{2.45}$$

With the same assumptions on $m_0$ of Proposition 2.5, we have

PROPOSITION 2.6. *Recalling* (2.22) *and* (2.42), *set*

$$\mathcal{B}_{\varepsilon,\tau,\eta} \doteq \mathcal{B}^1_{\varepsilon,\tau,\eta} \cap \mathcal{B}^2_{\varepsilon,\tau,\eta} \tag{2.46}$$

*by* (2.23) *and* (2.43), *for each* $\eta,\tau,q>0$ *there is a constant* $C=C(\eta,\tau,q)>0$ *such that for any* $\varepsilon>0$

$$\mathcal{P}(\mathcal{B}_{\varepsilon,\tau,\eta}) \ge 1 - C\varepsilon^q. \tag{2.47}$$

*Let* $n_{\varepsilon,\delta,\ell}(\tau) = [(\varepsilon^{-1}\tau \wedge S_{\delta,\ell})/T]$. *Then, for each* $\tau,\eta>0$ *there is a constant* $C=C(\tau,\eta)$ *such that, for any* $\varepsilon>0$,

$$V^\perp_*(\tau) \le C\varepsilon^{\frac{1}{2}-2\eta}, \quad \sup_{0\le n<n_{\varepsilon,\delta,\ell}(\lambda\tau)} \|v_n(T_n)\|_{\varepsilon,n} \le C\varepsilon^{\frac{1}{2}-2\eta}, \tag{2.48}$$

*on the set* $\mathcal{B}_{\varepsilon,\tau,\eta}$ *and*

$$\sup_{0\le n<n_{\varepsilon,\delta,\ell}(\lambda\tau)} |x_{n+1} - (x_0 - \frac{3}{4}\sum_{k=0}^{n}\langle \bar{m}'_{x_k}, v_k(T_{k+1})\rangle)| \le C\lambda\, T^{-1/2}\varepsilon^{-4\eta}, \tag{2.49}$$

*on the set* $\mathcal{B}_{\varepsilon,\tau,\eta}$.

PROOF. Let us consider first the term $V_*^\perp(\tau)$. Shortanding by $R_n$ the sum of all terms those compose $v_n$ except for $\sqrt{\varepsilon}\hat{Z}_n(T_{n+1})$ and calling $R_n^\perp$ its orthogonal projection, we have

$$v_n^\perp(T_{n+1}) = R_n^\perp + \sqrt{\varepsilon}\hat{Z}_n^\perp(T_{n+1}). \tag{2.50}$$

The first term is bounded by

$$\|R_n^\perp\| \le C\big[e^{-aT}V_* + TV_*^2 + TV_*^3 + (1+T)\varepsilon\big] \tag{2.51}$$

as it follows by the estimations done in Proposition 2.5. Therefore by (2.42), (2.51) and the first of (2.25)

$$\|v_n^\perp(T_{n+1})\| \le C\varepsilon^{\frac{1}{2}-2\eta} \tag{2.52}$$

for $\varepsilon > 0$ small enough, for each $n \le n_\varepsilon(\lambda\tau)$. For reasons that will be clear later we prefer to demonstrate before (2.49) than the estimate on $v_n(T_n)$. To this aim we need to refine some estimation done in Proposition 2.5. Thanks to Lemma 2.3 we know that:

$$\begin{aligned} x_n = x_0 + \sum_{k=0}^{n-1}(x_{k+1}-x_k) = x_0 + \sum_{k=0}^{n-1}\Big[ &-\frac{3}{4}\langle \bar{m}'_{x_k}, v_k(T_{k+1})\rangle \\ &-\frac{9}{16}\langle \bar{m}'_{x_k}, v_k(T_{k+1})\rangle\langle \bar{m}''_{x_k}, v_k(T_{k+1})\rangle + R(v_k(T_{k+1})) + (x_{k+1}-x_{k+1}^\varepsilon)\Big] \end{aligned} \tag{2.53}$$

where $x_{k+1}^\varepsilon = \xi(T_T(m_{T_k}^\varepsilon))$ and $R(v_k(T_{k+1}))$ is as in (2.11). From (2.53) it follows that:

$$\sup_{n\le n_{\varepsilon,\delta,\ell}(\lambda\tau)} |x_n - x_0 + \frac{3}{4}\sum_{k=0}^{n-1}\langle \bar{m}'_{x_k}, v_k(T_{k+1})\rangle| \le n_{\varepsilon,\delta,\ell}(\lambda\tau) \sup_{n<n_{\varepsilon,\delta,\ell}(\lambda\tau)} \tag{2.54}$$

$$\Big[\frac{9}{16}\langle \bar{m}'_{x_n}, v_n(T_{n+1})\rangle\langle \bar{m}''_{x_n}, v_n(T_{n+1})\rangle + \|R(v_n(T_{n+1}))\| + |x_{n+1}-x_{n+1}^\varepsilon|\Big]$$

By its definition

$$\sup_{n\leq n_{\varepsilon,\delta,\ell}(\lambda\tau)} \|R(v_n(T_{n+1}))\| \leq CV_*(\tau)^3 \tag{2.55}$$

and since $\|\bar{m}'\|_1 = 2$, we have $\langle \bar{m}'_{x_n}, v_n(T_{n+1})\rangle \leq 2V_*(\tau)$; furthermore, by $\langle \bar{m}', \bar{m}''\rangle = 0$, $\langle \bar{m}''_{x_n}, v_n(T_{n+1})\rangle \leq CV_*^{\perp}(\tau)$. The last term requires more attention. We need to refine the estimation done in 2.5. Actually, we know from (2.12) that:

$$|x_{n+1} - x^{\varepsilon}_{n+1}| \leq \int dx\, \bar{m}'_{x_{n+1}}(x)\big|m^{\varepsilon}_{T_{n+1}}(x) - T_T(m^{\varepsilon}_{T_n}(x),\varepsilon)\big| \tag{2.56}$$

To make a better estimation, let us use Barrier Lemma, there exists a $V > 0$ such that for $L_\varepsilon = \varepsilon^{-1} - VT$

$$\sup_{|x|\leq L_\varepsilon} |m^{\varepsilon}_{T_{n+1}}(x) - T_T(m^{\varepsilon}_{T_n}(x),\varepsilon)| \leq Ce^{-T}. \tag{2.57}$$

by splitting the integral in (2.56) into two parts with, respectively $|x| > L_\varepsilon$ and $|x| \leq L_\varepsilon$, using the explicit form of $\bar{m}'$, and using that $|x_{n+1}| \leq (1-\ell)\varepsilon^{-1}$ with $\ell \in (0,1)$, for $n < n_{\varepsilon,\delta,\ell}(\lambda\tau)$, such shown in the Proposition 2.5, we have that for any $N > 0$ there exists $\varepsilon_0 > 0$ such that for any $\varepsilon < \varepsilon_0$

$$|x_{n+1} - x^{\varepsilon}_{n+1}| \leq Ce^{-T} + e^{-(\ell\varepsilon^{-1}-VT)} \sup_{x\in\mathbb{R}} \left[m^{\varepsilon}_{T_{n+1}}(x) - T_T(m^{\varepsilon}_{T_n}(x),\varepsilon)\right] \leq \varepsilon^N, \tag{2.58}$$

therefore:

$$\sup_{n\leq n_{\varepsilon,\delta,\ell}(\lambda\tau)} |x_n - x_0 + \frac{3}{4}\sum_{k=0}^{n-1} \langle \bar{m}'_{x_k}, v_k(T_{k+1})\rangle| \leq C\lambda\tau T^{-\frac{1}{2}}\varepsilon^{-4\eta} \tag{2.59}$$

Consider now $v_n(T_n)$. Observe that:

$$\begin{aligned} v_n(T_n) &= m^{\varepsilon}_{T_n} - \bar{m}_{x_n} = v_{n-1}(T_n) + \bar{m}_{x_{n-1}} - \bar{m}_{x_n} + (m^{\varepsilon}_{T_n}(x) - T_T(m^{\varepsilon}_{T_{n-1}}(x))) \\ &= v^{\perp}_{n-1}(T_n) + \big[\frac{3}{4}\langle \bar{m}'_{x_{n-1}}, v_{n-1}(T_n)\rangle \bar{m}'_{x_{n-1}} - (\bar{m}_{x_n} - \bar{m}_{x_{n-1}}) \\ &\quad + (m^{\varepsilon}_{T_n}(x) - T_T(m^{\varepsilon}_{T_{n-1}}(x)))\big] \end{aligned} \tag{2.60}$$

now, using Taylor expansion,

$$\bar{m}_{x_n} - \bar{m}_{x_{n-1}} = -\bar{m}'_{x_{n-1}}(x_n - x_{n-1}) + \frac{1}{2}\bar{m}''_{x_{n-1}}(x_n - x_{n-1})^2 - \frac{1}{6}\bar{m}'''_{x_{n-1}}(x_n - x_{n-1})^3 + \alpha_{n-1}(x_n - x_{n-1})^4 \qquad (2.61)$$

where $\alpha_{n-1}$ is bounded. Thus by Lemma 2.3, using $x_n - x_{n-1} = (x_n^\varepsilon - x_{n-1}) + (x_n - x_n^\varepsilon)$ and recalling that

$$x_n^\varepsilon - x_{n-1} = -\tfrac{3}{4}\langle \bar{m}'_{x_{n-1}}, v_{n-1}(T_n)\rangle - \tfrac{9}{16}\langle \bar{m}'_{x_{n-1}}, v_{n-1}(T_n)\rangle\langle \bar{m}''_{x_{n-1}}, v_{n-1}(T_n)\rangle + R(v_{n-1}(T_n))$$

$$\bar{m}_{x_n} - \bar{m}_{x_{n-1}} = \frac{3}{4}\langle \bar{m}'_{x_{n-1}}, v_{n-1}(T_n)\rangle \bar{m}'_{x_{n-1}} - (x_n - x_n^\varepsilon)\bar{m}'_{x_{n-1}} + \alpha_n \qquad (2.62)$$

where

$$\alpha_n = \frac{1}{2}\bar{m}''_{x_{n-1}}(x_n - x_{n-1})^2 - \frac{1}{6}\bar{m}'''_{x_{n-1}}(x_n - x_{n-1})^3 + \alpha_{n-1}(x_n - x_{n-1})^4 + \bar{m}'_{x_{n-1}}\Big\{\frac{9}{16}\langle \bar{m}'_{x_{n-1}}, v_{n-1}(T_n)\rangle\langle \bar{m}''_{x_{n-1}}, v_{n-1}(T_n)\rangle - R(v_{n-1}(T_n))\Big\} \qquad (2.63)$$

from (2.60),(2.61)

$$v_n(T_n) = v_{n-1}^\perp(T_n) + \big[(m^\varepsilon_{T_n}(x) - T_T(m^\varepsilon_{T_{n-1}}(x))) - (x_n - x_n^\varepsilon)\bar{m}'_{x_{n-1}} + \alpha_n\big]$$

Note that from (2.25), in $\mathcal{B}_{\varepsilon,\tau,\eta}$, we have $\sup_{n\le n_\varepsilon(\lambda\tau)} |x_n - x_{n-1}| \le C\sqrt{T}\varepsilon^{\frac{1}{2}-\eta}$ therefore we have $|\alpha_n| \le CT\varepsilon^{1-2\eta}$. Now for each $n \le n_\varepsilon(\lambda\tau)$

$$\|v_n(T_n)\|_{\varepsilon,n} < \| v_{n-1}^\perp(T_n) \| + |x_n - x_n^\varepsilon| + |\alpha_n| + \|m^\varepsilon_{T_n}(x) - T_T(m^\varepsilon_{T_{n-1}}(x))\|_{\varepsilon,n} \qquad (2.64)$$

Let us estimate last term

$$\|m^\varepsilon_{T_n} - T_T(m^\varepsilon_{T_{n-1}})\|_{\varepsilon,n} \le \|m^\varepsilon_{T_n} - m_{T_n}\|_{\varepsilon,n} + \|m_{T_n} - T_T(m^\varepsilon_{T_{n-1}})\|_{\varepsilon,n}$$

using that for each $n \le n_{\varepsilon,\delta,\ell}(\lambda\tau)$ $|x_n| < (1-\ell)\varepsilon^{-1}$ and by the definition of $m^\varepsilon_{T_n}$, the first term above is identically zero. For the second let we use again the Barrier Lemma. Since $m^\varepsilon_{T_n} = m_{T_n}$ for $|x| < \varepsilon^{-1}$ we know that there exists a $V > 0$ such that $\sup_{|x|\le\varepsilon^{-1}-VT} |m_{T_n}(x) - T_T(m^\varepsilon_{T_{n-1}}(x))| \le$

$Ce^{-T}$. The proof is now concluded by choosing appropriately $V$ in such a way that $\{|x - x_n| < \varepsilon^{-1/10}\} \subset \{|x| \leq \varepsilon^{-1} - VT\}$ that is always possible for each $n \leq n_{\varepsilon,\delta,\ell}(\lambda\tau)$. It follows, by (2.64), that

$$\sup_{0\leq n\leq n_{\varepsilon,\delta,\ell}(\lambda\tau)} \|v_n(T_n)\|_{\varepsilon,n} < \sup_{0\leq n\leq n_{\varepsilon,\delta,\ell}(\lambda\tau)} \| \, v_{n-1}^{\perp}(T_n) \, \| \leq \varepsilon^{\frac{1}{2}-2\eta}$$

□

## 2.3. Recursive equation for the center

We define

$$\xi_{n+1} \doteq x_0 - \frac{3}{4} \sum_{k=0}^{n\wedge[S_{\delta,\ell}/T]} \langle \bar{m}'_{x_k}, v_k(T_{k+1})\rangle, \quad \xi_0 \doteq x_0, \tag{2.65}$$

$$\sigma_n \doteq -\frac{3}{4}\sqrt{\varepsilon}\langle \bar{m}'_{x_n}, \hat{Z}_n(T_{n+1})\rangle, \tag{2.66}$$

$$F_n \doteq \frac{3}{4}\varepsilon \int_{T_n}^{T_{n+1}} dt \, \langle \bar{m}'_{x_n}, 3\bar{m}_{x_n}\hat{Z}_n^2(t)\rangle, \tag{2.67}$$

and

$$h_n \doteq -\frac{3}{4}\varepsilon\langle \bar{m}'_{\xi_n}, \hat{h}\rangle \int_{T_n}^{T_{n+1}} dt \, G(\varepsilon t). \tag{2.68}$$

$\xi_{n+1}$, thanks to (2.11), is a linear approximation to the center $x_{n+1}$, for $n < [S_{\delta,\ell}/T]$. Moreover, conditionally to the centers $x_0, x_1, \ldots, x_n$, the random variables $\sigma_0, \sigma_1, \ldots, \sigma_n$ are indipendent Gaussian with mean zero and variance $\frac{3}{4}\varepsilon T(1 + o(1))$. We want to identify a recursive equation satisfied by $\xi_n$.

PROPOSITION 2.7. *For any $n < [S_{\delta,\ell}/T]$ we have*

$$\xi_{n+1} - \xi_n = \sigma_n + h_n + F_n + R_n \tag{2.69}$$

*where for any $\tau \in \mathbb{R}_+$ there exist $\eta_0, q > 0$ such that for any $\eta \in (0, \eta_0)$, on the event $B_{\varepsilon,\tau,\eta}$,*

$$\sup_{n<[S_{\delta,\ell}/T]} |R_n| \leq \varepsilon T\lambda^{-1}\varepsilon^q \tag{2.70}$$

*for any $\varepsilon$ small enough. Moreover, for any $\tau \in \mathbb{R}_+$ there exists $q > 0$ such that*

$$\lim_{\varepsilon\to 0}( \sup_{n<n_\varepsilon(\lambda\tau)} \Big| \sum_{k=0}^{n} F_k \Big| > \varepsilon^q) = 0. \tag{2.71}$$

The idea is the following. The component $\sigma_n$ will give rise to the Brownian motion, while the term $h_n$ will give the deterministic drift. The remainders, $R_n, F_n$, are respectively deterministically and stochastically negligible.

First of all, we decompose $v_n$ into five terms

$$v_n(t) = \Gamma_{0,n}(t) + \Gamma_{1,n}(t) + \Gamma_{2,n}(t) + \Gamma_{h,n}(t) + \Gamma_{z,n}(t) \tag{2.72}$$

where

$$\begin{aligned}
\Gamma_{0,n}(t) &\doteq g_{t-T_n,x_n} v_n(T_n) \\
\Gamma_{1,n}(t) &\doteq -3 \int_{T_n}^{t} ds\, g_{t-s,x_n}(\bar{m}_{x_n} v_n^2(s)) \\
\Gamma_{2,n}(t) &\doteq - \int_{T_n}^{t} ds\, g_{t-s,x_n}(v_n^3(s)) \\
\Gamma_{h,n}(t) &\doteq \varepsilon \int_{T_n}^{t} ds\, g_{t-s,x_n}(\hat{h}(\cdot) G(\varepsilon s)) \\
\Gamma_{z,n}(t) &\doteq \sqrt{\varepsilon}\hat{Z}_n(t)
\end{aligned} \tag{2.73}$$

Define now, for $i = 0, 1, 2, h, z$

$$R_{i,n} \doteq -\frac{3}{4}\langle \bar{m}'_{x_n}, \Gamma_{i,n}(T_{n+1})\rangle, \tag{2.74}$$

(in particular $R_{z,n} = \sigma_n$) and set

$$\tilde{R}_{h,n} \doteq R_{h,n} + \frac{3}{4}\varepsilon\langle \bar{m}'_{\xi_n}, \hat{h}\rangle \int_{T_n}^{T_{n+1}} dt\, G(\varepsilon t) \tag{2.75}$$

as the rest associated to $\Gamma_{h,n}$. For $i = 0, 1, h$, the terms $R_{i,n}$ do not contribute to the limiting equation for $\xi_n$, since $n \leq (\varepsilon T)^{-1}\lambda\tau$, as we will proof. Clearly $\sigma_n$ is not negligible because its typical magnitude is $\sqrt{\varepsilon T}$. It will be examined in the next section, where we shall see that,

summed over $n$ it gives a finite contribution because of cancellations related to its martingale nature. The last term $R_{1,n}$ is not small enough to be directely negligible even if it is smaller than the priori bound $\sqrt{T}\varepsilon^{1/2-2\eta}$. Let us prove Proposition 2.7.

PROOF. Using the notation just introduced, we are going to demonstrate (2.70) and (2.71). Observe that $R_{0,n}$ is identically zero, since $v_n(T_n) \perp \bar{m}'_{x_n}$, $g$ is self-adjoint and $g_{T,x_n}\bar{m}'_{x_n} = \bar{m}'_{x_n}$. For $i = h$

$$\begin{aligned}\left|\tilde{R}_{h,n}\right| &\leq \left|\frac{3}{4}\varepsilon\int_{T_n}^{T_{n+1}} dt\, G(\varepsilon t)\langle \bar{m}'_{\xi_n} - \bar{m}'_{x_n}, \hat{h}\rangle\right| \\ &\leq \frac{3}{4}C\varepsilon T|\langle \bar{m}'_{\xi_n} - \bar{m}'_{x_n}, \hat{h}\rangle| \leq CK\lambda T^{\frac{1}{2}}\varepsilon^{1-4\eta} \end{aligned} \tag{2.76}$$

where we used, as it is simple to show, that $y \mapsto \langle \bar{m}'_y, \hat{h}\rangle$ is globally Lipschitz with a costant $K$ and (2.49). Therefore $\tilde{R}_{h,n}$ is negligible. It is straightforward to see that $|R_{2,n}| \leq CTV_*^3$ so it is negligible too. The last term we have to controll is $R_{1,n}$. We divide it into a component deterministically small and the component stochastically small $F_n$. Define

$$\begin{aligned}\tilde{R}_{1,n} \doteq R_{1,n} - F_n &= \frac{9}{4}\int_{T_n}^{T_{n+1}} ds\langle \bar{m}'_{x_n},\, g_{t-T_n,x_n}\bar{m}_{x_n}v_n^2(s)\rangle - F_n \\ &= \frac{9}{4}\int_{T_n}^{T_{n+1}} ds\langle \bar{m}'_{x_n}, \bar{m}_{x_n}(v_n(s) - \sqrt{\varepsilon}\hat{Z}_n(s))(v_n(s) + \sqrt{\varepsilon}\hat{Z}_n(s))\rangle \end{aligned} \tag{2.77}$$

We decompose $[T_n, T_{n+1}] = [T_n, T_n + \log^2 T] \cup [T_n + \log^2 T, T_{n+1}]$ and estimate separately the two time integrals. For the first one

$$\begin{aligned}
&\Big| \int_{T_n}^{T_n+\log^2 T} ds \langle \bar{m}'_{x_n}, \bar{m}_{x_n}(v_n(s) - \sqrt{\varepsilon}\hat{Z}_n(s))(v_n(s) + \sqrt{\varepsilon}\hat{Z}_n(s))\rangle \Big| \\
&\leq V_*(\tau) \Big| \int_{T_n}^{T_n+\log^2 T} ds \langle \bar{m}'_{x_n}, v_n(s) - \sqrt{\varepsilon}\hat{Z}_n(s)\rangle \Big| \\
&\leq V_*(\tau) \Big| \int_{T_n}^{T_n+\log^2 T} ds \Big\{ \int_{|x-x_n|<\varepsilon^{-1/10}} dx \bar{m}'_{x_n}(x)(v_n(s) - \sqrt{\varepsilon}\hat{Z}_n(s))(x) \\
&+ \int_{|x-x_n|\geq\varepsilon^{-1/10}} dx \bar{m}'_{x_n}(x)(v_n(s) - \sqrt{\varepsilon}\hat{Z}_n(s))(x) \Big\} \Big| \\
&\leq V_*(\tau) \Big[ \log^2 T \Big( \|v_n(T_n)\|_{\varepsilon,n} + e^{-\varepsilon^{-1/10}} \|v_n(T_n)\| \Big) \Big] \\
&\leq V_*(\tau) \log^2 T (\varepsilon^{\frac{1}{2}-2\eta} + e^{-\varepsilon^{-\frac{1}{10}}} \sqrt{T} \varepsilon^{\frac{1}{2}-2\eta}) \\
&\leq \sqrt{T} \log^2 T \varepsilon^{1-4\eta}
\end{aligned}$$

where we used the second of (2.48). To bound the second integral we write, by the recursive expression of $v_n$,

$$v_n(t) - \sqrt{\varepsilon}\hat{Z}_n(t) = g^{\perp}_{t-T_n} v_n(T_n) + D_n(t)$$

where $\sup_{t\in[T_n+\log^2 T, T_{n+1}]} \|D_n(t)\| \leq CTV_*^2 \leq CT^2\varepsilon^{1-4\eta}$, while

$$\sup_{t\in[T_n+\log^2 T, T_{n+1}]} \|g^{\perp}_{t-T_n} v_n(T_n)\| \leq Ce^{-a\log^2 T} V_*(\tau)$$

therefore

$$\begin{aligned}
&\Big| \int_{T_n+\log^2 T}^{T_{n+1}} ds \langle \bar{m}'_{x_n}, \bar{m}_{x_n}(v_n(s) - \sqrt{\varepsilon}\hat{Z}_n(s))(v_n(s) + \sqrt{\varepsilon}\hat{Z}_n(s))\rangle \Big| \\
&\leq CT^{\frac{7}{2}} \varepsilon^{\frac{3}{2}-6\eta}
\end{aligned}$$

putting together all the above bounds it follows that $\tilde{R}_{1,n}$ is negligible. This concludes the proof of (2.70).

We are left with the proof of (2.71). By the Doob decomposition:

$$\sum_{k=0}^{n-1} F_k = M_n - \sum_{k=0}^{n-1} \gamma_k$$

where

$$\gamma_k \doteq \mathbb{E}(F_k|\mathcal{F}_{T_k})$$

and $M_n$ is an $\mathcal{F}_{T_n}$-martingale with bracket

$$\langle M\rangle_n = \sum_{k=0}^{n-1} \big\{\mathbb{E}(F_k^2|\mathcal{F}_{T_k}) - \gamma_k^2\big\}.$$

Actually $\gamma_k \equiv 0$, therefore $\sum_{k=0}^{n-1} F_k = M_n$. In fact, using that $\mathbb{E}(\hat{Z}_k(t,x)|\mathcal{F}_{T_k}) = \int_{T_k}^t ds\, g_{2(t-s),x_k}(x,x)$, for each $(t,x) \in [T_k, T_{k+1}] \times \mathbb{R}$

$$\gamma_k = -\frac{9}{4}\varepsilon \int_{T_k}^{T_{k+1}} dt \int_{T_k}^t ds \int dx \int dy\, \bar{m}'_{x_k}(x)\bar{m}_{x_k}(x) g^2_{t-s,x_k}(x,y) = 0$$

where we exploited the identity

$$\int dx \int dy\, \bar{m}'_{x_k}\bar{m}_{x_k} g^2_{t-s,x_k}(x,y) = \int dx\, \bar{m}'_{x_k}(x)\bar{m}_{x_k}(x) g_{2(t-s),x_k}(x,x) = 0$$

which holds because $x \mapsto g_t(x,x)$ is an even function of $x$. Once proved $\gamma_k = 0$ we are left with the bound of the martingale $M_n$. Given $q > 0$, by Doob's inequality,

$$\begin{aligned}
&\mathbb{P}\Big(\sup_{0\le n\le n_\varepsilon(\lambda\tau)} |M_n| \ge \varepsilon^q\Big) \le \varepsilon^{-2q}\, \mathbb{E}(\langle M\rangle_{n_\varepsilon(\lambda\tau)}) \\
&\le \varepsilon^{-2q} \sum_{k=0}^{n_\varepsilon(\lambda\tau)-1} \mathbb{E}\big[\mathbb{E}(F_k^2|\mathcal{F}_{T_k})\big] \le C^2\varepsilon^{-2q}\, n_\varepsilon(\lambda\tau)\, \varepsilon^2 T^4 \qquad (2.78)
\end{aligned}$$

where we used that there exists $C > 0$ such that for any $\varepsilon > 0$ and $k \le n_\varepsilon(\lambda\tau)$,

$$\sqrt{\mathbb{E}(F_k^2|\mathcal{F}_{T_k})} \le C\varepsilon \int_{T_n}^{T_{n+1}} dt \int dx\, \bar{m}'_{x_k}(x) \sqrt{\mathbb{E}(\hat{Z}_k^4|\mathcal{F}_{T_k})} \le C\varepsilon T^2,$$

which follows by a Gaussian computation. By (2.78) the proof of (2.71) follows. □

In the following lemma we prove that $\xi_n$ is bounded with probability close to one. In proving the convergence to the molecular motor we need such a controll for $n \le \lambda(\varepsilon T)^{-1}$.

LEMMA 2.8. *For each $\tau \in \mathbb{R}_+$ we have for $\mu = 1, \lambda$*

$$\lim_{L\to\infty} \limsup_{\varepsilon\to 0} \mathbb{P}\Big( \sup_{0\le n\le n_\varepsilon(\mu\tau)} |\xi_n| > L\mu\Big) = 0 \tag{2.79}$$

PROOF. Since for $n \ge [S_{\varepsilon,\delta,\ell}/T]$, by definition, $\xi_n = \xi_{[S_{\varepsilon,\delta,\ell}/T]}$, it is enough to prove the statement for $n < n_{\varepsilon,\delta,\ell}(\mu\tau)$. Recall (2.69) and let

$$A_n \doteq S_n + x_0 + \sum_{k=0}^{n-1} \big[F_k + R_k\big] \ \text{ with } \ S_n \doteq \sum_{k=0}^{n-1} \sigma_k \tag{2.80}$$

we know that $|x_0| \le \varepsilon^{1/2-\eta}$, for any $\eta < 0$, for (2.14). Recalling the definition of $\sigma_k$ it is easy to show that there exists a real $C > 0$ such that, for any $\varepsilon > 0$,

$$\mathbb{E}(\sigma_k|\mathcal{F}_{T_k}) = 0 \ \text{ and } \ \mathbb{E}(\sigma_k^2|\mathcal{F}_{T_k}) \le C\varepsilon T. \tag{2.81}$$

Given $\tau \in \mathbb{R}_+$ an application of Doob's inequality then yields

$$\lim_{L\to\infty} \limsup_{\varepsilon\to 0} \mathbb{P}\Big( \sup_{0\le n\le n_\varepsilon(\mu\tau)} |S_n| > L\sqrt{\mu}\Big) = 0 \tag{2.82}$$

By Proposition 2.7 and (2.80) we have

$$\xi_n = -\frac{3}{4}\,\varepsilon \sum_{k=0}^{n-1} \int_{T_k}^{T_{k+1}} ds\, G(\varepsilon s)\langle \bar m'_{\xi_k}, \hat h\rangle \ + \ A_n \tag{2.83}$$

By Proposition 2.7, (2.82) and the definition of the center we have

$$\lim_{L\to\infty} \limsup_{\varepsilon\to 0} \mathbb{P}\Big( \sup_{0\le n\le n_{\varepsilon,\delta,\ell}(\mu\tau)} |A_n| > L\sqrt{\mu}\Big) = 0 \tag{2.84}$$

and let us call $\bar L \doteq \sup_{0\le n\le n_{\varepsilon,\delta,\ell}(\mu\tau)} |A_n|/\sqrt{\mu}$. Actually

$$\sup_{0\le n\le n_{\varepsilon,\delta,\ell}(\mu\tau)} \Big|\frac{3}{4}\,\varepsilon \sum_{k=0}^{n-1} \int_{T_k}^{T_{k+1}} ds\, G(\varepsilon s)\langle \bar m'_{\xi_k}, \hat h\rangle\Big| \le C\varepsilon T n_{\varepsilon,\delta,\ell}(\mu\tau) \le C\mu\tau \tag{2.85}$$

so that

$$\sup_{0\le n\le n_{\varepsilon,\delta,\ell}(\mu\tau)} |\xi_n| \le (\bar L\mu^{-\frac{1}{2}} + C\tau)\mu = L_1\mu$$

By (2.84) and the above bound the limit (2.79) follows. □

PROOF. *of Theorem 2.4 item (i)* Let

$$X_\varepsilon(t) = \xi(m^\varepsilon(t \wedge S_{\delta,\ell}))$$

$X_\varepsilon$ is a continuous $\mathcal{F}_t$-adapted process. We have to show that for every $\tau, \eta > 0$

$$\lim_{\varepsilon\to 0} \mathbb{P}(\sup_{t\in[0,\varepsilon^{-1}\lambda\tau]} \|m(t) - \bar{m}_{X_\varepsilon(t)}\|_\varepsilon > \varepsilon^{\frac{1}{2}-\eta}) = 0 \tag{2.86}$$

First of all, from (2.17), Proposition 2.5, and estimates therein included we have

$$\lim_{\varepsilon\to 0} \mathbb{P}(S_{\delta,\ell} \le \varepsilon^{-1}\lambda\tau) = 0 \tag{2.87}$$

therefore it is enough, instead of (2.86), to show that

$$\lim_{\varepsilon\to 0} \mathbb{P}(\sup_{t\le\varepsilon^{-1}\lambda\tau\wedge S_{\delta,\ell}} \|m(t) - \bar{m}_{X_\varepsilon(t)}\|_\varepsilon > \varepsilon^{\frac{1}{2}-\eta}) = 0 \tag{2.88}$$

which follows from Proposition 2.5 and Lemma 2.3 □

## 2.4. Convergence to Molecular Motor

In this section we prove Theorem 2.4 item (*ii*). Recalling that $n_\varepsilon(\tau) = [\varepsilon^{-1}\tau/T]$, $T = \varepsilon^{-\frac{1}{10}}$ and (2.65), we define the continuous process $\xi_\varepsilon(\tau)$, $\tau \in \mathbb{R}_+$, as the piecewise linear interpolation of $\xi_n$, namely we set

$$\xi_\varepsilon(\tau) \doteq \xi_{n_\varepsilon(\tau)} + [\tau - \varepsilon T n_\varepsilon(\tau)][\xi_{n_\varepsilon(\tau)+1} - \xi_{n_\varepsilon(\tau)}]. \tag{2.89}$$

From (2.87), (2.47) and (2.49) for any $\theta, \varepsilon > 0$ there exists a positive $q$ such that

$$\lim_{\varepsilon\to 0} \mathbb{P}(\sup_{\tau\in[0,\lambda\theta]} \left|X_\varepsilon(\varepsilon^{-1}\tau) - \xi_\varepsilon(\tau)\right| > \varepsilon^q) = 0. \tag{2.90}$$

Therefore we shall identify the limiting equation satisfied by $\xi_\varepsilon$ to prove item (*ii*) of Theorem 2.4. Following Lemma 6.1 of [**4**] and Proposition 8.2 of [**3**] we state without proof the following lemma. Let $S_\varepsilon(\tau)$ be the continuous process defined, as in (2.89), by the linear interpolation of $S_n$,

LEMMA 2.9. *As $\varepsilon \to 0$, the process $\{S_\varepsilon\}$ converges weakly in $\mathcal{C}(\mathbb{R}_+)$ to a Brownian motion with diffusion coefficient $\frac{3}{4}$.*

The proof relies on standard martingale arguments and Levy's theorem. We want to show that $\xi_\varepsilon$ converges by subsequences to a continuous process and that any limit point solves the integral equation (2.15). The boundedness of $\xi_\varepsilon$ follows by Lemma 2.8, we are going to prove its tightness in the next lemma and therefore Theorem 2.4 will follow by the uniquenes in law of (2.15).

LEMMA 2.10. *For each sequence $\varepsilon \to 0$, the process $\{\xi_\varepsilon\}$ is tight in $\mathcal{C}(\mathbb{R}_+)$.*

PROOF. For the initial hypotesis $\xi_\varepsilon(0) \to 0$. Using Theorem 8.2 of [**5**] it is enough to prove that for any $\tau \in \mathbb{R}_+$ and $\eta > 0$,

$$\lim_{\delta\to 0} \limsup_{\varepsilon\to 0} \mathbb{P}\Big( \sup_{\tau_1,\tau_2\in[0,\tau],|\tau_2-\tau_1|<\delta} |\xi_\varepsilon(\tau_2) - \xi_\varepsilon(\tau_1)| > \eta\Big) = 0. \tag{2.91}$$

By (2.89) and (2.79) this follows if, for each $L > 0$,

$$\lim_{\delta\to 0} \limsup_{\varepsilon\to 0} \mathbb{P}\Big( \sup_{\tau_1,\tau_2\in[0,\tau],|\tau_2-\tau_1|<\delta} |\xi_{n_\varepsilon(\tau_2)} - \xi_{n_\varepsilon(\tau_1)}| > \eta, \sup_{0\le n\le n_\varepsilon(\tau)} |\xi_n| \le L\Big) = 0 \tag{2.92}$$

Now, from (2.47), (2.87) and Proposition 2.7

$$|\xi_{n_\varepsilon(\tau_2)} - \xi_{n_\varepsilon(\tau_1)}| = \Big| \Big[ -\sum_{k=n_\varepsilon(\tau_1)}^{n_\varepsilon(\tau_2)-1} \varepsilon \int_{T_k}^{T_{k+1}} ds\, G(\varepsilon s) \langle \bar{m}'_{\xi_k}, \hat{h}\rangle \Big] + S_{n_\varepsilon(\tau_2)} - S_{n_\varepsilon(\tau_1)}$$

$$+ R_\varepsilon(\tau_1,\tau_2)\Big|,$$

where for each $\tau \in \mathbb{R}_+$ there exists $q > 0$ so that

$$\limsup_{\varepsilon\to 0} \mathbb{P}\Big( \sup_{\tau_1,\tau_2\in[0,\tau]} |R_\varepsilon(\tau_1,\tau_2)| > \varepsilon^q\Big) = 0.$$

By Lemma 2.9 it is now straightforward to conclude the proof of (2.92).

□

LEMMA 2.11. *For each $\delta > 0, \tau \in \mathbb{R}_+$, for $\mu = 1, \lambda$*

$$\lim_{\varepsilon\to 0} \mathbb{P}( \sup_{s\in[0,\mu\tau]} |\xi_\varepsilon(s) - S_\varepsilon(s) + \int_0^s du \langle \bar{m}'_{\xi_\varepsilon(u)}, h\rangle G(u)| > \delta\mu) = 0 \quad (2.93)$$

*with $h$ defined in* (2.2) *on the whole real axe.*

PROOF. By (2.47) and (2.49) it is enough to show that

$$\lim_{\varepsilon\to 0} \mathbb{P}( \sup_{s\in[0,\mu\tau]} |\xi_\varepsilon(s) - S_\varepsilon(s) + \int_0^s du \langle \bar{m}'_{\xi_\varepsilon(u)}, h\rangle G(u)| > \delta\mu, \sup_{n\le n_\varepsilon(\mu\tau)} |\xi_n| \le (1-\ell)\varepsilon^{-1}) = 0 \quad (2.94)$$

Recalling the definition of $\xi_n$ in (2.65), the second bound in (2.25) and Lemma 2.3, it yields $|\xi_{n+1} - \xi_n| \le C\sqrt{T}\varepsilon^{1/2-\eta}$ for $n \le n_\varepsilon(\mu\tau)$ on a set of probability converging to one, as $\varepsilon \to 0$ by (2.47). By definition (2.89), for each $\tau \in \mathbb{R}_+$ and $\delta > 0$ and $L > 0$ we have

$$\lim_{\varepsilon\to 0} \mathbb{P}( \sup_{s\in[0,\mu\tau]} | - \sum_{k=0}^{n_\varepsilon(s)} \varepsilon \langle \bar{m}'_{\xi_k}, \hat{h}\rangle \int_{T_k}^{T_{k+1}} d\tau\, G(\varepsilon\tau) + \int_0^s du \langle \bar{m}'_{\xi_\varepsilon(u)}, h\rangle G(u)| > \delta\mu, \sup_{n\le n_\varepsilon(\mu\tau)} |\xi_n| \le (1-\ell)\varepsilon^{-1}) = 0 \quad (2.95)$$

as it can be easily seen by the change of variable $u = \varepsilon t$ in the integral on the second term of (2.95), (2.89), (2.90), using that $\hat{h} = h$ in $\mathcal{T}_\varepsilon$ and that $\sup_{|\xi_k|\le(1-\ell)\varepsilon^{-1}} \left| \int dx\, \bar{m}'_{\xi_k}(x)\hat{h}(x) - \int dx\, \bar{m}'_{\xi_k}(x)h(x)\right| \le e^{-\ell\varepsilon^{-1}}$ and finally, using that

$$\max_{k\le n_\varepsilon(u)} \sup_{u\in[T_k,T_{k+1}]} |\langle \bar{m}'_{\xi_k}, h\rangle - \langle \bar{m}'_{\xi_\varepsilon(u)}, h\rangle| n_\varepsilon(u) \le 4C n_\varepsilon(u) h_0 L\sqrt{T}\varepsilon^{1/2-\eta}.$$

The proof of (2.93) is now completed by using (2.69), (2.47) and (2.87). □

PROOF. *of Theorem 2.4 item (ii)* See proof of *Theorem 2.1, item (ii)* in [**4**]. □

It remains to controll that the drift $D(\cdot,\tau)$ is in $\mathcal{C}^1(\mathbb{R})$ for every $\tau$ in $R_+$ and that is a periodic asymmetric and mean-zero function of $Y$. This follows by the same characteristics of $h$, as it can be easily seen by a simple change of variable $Z = X - Y$

$$D(Y,\tau) = -G(\tau)\int dX\,\bar{m}'_Y(X)h(X) = -G(\tau)\int dZ\,\bar{m}'(Z)h(Z+Y). \tag{2.96}$$

By using the $L+1$-periodicity of $h$ it follows the $L+1$-periodicity of $D$; the same argument leads to the asymmetry of $D$. Finally

$$\int_L^1 dY\,D(Y,\tau) = -G(\tau)\int dZ\,\bar{m}'(Z)\int_L^1 dY\,h(Z+Y) = 0 \tag{2.97}$$

Therefore, following the definition in [**18**], equation (2.15) describes an on-off Molecular Motor.

## 2.5. Net current of On-Off molecular brownian motor

In this section we prove that a positive net current arises in the asymptotic limit for $t \to \infty$ of equation (2.15). The probability density of equation

$$dx(t) = D(x,t)dt + db(t), \text{ with } D(x,t) \doteq -G(t)V'(x)$$

(where we call for semplicity $V'(x) = \langle \bar{m}'_x, h\rangle$) is governed by the Fokker-Planck equation

$$\partial_t P(x,t) - \partial_x\big(G(t)V'(x) + \frac{3}{4}\partial_x\big)P(x,t) = 0 \tag{2.98}$$

where $D(x,t)$ is the drift and $3/4$ is the diffusion. The drift is $\mathcal{C}^1(\mathbb{R}^2)$ and $L$-periodic in space while both the drift and the diffusion are $T$-periodic in time. The drift has zero space mean value.

This kind of equation represents a *pulsating motor*. The brownian motors have a typical transport phenomenon that is the *ratchet effect*, which consists in the emergence of a unidirectional motion in $1-d$ space-periodic systems, kept out of equilbrium by zero-mean forces.

The ratchet effect emerges in the existence of a non zero asynptotic mean current,

$$I = \lim_{t\to\infty} \frac{1}{t} \int dx\, P(x,t)x$$

Restricting to the long time limit, from [**11**] and with some work, it can be proven the following theorem

THEOREM 2.12. *There exists a unique solution $\hat{P}(x,t)$ to the Fokker-Planck equation* (2.98)*, $L-$periodic in $x$ and $T-$periodic in $t$, with $T = T_N + T_D$. Moreover, for each $L-$periodic function $P_0(x) \geq 0$ such that*

$$\int_0^L dx P_0(x) = 1,$$

*if $P(x,t)$ is the solution to* (2.98) *with initial data $P_0(x)$, then*

$$\begin{aligned} I &= \lim_{t\to\infty} \tfrac{1}{t} \int_0^t ds \int_0^L dx (G(t)V'(x))P(x,t) \\ &= -\tfrac{1}{T} \int_0^T dt \int_0^L dx (G(t)V'(x))\hat{P}(x,t) \end{aligned} \tag{2.99}$$

Obviously a non vanishing current $I$ is only possible for a periodic $V(x)$ with broken symmetry (ratched) as in our case. Even then, in the fast oscillation limit $T \to 0$, $G(t)$ changes very quickly and the Brownian particle (2.15) will behave like a Smoluchowsky-Feymann ratched $dx(t) = -V'(x)dt + db(t)$ for which $I = 0$. Similarly in the adiabatic limit, $T \to \infty$, $G(t) \approx const$ and once again $I \to 0$. It is therefore not obvious whether directed motion $I \neq 0$ can be generated at all by our ratched.

It becomes quickly clear that a closed analytical solution of (2.98), (2.99) is really difficult or even impossible. A way to approach this problem, focusing on $(x,t)$-periodic solutions to (2.98), is to solve the Fokker-Planck equation perturbatively for fast or slow oscillation. Here we study the asymptotic analysis for fast oscillations.

We introduce a parameter $\lambda \in (0,1)$, rescaling our system, in a way that the time period is asymptotically small in the limit for $\lambda \to 0$

$$G_\lambda(t) = G(t/\lambda), \quad G_\lambda(t) = G_\lambda(t + \lambda T).$$

By this way we can take $T$ fixed and let $\lambda$ go to zero. We introduce the class of models dependng on $\lambda$

$$dx(t) = -V'(x)G_\lambda(t)dt \, + \, db(t),$$

calling $\hat{P}_\lambda(x,t) = \hat{P}_\lambda(x + L, t + \lambda T)$ the unique periodic solution that solves

$$\partial_t P_\lambda(x,t) - \partial_x\big(G_\lambda(t)V'(x) + \frac{3}{4}\partial_x\big)P_\lambda(x,t) = 0,$$

we have

$$I_\lambda = -\frac{1}{T}\int_0^T dt \int_0^L dx(G_\lambda(t)V'(x))\hat{P}_\lambda(x,\lambda t).$$

We introduce now the new distribution

$$W_\lambda(x,t) = \hat{P}_\lambda(x,\lambda t) = \hat{P}_\lambda(x,\lambda(t+T)) = W_\lambda(x,t+T),$$

that solves

$$\partial_t W_\lambda(x,t) = \lambda\,\partial_x\big(G(t)V'(x) + \frac{3}{4}\partial_x\big)W_\lambda(x,t). \tag{2.100}$$

We expand $W_\lambda(x,t)$ in series for small $\lambda$, $W_\lambda = \sum_{k=0}^n \lambda^k W_k + \lambda^{n+1}R_\lambda^n$, where $R_\lambda^n(x,t)$ is uniformly bounded as $\lambda$ converges to zero (we omit the details). The normalization and the periodic boundary conditions on $W_\lambda$ imply

$$\begin{cases} W_k(x+L,t+T) = W_k(x,t), \\ \int_0^L dx\, W_k(x,t) = \delta_{k,0}, \end{cases}$$

for each $k \geq 0$ and $\delta_{k,0}$ is the Kronecker delta.

By equation (2.101), the functions $W_k$ can now be readily determined by comparing the coefficients of equal order of $\lambda$. The contribution of each term to the current is given by

$$I_k = -\frac{1}{T}\int_0^T dt \int_0^L dx (G(t)V'(x))W_k(x,t),$$

where we used that $G_\lambda(t/\lambda) = G(t)$.

Here we just mention that, calling $\bar{G} = 1/T \int_0^T dt\, G(t)$, $\bar{c} = 4\bar{G}/3$ and $\bar{Z} = \int_0^L dx\, e^{-\bar{c}V(x)}$, we have

$$W_0(x,t) = W_0(x) = \frac{e^{-\bar{c}V(x)}}{\bar{Z}},$$

that finally yields $I_0 = 0$, for the periodicity of $V(x)$.

We have to compute up to order $\lambda^2$ to have a non-zero contribute, which actually is

$$I_2 = \frac{4L\bar{G}\langle \Delta_1(t)^2 \rangle}{\bar{Z}\int_0^L dx\, e^{\bar{c}V(x)}} \int_0^L dx\, V'(x)(V''(x))^2$$

where $\Delta_1(t) = \int_0^t ds\, (G(s) - \bar{G}) - 1/T \int_0^T dt \int_0^t ds\, (G(s) - \bar{G})$.

It can be shown that our potential $V(x)$, for $L > 3$, resembles $U(x) = U_0[\sin(2\pi x/L) + (1/4)\sin(4\pi x/L)]$, see [**18**], for which it is easy to see that $I_2 > 0$. Therefore

$$I = I_2 + O(\lambda^3)$$

has a positive leading order. We can conclude that in the long time asymptotics of our model, particles pick up a positive drift. For detailes about calculations of $W_k$ and $I_k$ we refer to the Appendix.

## 2.6. Appendix

In this appendix we give further detailes on the derivation of the terms $W_k$ and $I_k$. Starting from the Fokker-Planck equation, (2.100),

solved by $W_\lambda$, we have

$$\partial_t W_\lambda(x,t) = \lambda \mathcal{L}_t W_\lambda(x,t)$$

where the operator $\mathcal{L}_t$ is defined by

$$\mathcal{L}_t f(x) = \partial_x \big[ G(t)V'(x) + \sigma \partial_x \big] f(x), \quad \sigma = 3/4,$$

therefore

$$\partial_t W_0 + \lambda \partial_t W_1 + \lambda^2 \partial_t W_2 + \ldots = \lambda \mathcal{L}_t W_0 + \lambda^2 \mathcal{L}_t W_1 + \lambda^3 \mathcal{L}_t W_2 + \ldots$$

finally we define the new operator

$$\bar{\mathcal{L}} f(x) = \partial_x (\bar{G} V'(x) f(x)) + \sigma \partial_x^2 f(x),$$

remembering that $\bar{G} = 1/T \int_0^T dt\, G(t)$.

For what concerns the first term $W_0$, comparing the $\lambda^0$ terms in the right and left side of the above equality, we have $\partial_t W_0 = 0$, therefore $W_0(x,t) = W_0(x)$, and using $\partial_t W_1 = \mathcal{L}_t W_0$, from the periodicity in $t$ of $W_1$,

$$0 = \frac{1}{T} \int_0^T dt\, \partial_t W_1(x,t) = \frac{1}{T} \int_0^T \mathcal{L}_t W_0(x) = \bar{\mathcal{L}} W_0(x),$$

it follows that $W_0(x,t) = W_0(x) = \frac{e^{-\bar{c}V(x)}}{\bar{Z}}$, where $\bar{c} = \bar{G}/\sigma$ and $\bar{Z} = \int_0^L dx\, e^{-\bar{c}V(x)}$. Therefore

$$I_0 = -\frac{1}{T} \int_0^T dt \int_0^L dx (G(t)V'(x)) W_0(x,t) = 0.$$

Let us note that

$$\mathcal{L}_t f(x) = \bar{\mathcal{L}} f(x) + \Delta(t) \partial_x (V'(x) f(x))$$

where $\Delta(t) = G(t) - \bar{G}$ is a $T$-periodic mean-zero function.

For the next orders, we use the iterative equation,

$$\partial_t W_k = \Delta(t) \partial_x (V' W_{k-1}) + \bar{\mathcal{L}} W_{k-1}$$

joint with the periodic conditions. For $k = 1$, it gives

$$\partial_t W_1 = \Delta(t)\partial_x(V'W_0) + \bar{\mathcal{L}}W_0(x) = \Delta(t)\partial_x(V'W_0)$$

therefore

$$W_1(x,t) = \alpha_1(x) + \int_0^t ds\, \Delta(s)\partial_x(V'W_0),$$

once again, we use the periodicity on $t$ to obtain $\alpha_1(x)$

$$0 = \frac{1}{T}\int_0^T dt\, \partial_t W_2(x,t) = \bar{\mathcal{L}}\alpha_1(x) + \bar{\mathcal{L}}\frac{1}{T}\int_0^T dt \int_0^t ds\, \Delta(s)(\partial_x(V'W_0))(x)$$

$$+\frac{1}{T}\int_0^T dt\, \Delta(t)\partial_x(V'\alpha_1)(x) + \frac{1}{T}\int_0^T dt\, \Delta(t)\int_0^t ds\, \Delta(s)\partial_x(V'\partial_x(V'W_0))(x).$$

It's easily shown that the integral $\frac{1}{T}\int_0^T dt\, \Delta(t)\int_0^t ds\, \Delta(s) = 0$, then

$$\bar{\mathcal{L}}\big(\alpha_1(x) + \frac{1}{T}\int_0^T dt \int_0^t ds\, \Delta(s)\partial_x(V'W_0)(x)\big) = 0$$

and consequently

$$\alpha_1(x) + \frac{1}{T}\int_0^T dt \int_0^t ds\, \Delta(s)\partial_x(V'W_0) = C_1 W_0,$$

finally, defining the $T$-periodic mean-zero function $\Delta_1(t) = \int_0^t ds\, \Delta(s) - 1/T\int_0^T dt \int_0^t ds\, \Delta(s)$, we have

$$W_1(x,t) = C_1 W_0(x) + \Delta_1(t)\partial_x(V'W_0)(x)$$

where $C_1 = 0$ from the periodicity condition for $\alpha_1(x)$. From the final form of $W_1$ easily follows that

$$I_1 = -\frac{1}{T}\int_0^T dt \int_0^L dx(G(t)V'(x))W_1(x,t) = 0.$$

We can now study $W_2$,

$$\partial_t W_2 = \bar{\mathcal{L}}W_1 + \Delta(t)\partial_x(V'W_1) = \Delta_1(t)\bar{\mathcal{L}}(\partial_x(V'W_0)) + \Delta(t)\Delta_1(t)\partial_x(V'\partial_x(V'W_0))$$

integrating on $t$

$$W_2(x,t) = \alpha_2(x) + \int_0^t ds\Delta_1(s)\bar{\mathcal{L}}(\partial_x(V'W_0))(x)$$

$$+\frac{1}{2}[{\Delta_1}^2(t)-{\Delta_1}^2(0)]\partial_x(V'\partial_x(V'W_0))(x)$$

Let us determine $\alpha_2(x)$

$$0=\frac{1}{T}\int_0^T dt\,\partial_t W_3(x,t)=\frac{1}{T}\int_0^T dt\,\bar{\mathcal{L}}W_2(x,t)+\frac{1}{T}\int_0^T dt\,\Delta(t)\partial_x(V'W_2)(x,t)$$

$$=\bar{\mathcal{L}}\big(\alpha_2(x)+\langle\int_0^t ds\Delta_1(s)\rangle\bar{\mathcal{L}}(\partial_x(V'W_0))(x)$$

$$+\frac{1}{2}[\langle{\Delta_1}^2(t)\rangle-\langle{\Delta_1}^2(0)\rangle]\partial_x(V'\partial_x(V'W_0))(x)-\langle{\Delta_1}^2(t)\rangle\partial_x(V'\bar{\mathcal{L}}\partial_x(V'W_0))(x)\big)$$

Let

$$g(x)=\alpha_2(x)+\langle\int_0^t ds\Delta_1(s)\rangle\bar{\mathcal{L}}(\partial_x(V'W_0))(x)+\frac{1}{2}[\langle{\Delta_1}^2(t)\rangle-\langle{\Delta_1}^2(0)\rangle]$$

$$\partial_x(V'\partial_x(V'W_0))(x)$$

and

$$F(x)=\langle{\Delta_1}^2(t)\rangle\partial_x(V'\bar{\mathcal{L}}\partial_x(V'W_0))(x)$$

therefore

$$g(x)=\gamma e^{-\bar{c}V(x)}+e^{-\bar{c}V(x)}\int_0^x dy\,\frac{e^{\bar{c}V(y)}}{\sigma}\big[F(y)+c\big]$$

where $c$ and $\gamma$ are obtained by imposing normalization and periodicity. Therefore

$$\alpha_2(x)=g(x)-\langle\int_0^t ds\Delta_1(s)\rangle\bar{\mathcal{L}}(\partial_x(V'W_0))(x)$$

$$-\frac{1}{2}[\langle{\Delta_1}^2(t)\rangle-\langle{\Delta_1}^2(0)\rangle]\partial_x(V'\partial_x(V'W_0))(x)$$

from the periodicity of $\alpha_2(x)$, we have

$$c=-\frac{\langle{\Delta_1}^2(t)\rangle}{\int_0^L dx\,e^{\bar{c}V(x)}}\int_0^L dx\,e^{\bar{c}V(x)}\partial_x(V'\bar{\mathcal{L}}\partial_x(V'W_0))(x)$$

and

$$W_2(x,t)=\gamma e^{-\bar{c}V}+e^{-\bar{c}V(x)}\int_0^x dy\,\frac{e^{\bar{c}V(y)}}{\sigma}\big[F(y)+c\big]$$

$$+\Delta_2(t)\bar{\mathcal{L}}(\partial_x(V'W_0))+\tilde{\Delta}_2(t)\partial_x(V'\partial_x(V'W_0))(x)$$

where

$$\Delta_2(t) = \int_0^t \Delta_1(s)ds - \langle \int_0^t \Delta_1(s)ds \rangle$$

and

$$\tilde{\Delta}_2(t) = \frac{1}{2}[\Delta_1^2(t) - \langle \Delta_1^2(t) \rangle],$$

both periodic mean-zero functions. It follows that $I_2 = -\frac{1}{T}\int_0^T dt \int_0^L dx (G(t)V'(x))W_2$ is such that, integrating by parts repeatedly

$$I_2 = \frac{L\langle \Delta_1^2(t) \rangle}{\int_0^L dx\, e^{\bar{c}V(x)}} \int_0^L dx\, e^{\bar{c}V(x)} V' \bar{\mathcal{L}}(\partial_x (V' W_0))(x)$$

$$-\big(\frac{1}{T}\int_0^T dt\, G(t)\Delta_2(t) + \langle \Delta_1^2(t) \rangle \int_0^L dx\, V' \bar{\mathcal{L}}(\partial_x (V' W_0))\big)$$

$$-\frac{1}{T}\int_0^T dt\, G(t)\tilde{\Delta}_2(t) \int_0^L dx\, V' \partial_x (V' \partial_x (V' W_0))$$

$$= \frac{4L\bar{G}\langle \Delta_1^2(t) \rangle}{\bar{Z}\int_0^L dx\, e^{\bar{c}V(x)}} \int_0^L dx\, V'(x)(V''(x))^2$$

Therefore the sign of the current is given by the asymmetry of the drift through the term $\int_0^L dx\, V'(x)(V''(x))^2$. Note that if $V(x)$ was a symmetric function the current would be zero.

CHAPTER 3

# Molecular dynamics simulation of vascular network formation

Blood vessel formation may be divided into two different processes. In the first stage, occurring in embryonic development, ECs organize into a primitive vascular network (*Vasculogenesis*). In a second moment, existing vessels split and remodel in order to extend the circulation of blood into previously avascular regions by a mechanism of controlled migration and proliferation of the ECs (*Angiogenesis*) [**35**]. ECs are the most essential component of the vessel network: each vessel, from the largest one to the smallest one, is composed by a monolayer of ECs (called *endothelium*), arranged in a mosaic pattern around a central lumen, into which blood flows. In the capillaries the endothelium may even consist of just a single EC, rolled up on itself to form the lumen.

Although there are several mechanisms involved during vessel formation, in this work we shall focus on the characteristic migration motion of cells driven in response to an external chemical stimulus: the chemotaxis. ECs secrete an attractive chemical factor, the Vascular Growth Factor-A (VEGF-A), while they start to migrate. Each of them perceives the chemical signal with its receptors at its extremities and starts to move along the chemical concentration field gradient, toward areas of higher concentration corresponding to higher density of cells. ECs are able to move extending tiny protrusions, the *pseudopodia*, on the side of the higher concentration. The pseudopodia attach

to the substratum, via adhesion molecules, and pull the cell in that direction.

In parallel with chemotaxis, another mechanism resulting in cell motion is the *haptotaxis*, i.e. the movement of cells along an adhesive gradient: the substratum is not usually homogeneous and its varying density can affect cell adhesion and hence migration. We will not consider haptotaxis in this work. Cell-cell and cell-membrane contacts are really essential in the process of vascular network formation and their loss can cause cell apoptosis (death) [**35, 36, 37, 38, 39, 40**].

The study of the particular biological process of vascular network formation and its relations to tumor vascularization has also been accomplished by means of several mathematical models. First studies were presented by Murray et al. [**25, 28**], who explained the phenomenon by focusing mainly on its mechanical aspects, i.e. on the interaction between cells and the substrate. Gamba et al. [**29, 30, 31, 32**] proposed a continuous model, based on chemotaxis, which applies to early stages of *in vitro* vasculogenesis, performed with Human Umbilical-Vein ECs (HUVEC) cultured on a gel matrix. More recently, some of these authors managed to unify both the mechanical aspect and the chemical one into a more complete model [**33, 34**].

## 3.1. Review of the experimental data

The experimental data on which all theoretical studies till now hinge, are those collected by tracking the behavior of cells initially displaced at random onto a proteic gel matrix, generically original living environment. In our analysis, we explicitly refer to the *in vitro* vasculogenesis experiments of Gamba et al. [**29**], and shall use the same numerical values of parameters therein introduced. In the experiments, HUVEC cells are randomly dispersed and cultured on a gel matrix (*Matrigel*)

of linear size $l = 1,2,4,8$ mm. Cells sediment by gravity on the matrix and then move on its horizontal surface, showing the ability of self-organizing in a structured network characterized by a natural length scale. The whole process takes about $T = 12$ hours.
Four fundamental steps can be distinguished in the experiments [**41**]:

- During the first two hours, the ECs start to move by choosing a particular direction dictated by the gradient of the concentration of the chemical substance VEGF-A. Single ECs migrate until collision with neighboring cells, keeping a practically fixed direction with a small superimposed random velocity component. The peculiarity of ECs of maintaining the same direction of motion is known as *persistence*, and has been explained by cells inertia in rearranging their shapes. In fact, in order to change direction of motion, ECs have first to elongate towards the new direction, with the result that to change path is a relatively slow process. In this phase of amoeboid motion, the mechanical interactions with the substrate are weak.
- After collision, ECs attach to their neighboring cells eventually forming a continuous multicellular network. They assume a more elongated shape and multiply the number of adhesion sites. In this phase the motion is slower than in the previous step.
- In the third phase the mechanical interactions become essential as the network slowly moves, undergoing a thinning process that would leave the overall structure mainly unalterated.
- Finally cells fold up to create the lumen.

The final capillary-like network can be represented as a collection of nodes connected by chords, whose experimentally measured average length stays around 200 $\mu$m for values of the cell density between 100 to

200 cells/mm$^2$. Outside this range no network develops. More precisely, below a critical value of 100 cells/mm$^2$, groups of disconnected structures form, while at higher densities (above 200-300 cells/mm$^2$) the mean chord thickness grows to hold an increasing number of cells and the structure resembles a continuous carpet with holes (*swiss cheese* pattern).

## 3.2. Theoretical model

In this section I better explain the model presented in the Introduction. As already mentioned this is an off-lattice particle model of vasculogenesis where the equations of motion are governed by the gradient of the concentration of a chemoattractant substance produced by the particles themselves. The discrete $N$-particle system we are proposing, gives evidence of the important role of the pure chemotaxis process in forming well structured networks with a characteristic chord length size.

We refined our model with increasing complexity, by gradually adding features that would allow a closer resemblance with experiments. Particles, which we shall also refer to as "cells" in the following, are constrained inside a square box of given edge $L$ with periodic boundary conditions. The number of cells will be kept constant during the simulations, i.e. we will consider neither cell creation nor cell destruction.

At first, we consider cells as adimensional point-like particles moving only under the effect of the concentration gradient of the chemoattractant substance $\nabla c(\mathbf{x}, t)$. The chemoattractant is released by cells. It diffuses according to a diffusion coefficient $D \approx 10\ \mu\text{m}^2/\text{s}$ and degrades within a characteristic finite time $\tau \approx 64$ min. The combination of the diffusion and degradation processes introduces a characteristic length

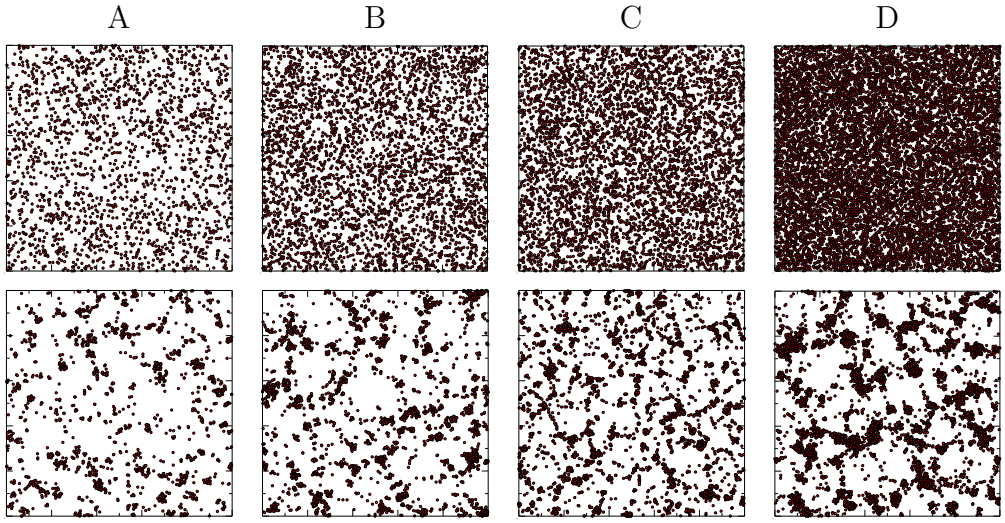


FIGURE 3.1. Results of the simulations of point-like particle under the sole effect of chemotaxis inside the box with edge 1 mm= $5\ell$; $\ell = \sqrt{D\tau}$ indicates the characteristic length of the process. Each column involves different particle numbers: (A) 2000 cells, (B) 3750 cells, (C) 5000 cells, (D) 11250 cells. The top row shows the initial random particle displacement. The bottom row shows the systems after the dynamics produced a network-like resembling structure. Since this structure appears during a brief transient before the expected structural collapse into a single agglomerate, the simulation times of these snapshots were chosen qualitatively after visual inspection and roughly correspond to $T = 2$ hours of laboratory time (much less than experimental times due to the large cell densities resulting in unrealistically large chemo-attractant concentration gradients). In these simulations we used the dimensionless $\alpha = 1$.

$\ell = \sqrt{D\tau}$ in the system, with $\ell \approx 200$ $\mu$m. As a further step, we introduced in the system a dynamical friction proportional to the velocity of cells in order to simulate the dragging force to which cells are subjected in the matrigel. The net result of this friction is to slow down the overall simulation time, leaving unaltered the main features of the system history. Although point-like cells are a very simplified representation of real cells, their motion, driven by chemotaxis, yields the formation of the expected network of filaments with a characteristic length $\ell$ (see bottom row of Fig. 3.1).

In order to further refine the simulation, we introduced an inelastic isotropic repulsion mechanism between cells (see the following paragraph for its definition), imitating the fact that cells do not penetrate each other in reality. Since the chemotactic field acts as an attractive potential between cells, the result of both processes is to stick together cells after collision. Cells are no more adimensional but now possess their own effective radius $r \approx 10$ $\mu$m. The introduction of a cell effective radius changes sensibly the simulation. One important side effect is that of imposing a limit on the density of cells in the simulation, which must lie well below the close-packing density. The last refinement deals with the problem of the "cell persistence" of motion, i.e. the observed large inertia of cells in changing the direction of their motion. The solution to this issue in terms of pure galilean inertia proposed by Gamba et al. in their continuous model [**29**] has been criticized in [**42**], where it was pointed out that cells must rely onto a more involved mechanism of resistance to changes of direction. As a result some of the authors of [**29**] recently proposed variations of their model to explicitly include cell persistence [**34, 41**]. In our case, we use the advantage of a molecular dynamic simulation to have full control of all forces acting on all cells at each time step. For each cell, we simply reduce the component of the gradient of the chemical field along the direction orthogonal to

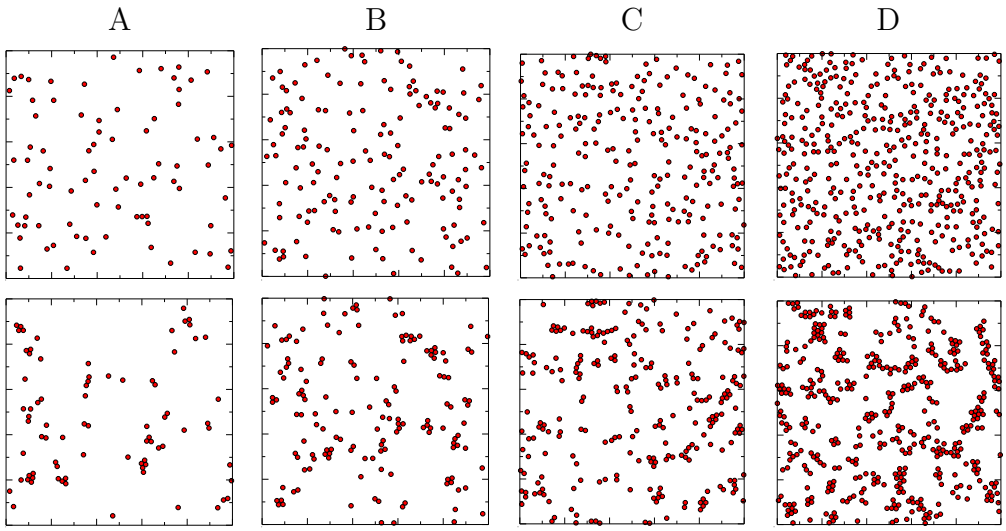


FIGURE 3.2. Simulation results of particles in presence of an inelastic repulsion potential between cells and a persistence force together with chemotaxis, inside the box with edge 1 mm= $5\ell$; $\ell = \sqrt{D\tau}$ indicates the characteristic length of the process. Each column involves different particle numbers: (A) 80 cells, (B) 150 cells, (C) 250 cells, (D) 450 cells. The first row shows the initial random particle displacement. The second row shows the systems after the dynamics produced a possible network-like structure. The simulation times at which the networks form were chosen qualitatively after visual inspection, as in Fig. 3.1. The chosen final simulation time corresponds to about $T \simeq 13$ hours, i.e. a value comparable with the observed network formation times of experiments. The diameter of cells is of $20\mu m = 0.1\ell$ and is faithfully represented in scale. In these simulations we fixed the dimensionless constants to $\alpha = 1$, $\gamma = 1$, $\kappa = 1000$, $\nu = 1$, $\eta = 100$.

the direction of cell motion by a factor $\beta_i = \kappa|\mathbf{v}_i|/(\kappa|\mathbf{v}_i| + |\nabla c(\mathbf{x}_i)|)$ with $\kappa$ a constant modulating the effect of persistence and $(\mathbf{x}_i, \mathbf{v}_i)$ the position and velocity of the $i$-th cell.

To summarize, the dynamical system of equations we solve with $i = 1 \dots N$ is

$$\begin{cases} \dot{\mathbf{x}}_i(t) = \mathbf{v}_i(t) \\ \dot{\mathbf{v}}_i(t) = \mu \nabla c(\mathbf{x}_i(t), t) + \mathbf{F}_{\mathrm{IR}} + \mathbf{F}_{\mathrm{T}} + \mathbf{F}_{\mathrm{F}} \\ \partial_t c(\mathbf{x}, t) = D\Delta c(\mathbf{x}, t) - \frac{c(\mathbf{x},t)}{\tau} + \alpha \sum_{j=1}^{N} J(\mathbf{x} - \mathbf{x}_j(t)), \end{cases} \tag{3.1}$$

where $D$, $\alpha$, and $\tau$ are respectively the diffusion coefficient, the rate of production and the characteristic degradation time of the soluble chemo-attractant mediator, and $\mu$ measures the strength of the cell response to the chemical factor. Here $c(\mathbf{x}, t)$ is the total chemical field acting on the position $\mathbf{x}$ at time $t$. By linearity it is given by the sum of the chemotactic fields $c_j(\mathbf{x}, t)$ generated by all cells $\sum_{j=1}^{N} c_j(\mathbf{x}, t)$.
The force $\mathbf{F}_{\mathrm{IR}}$ stands for the inelastic isotropic repulsion force between two colliding cells. Let $\mathbf{d}_{ij}$ be the vector joining the centers cells $j$ and $i$, we define the force $\mathbf{F}_{\mathrm{IR}} = \sum_{j \neq i}^{N} \nu(2r - d_{ij})\hat{\mathbf{d}}_{\mathbf{ij}} - \eta\langle \mathbf{v}_i, \hat{\mathbf{d}}_{\mathbf{ij}} \rangle \hat{\mathbf{d}}_{\mathbf{ij}}$ for $d_{ij} < 2r$ (overlapping cells) and zero otherwise, where $r$ is the cell radius, $\nu$ is an elastic constant, $\eta$ is an inelastic coefficient and $\hat{\mathbf{d}}_{\mathbf{ij}} = \mathbf{d}_{ij}/d_{ij}$.
$\mathbf{F}_{\mathrm{T}} = -\beta_i \mu \nabla c_{i,\perp \mathbf{v}}$ the cell persistence force discussed above, with the symbol $\nabla c_{i,\perp \mathbf{v}}$ standing for the projection of the gradient $\nabla c(\mathbf{x}_i)$ orthogonal to the direction of $\mathbf{v}_i$.
$\mathbf{F}_{\mathrm{F}} = -\gamma \mathbf{v}_i$ is the non-conservative friction term.
The function $J(\mathbf{x})$ is responsible of chemo-attractant production. It is an even non-negative function of $\mathbf{x}$, normalized to unity in the whole space. We took $J(\mathbf{x})$ as a step function with constant value inside the circle $|\mathbf{x}| < r$ and zero outside.

In order to match the experimental set up conditions, cell initial positions were extracted at random with a poissonian process, while

all velocities were set to zero. In the case of two-dimensional cells with repulsion, cells were dropped in the random extracted position only if no overlap with other cells occurred, otherwise another position had to be extracted. The concentration of the chemo-attractant was also initially set to zero.

We integrated the equations of motion by means of a standard Verlet algorithm [**43**] with time step $4\times10^{-5}\tau \simeq 0.15$ s, while the numerical solution of the diffusion partial differential equation was accomplished by using a second order explicit finite differences scheme [**44**] on a square grid with step equal to $2.5 \times 10^{-2}\ell \simeq 5\mu$m. The edge $L$ of the simulation box was set to $5\ell \simeq 1$ mm. By posing $x^* = x/\sqrt{D\tau}$, $t^* = t/\tau$ and $c^* = c\mu\tau/D$ the equations can be written in terms of the dimensionless starred unknowns, so that all the dependence on the constant parameters $D$, $\mu$, $\tau$ is carried upon a rescaled value of $\alpha^* = \alpha\tau^2\mu/D$ and all forces $\mathbf{F}^*_{\{\mathrm{IR,T,F}\}} = \mathbf{F}_{\{\mathrm{IR,T,F}\}}\tau^2/\sqrt{D\tau}$.

As already mentioned, we performed our simulations with increasing complexity. Firstly we consider point-like model cells moving inside the chemotactic field. Secondly, we switched on the inelastic cell-cell repulsion term $\mathbf{F}_{\mathrm{IR}}$ and the velocity dependent persistence force $\mathbf{F}_{\mathrm{T}}$. In both cases, we included the dynamical non-conservative friction force $\mathbf{F}_{\mathrm{F}}$ in the simulations, the presence of which did not change substantially the results.

## 3.3. Results

The results of the simulation of point-like cells under chemotaxis, without the effect of repulsion and persistence forces, are shown in Fig. 3.1, where the system is analyzed depending on the number of particles. These simulations, far from representing the dynamics of real cell populations, are nevertheless interesting since they deliver a picture of the

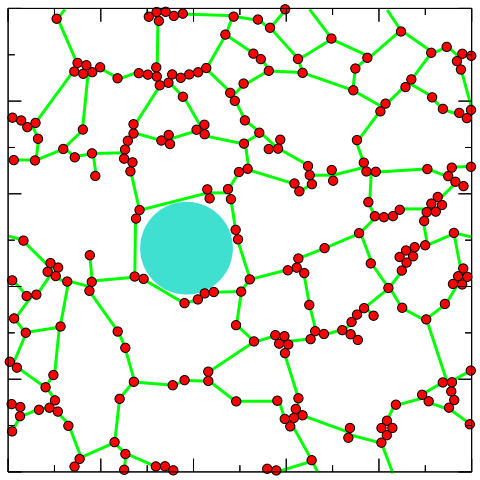

FIGURE 3.3. Same as Fig. 3.2C but here we draw by hand the possible resulting network. In order to compare empty regions with the characteristic area $\ell^2$ we show a circle with diameter equal to $\ell$. The underlying network was drawn in a qualitative way by connecting nearby cells. We suggest that a more realistic model with elongating cells might reproduce the displayed network structure.

capillary network with a characteristic chord size of length $\ell \approx 200$ $\mu$m and uncover the different behavior of the system with respect to the cell density. For $N = 2000$, network chords do not develop and after a short transient of slow motion, in which the chemical substance diffuses throughout the simulation box, cells collapse all together. The situation improves as the number of particles increases and the best network is obtained for $N = 5000$. In that case, thin filaments are visible with a thickness of very few cells. Finally, for $N = 11250$ chords are obtained with a thickness of many cells. In some senses this last situation resembles the *swiss cheese* pattern visible in the experiments. The characteristic length is still detectable in the form of holes with

characteristic area value around $\ell^2$.
We notice that in the case of pointless particles, cell densities resulting in vascular networks are very large compared to the experimental ones. This is obviously an issue stemming from the vanishing excluded volume of the chosen model particles that represent cells. Moreover, these unrealistic high cellular densities result in a correspondingly high production of chemo-actractant and consequently high chemotactic field gradients, so that the simulation runs faster than the characteristic times of experiments. In fact, with these semplified model we find the formation of network resembling structures after $T \simeq 2$ hours, much less than the experimental value of 12 hours.

Without both the repulsion and persistence terms, the organized capillary network structure arises as a brief transient, after which cells collapse all together. The appearance of network structures only during a transient is a feature shared by other different models of continuous type [**45**]. At this stage, the dynamical friction term, although strictly unnecessary, helps to lengthen the duration of the transient. Therefore, as a first result we observe that a simple molecular dynamics model captures the essence of the process of chemotaxis, which is capable of organizing cells in a non-trivial functional network displacement, although only during a brief transient.

As an attempt to stabilize the temporary capillary network, we introduce the inelastic repulsion force $\mathbf{F}_{\mathrm{IR}}$, intended to glue together colliding cells of certain effective radius (in co-operation with the actractive chemotactic field) and to reduce bouncing effects (due to its inelastic character), and the persistence force $\mathbf{F}_{\mathrm{T}}$, which should provide a better alignment of cells such to enhance the network-like structure. The inelastic repulsion term $\mathbf{F}_{\mathrm{IR}}$, because of the effective cell radius introduced, imposes a limit on the number of cells that can be inserted

in the simulation box without overlap. Our simulations were set up with cell densities equal to the experimental values, i.e. varying from 80 cells/mm$^2$ to 450 cells/mm$^2$.

Despite our intention of improving the model, we find there is no clear formation of capillary networks. By examining Fig. 3.2A and Fig. 3.2B, we find disconnected patterns for $N = 80 \sim 150$ cells, as also foreseen by the experiments, while we do not find a clear evidence of network formation with $N = 250$ cells, although empty spaces of characteristic area $\ell^2$ can be observed in Fig. 3.2C and Fig. 3.2D. In particular, the case of $N = 450$ cells shows thick structures of cells reminiscent of the *swiss cheese* pattern, but still disposed in a rather unorganized geometry. In Fig. 3.3, we show the possible resulting network in the case of 250 cells, by drawing cell connections by hand (by connecting cell neighbors by eye) and by superposing a circle with diameter $\ell$. As in the simpler point-like cell model, the observed (unclear) network-like structures continue to appear during a short transient, although with longer lifetimes, after simulation times of $T \simeq 13$ hours, comparable with the experimental ones. Thus, the introduction of the persistence and inelastic repulsive forces tends to stabilize the network-like geometry.

The network-like capillary structure raising only during a transient in the simulation is an unrealistic feature common to the hydrodynamical models as well [**29, 45**]. A possible explanation of this fact, which may lead to more realistic simulations, is that cells have been modeled as (quasi) static geometrical entities. In fact, in reality, cells elongate their shape in the act of moving toward higher chemo-attractant concentrations [**46**], which is a process intimately bound to the phenomenon of cell persistence of motion. This is the main reason that led us to introduce the persistence force $\mathbf{F}_{\mathrm{T}}$. With this term, in fact, the

transient phase gets longer and the network structures become slightly more clear. In the elongated form and after they come in contact, the real cells stick together, in some sense imitating those connections that we added by hand in Fig. 3.3.

## 3.4. Conclusions and prospectives

We showed that two-dimensional molecular dynamics simulations of point-like cells whose motion is governed by the process of chemotaxis, reproduce the main features of real cells to form networks having chords with a characteristic length. However, this networks are metastable and collapse after a brief transient. Similar results are present in literature, where the problem is faced by solving PDE of hydrodynamic type, with individual cells represented by gaussian bumps. To our knowledge our method is the first attempt to describe endothelial cell systems in terms of a discrete collection of particles, whose motion can be tracked throughout the whole history of capillary network formation. The peculiar advantage of molecular dynamics methods is the extreme ease with which one can introduce forces acting to individual particles.

In particular, in order to stabilize the metastable network state, we introduce both an inelastic repulsion force between cells and the so called "persistence" force, which mimics the observed tendency of cells to preserve the direction of their motion. Unfortunately, this model, although more complete and closer to reality, is not fully able to reproduce the formation of a clear capillary network in correspondence of realistic cell densities beyond the percolation threshold. A vague network-like structure appears during a short transient, whereas the introduction of the persistence of motion force and the inelastic repulsive force helps to lengthen this metastable geometry, before all cells

collapse in a unique large cluster. We ascribe this unsuccess to the geometry of single cells, which in reality change their shape by elongating towards the direction of motion, a feature that we have not considered at this stage.

As already mentioned in the Introduction this is the main reason while we made a new model considering the elongation and reorientation of cells. We want them to elongate in the direction of motion while they move. The longer axe of cells reaches up to 100-times the original radius length and cells continually update their "head" and "tail". Actually, even if in reality cells make exchange of matter with the substratum (i.e. *endocytosis*) in order not to loose their lower dimension, we keep the conservation of mass, not considering this feature [**47**]. We just put a cut off not to let the long axe exceed $100\,r$.

In the sequel, the model we are testing. The main idea is the same of model (3.1), the space is the $L$-side periodic boundary box and the number $N$ of cells is kept constant. We consider cells like rectangulus. The $i$-th cell is described by means of the position and velocity $(\mathbf{x}_i, \mathbf{v}_i)$ of its center, whose equations are conceptually the same of the spherical case; it has a longer semi-axe $\xi_i$ which elongates towards the direction of the gradient of $c$. The orientation of the cell is given by the component $\theta_i = \widehat{\xi_i \mathbf{x}}$, where $\mathbf{x}$ is the $x$-axe. Finally we consider the other semi-axe $\eta_i$ and the angles $\psi_i = \widehat{\mathbf{v}_i \mathbf{x}}$, $\phi_i = \widehat{\nabla c \mathbf{x}}$. The final system, with $i = 1 \dots N$ is

$$\begin{cases} \dot{\mathbf{x}}_i(t) = \mathbf{v}_i(t) \\ \dot{\mathbf{v}}_i = \mu \nabla c(\mathbf{x}_i(t), t) + \mathbf{F}_T + \mathbf{F}_{IR} + \mathbf{F}_F \\ \dot{\xi}_i = K_0 |\nabla c| cos(2\theta_i) - K_1(\xi_i - r) - K_2 \dot{\xi}_i \\ \dot{\theta}_i = -K_3 |\nabla c| sen(2(\theta_i - \phi_i)) - K_4 \dot{\theta}_i \\ \partial_t c(\mathbf{x}, t) = D \Delta c(\mathbf{x}, t) - \frac{c(\mathbf{x},t)}{\tau} + \alpha \sum_{j=1}^{N} J(\mathbf{x} - \mathbf{x}_j(t)), \end{cases} \tag{3.2}$$

where $K_{0,1,2,3,4}$ are constants. The first two equations and the one for $c$ are exactly the same of system (3.1).

$\mathbf{F}_F = -\gamma * \dot{\mathbf{x}}_i$ is, as before, the non-conservative friction term. The inelastic isotropic repulsion force between two colliding cells, $\mathbf{F}_{IR}$, is set to zero if no overlap occurs and it is given by $\mathbf{F}_{IR} = \sum_{j \neq i}\{C_0 * A_{i,j}\mathbf{n}_{ij} - C_1 * \langle \mathbf{v}_i, \mathbf{n}_{ij} \rangle\}$, where $A_{i,j}$ is the overlapping area between the $i$-th cell and the $j$-th one and $C_{0,1}$ are constants. For $\mathbf{n}_{ij}$ we made this choice: we consider for each cell the side with a greater overlapping in the other cell; then we take for the side of the $i$ cell the outgoing normal and we call it $\mathbf{n}_{i\to j}$, and we do the same for the $j$-th cell's side, obtaining $\mathbf{n}_{j\to i}$. Finally we set $\mathbf{n}_{ij} = \mathbf{n}_{j\to i} - \mathbf{n}_{i\to j}$ and $\mathbf{n}_{ji} = -\mathbf{n}_{ij}$.

The persistence force acting on the centers is given by $\mathbf{F}_T = -C_2 * (\xi_i - r)(1 - cos(2(\theta_i - \psi_i)))\dot{\mathbf{x}}_i$, where $C_2$ is constant. Therefore it is proportional to the factor $(1 - cos(2(\theta_i - \psi_i)))$ which is in $[0, 2]$ and whose value depends on how much the cell deviates from the direction of the gradient $\nabla c$: more the velocity and the gradient are aligned, weaker it is. Actually, it is zero when the cell is perfectly directed like the chemical field. This is consistent with the nature of the persistence force which reflects the resistance of the skeleton in changing the direction of motion and in re-arranging the shape of the cell. This is why the force is also proportional to the elongation of the axe, by the term $(\xi_i - r)$.

In the equation for $\xi_i$, the first component $K_0|\nabla c|cos(2\theta_i)$ gives rise to the elongation due to the chemical field, $-K_1(\xi_i - r)$ is a physical resistance in elongating, due to the presence of the skeleton, while the last term is just a dynamical friction.

In the equation for the orientation $\theta_i$, the term $-K_3|\nabla c|sen(2(\theta_i - \phi_i))$ is a term to let the cell align with the direction of the chemical field. Once again the last term is a non-conservative friction.

At time 0 the angle $\theta_i$ and the centers $\mathbf{x}_i$ are chosen at random, while the two semi-axes $\xi_i, \eta_i$ are put equal to $r$, which is the radius of the cell at rest, whose value is the same of the previous model. The semi-axe $\eta_i$ it is simply given, at each time step, by the conservation of initial area, i.e. $\eta_i = \pi r^2/4\xi_i$. As in (3.1) the chemical field and the velocities are initially set to zero.

At the moment I am performing simulations of this model and I do not have yet any definitive result. Having a good representation of elongating-cells model, with a better description of network, it would let answer to an intriguing open question. In fact it would be very interesting to understand the collective behaviour of cells once they agglomerate. Are they acting like one big cell or are they just moving like a colony of cells? These are open questions also in Biology [**26, 27**]. And it would be the next step of the problem, once obtained a stable elongation model.

CHAPTER 4

# A model to reproduce the physical elongation of dendrites during swarming migration and branching

## 4.1. Experimental results

*Bacillus subtilis* is a non-pathogenic but important constituent of soil and of the plant rhizosphere. This bacterial species is also one of the major model organisms used in the laboratory throughout the world to study the fundamental questions concerning bacterial growth, metabolism, physiology and enzyme production. *B. subtilis* is now also an important model for studying the life style and social behaviour of bacteria as large communities - the normal form of most bacteria in nature. A particularly remarkable form of such community growth is the ability of *B. subtilis* to "swarm" over the surface of low concentration agar ($0.7\% - 1\%$). *Swarming* is a process of rapid mass migration of cells over a surface, involving a co-operative interaction between cells but not necessarily involving cell aggregation. The Orsay group and scientists of IBPC in Paris are studying the swarming of strains of *B. subtilis* over a fully defined medium (B-medium). This is done in a Petri dish (a swarm plate), in which the bacteria migrate from a central inoculum as hyper-branching dendrites, forming radiating patterns covering several square centimeters in a few hours [**59, 60**].

The presence of *flagella* and the secretion of a surfactant (*surfactin*) by the bacteria, plus the products of at least 15 genes, are absolutely essential for swarming. Following inoculation of the plate with $10^4$ cells,

the bacteria multiply with an assumed generation time (doubling time) of about $100\,min$, when cells are that growing in a measured classical shaking liquid culture. After $11-12\,h$ of growth, the inoculum forms the mother colony ($MC$), approximately $30\,\mu m$ thick, $2\,mm$ in diameter. This growth period is presumably necessary to build a critical mass and an accumulation of a chemical signal sufficient to trigger in some cells the ability to form dendrites.

The first visible sign of initiation of swarming is the spreading outwards from the edge of the $MC$ of a transparent zone of surfactin. Approximately one hour later, hemispherical "buds" approximately $500-800\,\mu m$ in diameter, abruptly appear (burst) from the edge of the $MC$. These subsequently form the heads (tips) of the rapidly elongating $10-14$ dendrites. Surfactin production is essential for formation of the pre-dendrite buds and experiments suggest that its presence modifies the surface of agar gel, presumably by inducing the formation of a thin layer of fluid close to the agar surface. It is important to note that at about $14\,h$, when dendrites are approximately $2\,mm$ long, the $MC$ can be excised with no significant effect on swarming. Flagella, whose deployment presumably depends on an appropriate fluid film on the agar surface, are also essential for development of the bud and for driving dendrite migration. Importantly, the entire process of bud formation and elongation of the radiating dendrites, up to a dendrite length of $1.5\,cm$, occurs as a monolayer of cells. The cells in dendrites, except at the tip, are distributed on irregular mesh-like organization, including closely packed but clearly separated cells. Dendrites can be divided into two distinct regions, a long stem containing largely non-motile cells, that are termed *supporters*, although with an average of $10-12$ flagella, which remarkably are maintained at an overall constant population density, and the extreme $1\,mm$ at the tip where the population density increases sharply by 2-fold. This tip region contains

hyper-motile cells that are termed *swarmers*, specialized with an average 24 flagella, which appear to constitute the 'motor' for elongation.

Other important facts to be taken into account when analyzing the mechanism of community expansion and branching include that dead cells in dendrites or in the $MC$ are rare, perhaps less than 1%. Moreover swarm migration speed is constant with a constant rate of about $3.5\,mm/h$. When dendrites reach approximately $1.5\,cm$ in length, equivalent to $5-6\,h$ following emergence of pre-dendrite buds, a dramatic switch from monolayered to multilayered dendrites slowly spreads progressively from the base of dendrites, as the swarm begins to develop the classical biofilm form up to $50\,\mu m$ thick. These observations demonstrate that nutrients are in great excess for at least $24\,h$ encompassing the swarming process and subsequent maturation of the bilayer. Moreover, it has been shown that diluting the nutrients in the swarms plates at least $4-$fold, prior to inoculation, has little obvious effect on the pattern of swarming (unpublished data).

The switch from mono to multi-layers may depend on dendrites reaching a critical length but the mechanism is not clear. However, surfactin is important since in cells enginereed to make less surfactin, the switch occur early and many side branches arrest early. In liquid cultures, apparently, all cells multiply exponentially with a doubling time of $100\,min$. Importantly the doubling time of the cells in the swarm has not yet been measured. At this stage we have simple untemped conjectures to explain this paradox but it is been required more experimental research. One hypothesis suspects that swarmers may not be dividing while perhaps supporters may not be growing exponentially. Another hypothesis, more favoured, is that supporters divide but more slowly than swarmers, which could divide to produce one swarmer and one supporter.

Recent studies, using genetic analysis ([**56**]) and now fluorescent microscopy to measure the level of production (expression) from the gene encoding the major flagellum subunit *in situ*, have identified a specific subpopulation of hyper-flagellated cells (*swarmers*). These are dominant in the formation of buds and then subsequently spearhead dendrites in the tips. The appearance of these swarmers in the mother colony could be a purely stochastic process but there are no experimental data on the nature of the mechanism that produces the swarmer subpopulation. These hyper-motile cells are in contrast to the cells forming the stem of dendrites, the supporters that are non-motile. Our making hypothesis, based on the results indicated above and on a high resolution film of tip migration which is still being analyzed in more detail, is that supporters contribute to dendrite elongation by growth and division (multiplication), while swarmers actively drive extension from the tips, generating hydrodynamic forces dependent upon their hyper-motility. A general prediction of such a model at the moment is that if the swarmers go too slow or supporters 'accumulate' too fast, then there will be a traffic jam, with the population density in tips becoming so high that no movement is possible. For example, instead, this happens if the humidity is suddenly reduced and we see swarming stop and the tip cells pack tightly together in a mosaic of $5-6$ cells. Moreover in these conditions cells in tips are induced to multiply and form a multilayer, a process that spreads backwards down the dendrites. Thus, the hypothesis proposes that the swarm front results from the co-operative action of two sub-populations to promote dendrite extension. In contrast to the mechanical forces, we note, however, that the piloting mechanism or guidance system that ensures radial migration, likely depends on a self-generated chemical gradient, but so far this remains completely unknown.

We shall now summarize a number of notable features of the migration process and consequent pattern development that should be taken into account when constructing mathematical models, if these are to describe the swarming process adequately. Migrating dendrites on encountering a large obstacle (like a cover slip on an *E.coli* colony) are induced to make a ninety degrees turn but then in most cases these return to the radial direction. In addition, dendrites rarely merge and appear to avoid each other. This behaviour is consistent with the diffusion of a chemical repellent generated by the cells, or that the cells are constrained within a physical track that keeps dendrites well separated. Significantly, the limited number of primary dendrites established at the initiation of swarming are usually supplemented at much later times by additional dendrites arising from the $MC$. This might indicate that the differentiation event to form swarmers (capable of breaking out of the $MC$) is based on a stochastic process that can occur more than once. The nature of branching of *B. subtilis* has been little studied so far since most studies have been restricted to analysis of $1.5\,cm$ dendrites, before significant amounts of branching occur. However, it is clear that, by tip splitting, although a significant number of branches abort and remain very short and are often restricted to one side of the dendrite stem, this is particularly true when surfactin production is reduced. All new branches tend quickly to adopt a radial direction during subsequent elongation. Importantly, while the overall frequency of branching increases towards the edge of the swarm plate, dendrite stems progressively also become thinner (Figure 4.1).

**A mathematical approach to swarming analysis is now essential.** A surprising characteristic of the swarming process is the paradox that while cells are expected to grow and divide exponentially, as cells do in a liquid culture, the rate of swarming migration remains

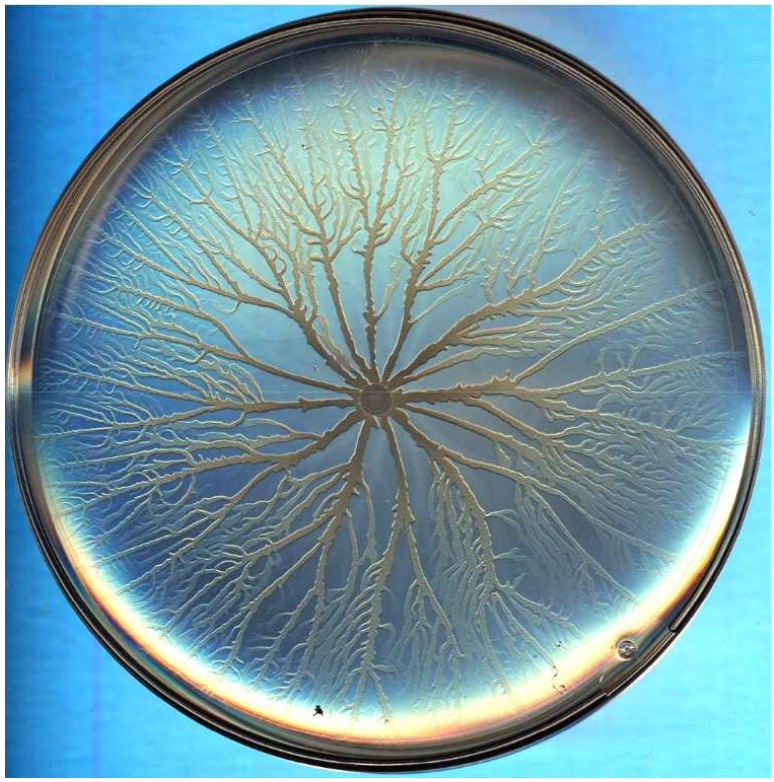

FIGURE 4.1. An experimental swarming pattern displayed by *B. subtilis* 168 on B-medium. Bacteria were inoculated in the centre of the plate and incubated for 24 $h$. dendrites elongate radially from the central mother colony (approximately 3.5 $mm\,per\,h$) and begin branching after 1.5 $cm$. Highly reproducible patterns are obtained, characterized by increased frequency of progressively thinner branches. Dendrites generally appear to evade each other and rarely fuse. Side branches tend to be biased to one side and rather frequently abort after a relatively short distance. Moreover they frequently commence at $40-90^{\circ}$ to the main branch, but then adopt a radial direction. Picture from [**65**].

constant. This, combined with the constant population density over most of the dendrite, clearly indicates that not all cells in the dendrites can be growing at the same rate. This would be an extremely unusual behaviour for a bacterial population and it is important to establish now which subpopulations may be subject to growth rate control.

Great progress has been made in the last five years to better understand the biology of the development of the swarm community. However, the major questions have emerged from the studies that we conclude mathematical modeling should make an essential contribution.

These observations lead us to look for answers to these three questions. What principles determine the guidance system of the cells to promote initial migration? How do dendrites elongate (i.e. how do cells grow in dendrites as well as what are the forces that pushes the tips forwards)? What determines the onset of branching and its frequency?

## 4.2. Critical review of previous models and ongoing ideas

**PDE models of cell communities auto-organization.** Different biophysical factors involved in pattern formation have given rise to various types of modeling. One class of models concerns auto-chemotaxis and give rise to a Fokker-Planck equation that is commonly called the Keller-Segel system. This model is mathematically very challenging and has motivated numerous studies (see [**57, 58, 67**] and citations therein); in particular this kind of model typically leads to cell aggregation in one or several discrete spots and biologists will need to know what this means.

Other models are based on the multiplication of cells resulting from nutrients initially present in the medium and consumed by the expanding community, combined with active and random motion of bacteria. This approach has also been widely used and can generate dendritic

patterns in the absence of oriented drift (preferred direction of motion) in contrast to the Keller-Segel model which describes cells moving preferentially towards higher concentration of the chemo attractant. Many additional factors have been incorporated into models, such as the observed higher motility of cells at the tips of dendrites, [**63**], or a surfactant secreted by the cells that may change the liquid surface and thus the migration of cells, [**54, 61**]. In what follows we consider cells in a domain $\Omega$ and, here, we explicitly refer to [**65**].

The nutrient-based models used to generate dendritic patterns of cell communities are mostly formulated in terms of three quantities

- the population density $n(x,t)$ of active cells at the location $x \in \Omega$. Under the effect of their active flagella, active cells undergo a random movement resulting in a diffusion of intensity $D_n$, and they multiply according to the nutrient available locally;
- the nutrient concentration $v(x,t)$ diffuses according to Einstein's rule and, because the nutrient is limited, it can diminish locally due to its consumption by multiplying cells;
- the population density of passive cells $f(x,t)$. For these cells the effect of their motion and multiplication is neglected. Active cells become passive according to some rules that differ from one model to the other, and they stay passive, i. e. they do not move or multiply.

These assumptions lead to write general systems of the form

$$\begin{cases} \partial_t n(x,t) - D_n \Delta n(x,t) = n[vG(n,v) - H(n,v)], \\ \partial_t v(x,t) - D_v \Delta v(x,t) = -nvG(n,v), \\ \partial_t f(x,t) = nH(n,v). \end{cases} \tag{4.1}$$

This kind of model has been introduced to model chemical reactions, and the Gray-Scott system, [**55**], is the simplest and classical

FIGURE 4.2. Final total population density $(n+f)$ for a simulation of the Gray-Scott model [**55**]. The dendritic pattern is determined by the passive cells in this type of model. Picture from [**65**].

example. It explains the instability that generates the digitation process. It is related to concentration effects of the equation on active cells; its solution $n$ exhibits high values on the tip of the dendrite and moves outwards where nutrients are replete (see numerical simulation in [**65**]). These concentration points are traveling pulses that undergo secondary instabilities which explain their branching. They leave behind them the column of passive bacteria forming the dendritic pattern. Other biophysical processes can be taken into account in this kind of model in order to explain the behaviour of specific bacterial communities. Several interesting choices of $G$ and $H$, relevant for biology, are

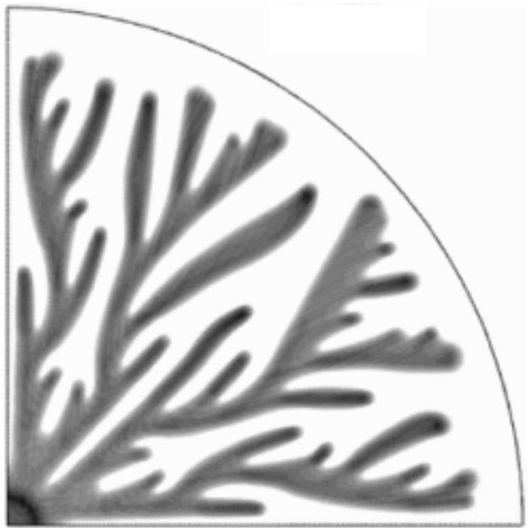

FIGURE 4.3. Final total population density $(n + f)$ for a simulation of the Mimura model [**66**]. The dendritic pattern is determined by the passive cells in this type of model. Picture from [**65**].

due to Levine and Kessler [**62**] and Mimura et al. [**66**]. In Figure (4.3) it is shown a solution to Mimura system compared to the Gray-Scott model shown in Figure (4.2).

When the bacteria emit a chemoatractant or chemorepellent substance, this results in additional terms in the reaction-diffusion systems described above. Assuming that the medium is rich enough and therefore the nutrient is not limiting, we arrive at systems with the form

$$\begin{cases} \partial_t n(x,t) - D_n \Delta n(x,t) + div[n(\nabla c_a - \nabla c_r)] = n[H(n) - G(n,c_r)], \\ \partial_t f(x,t) = nG(n,c_r), \\ \partial_t c_a(x,t) - D_a \Delta c_a(x,t) + \tau_a c_a = \rho_a H_a(n,f), \\ \partial_t c_r(x,t) - D_r \Delta c_r(x,t) + \tau_r c_r = \rho_r H_r(n,f). \end{cases} \tag{4.2}$$

Here $c_a$ and $c_r$ represent the concentration of chemoattractant and chemorepellent. These are assumed to diffuse according to Einstein's rule with coefficients $D_a$ and $D_r$, they are degraded with the rates $\tau_a$ and $\tau_r$ (depending possibly on the cell population densities $n$ and $f$), and they are secreted by the cells with rates $\rho_a$ and $\rho_r$. Their actions are represented by Fokker-Planck terms in the equation for $n$, together with the Keller-Segel model mentioned earlier.

In this combination of reaction-diffusion models together with drift terms, the latter represent chemoattraction/chemorepulsion and have a tendency to dominate the dynamics. This yields much more dynamic profiles and stronger aggregation effects on active cells.

**Experimental findings as a basis for new modeling approach.** Whereas the models presented here clearly produce dendrites of various shapes, a critical analysis of the experimental data reveals that many features cannot be explained by these models. Moreover, as we will now discuss, these observations make it clear that an entirely new class of model will be needed for a detailed description of swarming in *Bacillus subtilis* and probably other bacteria. The major point concerns the mechanism of branch formation. The models (4.1) and (4.2), as well as most of the models found in the literature, suppose that the proliferation of the bacteria is limited by the availability of a chemical nutrient which satisfies a diffusion equation. In some situations described in the literature this appears to be true, and apparently convincing agreement between patterns from models and experiments has been obtained [**54**]. This however, may in reality be an illusion.

For the swarming experiments described in our studies (see Section 4.1), certainly, nutrients do not become limiting for growth, as shown by the continued visible increase in cell numbers for many hours after completion of the swarming process.

The importance of this experimental observation for modeling stems from the fact that a gradient in nutrient concentration is required in these models to create dendrites, since this promotes faster growth of bacteria in the tips that have easier access to the nutrients. In the absence of nutrient limitation, the question arises which physical or chemical effect pilots the outward migration of the bacteria and leads to branch formation.

Two different potential alternative mechanisms can be envisaged for *Bacillus subtilis*. A first hypothesis is suggested by the fact that mutants with reduced surfactin production swarm slowly or do not exhibit swarming [**56**]. Moreover, the normal swarming process is accompanied by spatial gradients of surfactin concentration. Since surfactin is a surfactant, concentration gradients give rise to Marangoni forces, which have been shown to create branching patterns in the spreading of liquid droplets [**70**]. However under swarming conditions such surfactin pattern is not seen (A. Daerr, personal communication). Many models to explain also swarming assume that the surface of the agar is covered by a thin liquid film [**54**]. However, the reality is more complex since a simple experiment shows that a droplet of pure water deposited on the surface of the agar gel used in swarming experiments (0.7% agar) does not spread over the surface, but remains sessile (M. Banaha, Thesis Phd, 2009). This obviously implies that the surface of the agar cannot be covered by a continuous liquid film. Nevertheless, in the presence of surfactin, a very thin film develops in the vicinity of the deposited droplet and expands slowly ([**48**], M. Banaha, Thesis Phd, 2009). While the presence of this film is apparently necessary for swarming, presumably because this allows the movement of the bacteria, it is unlikely alone to provide a mechanism for the formation of branching dendrites. Minimally, a better understanding of the wetting

properties of surfactants is needed before incorporating them into new models, even at a qualitative level.

For example, the observed hyper motility of cells in dendrite tips in an important factor that is likely the key to the swarming mechanism. It is important to establish precisely the length of the hyper-motility zone throughout the swarming process in normal swarms and in a mixed swarm, for example, between a $WT$ and an *swrB* mutant, defective in producing swarmers and non swarmers (supporters) in the dendrite stem. The results may help to distinguish the mechanisms for the formation of the high population density/high motility zone, the effect of surface tension, the squeezing pressure on swarmers from the advancing supporters, or the size of the swarmer subpopulation, which is determined in the $MC$ (Hamze et al., in preparation). One possible idea is that supporters 'advance' by growth, following the track produced by swarmers; then, by multiplication, the supporters compete for space with swarmers, maintaining the high population density in tips and the forward direction of swarmers. Importantly, several physical studies show that a high population density of bacteria in tips is sufficient to induce hyper-motility with whirls and jets even with no swarmers ([**69**]), but how is the high population density produced during the initiation of swarming as buds form?

A second hypothesis, which was the basis for formulating models (4.2), is that the outward migration of the bacteria is driven by a long-range chemorepellent. Whereas, as yet, no substance generating such a chemotactic movement of the bacteria has been identified experimentally, the fact that dendrites avoid each other is consistent with the existence of a chemorepellent.

However, the postulated mechanisms underlying branching and the overall growth of dendrites are quite different in the existing models

and in the experiments. In particular, the models presented in Section 4.2, as well as most of those in the literature, introduce two states of the bacteria: active cells which diffuse and reproduce, and passive ones that do neither move nor reproduce. And this feature, as already mentioned in Section 4.1, is not realistic compared to most experimental studies. In fact is not clear yet if the driving mechanism for the swarming is cell migration, cell division or both.

The experimental observations differ markedly from models. Thus, although the tips of the observed dendrites can be described as hot spots (as in models), characterized by a hyper motile cells higher population density, the doubling time for bacteria growth under the conditions considered here is much longer than the typical migration speed, indicating that the driving mechanism for swarming is cell migration and not cell division. Moreover, although not as highly motile, the bacteria in the stems are by no means inactive. Some cells at least appear to perform a random-walk type motion with a global drift towards the tips that may support tip motion since cutting the stem stops swarming advance in the tip (S. J. Séror, I. B. Holland, personal communication).

In summary, many fundamental aspects of the swarming process are not well reproduced by the models available at present. Furthermore, as we have discussed above, some experimental observations indicate that the structure of the models has to be profoundly modified.

On the other hand, mathematical modeling has clearly predicted the participation of distinctive cell types involved in swarming, active leaders and passive cells forming the bulk of the dendrite. Experimental evidence from studies in *P. mirabilis* and now in *B. subtilis* (Hamze et

al submitted), with the demonstration of distinctive cell types, swarmers and supporters, formally equivalent to active and passive types respectively, confirms the reality of these predictions.

In addition, modeling studies more importantly make the exciting prediction of differential growth regulation for the two kind of cells and this feature would be a novel concept in the field of bacterial communities. Nevertheless, such growth regulation could explain some, so far, puzzling experimental observations. Future studies will be directed to testing this hypothesis, in addition to other experiments clearly needed to guide further model development. Moreover, a better understanding of the structure of the agar surface and its consequences for the local motility of the bacteria is desirable. Finally, models with several different population density fields of bacteria, reflecting distinct cell types, are certain to be required to account for the full complexity of the swarming process.

## 4.3. New model and numerical results

Based on the observations done in the previous sections we present a new class of models. Its major feature is that it does not use any nutrient since the agar is rich enough of such substances, from the beginning. This makes our model completely new from the pre-existing ones.

The dendrites are represented by two types of cells. In the tip there are active cells that follow the drift fields of both the surfactin, that is supposed to be the major guidance mechanism for them, and of another chemical substance (it might be also a surfactant) that acts as a chemoattractant and pack together cells in the tips. Swarmer cells divide, but we assume that after division, one of the two cells becomes a supporter; this assumption is based on the experimental

observation that the swarmers density remains constant. The tail is made by supporters cells, which reproduce and that just follow the trace left by the swarmers (by this way we suppose that the growth of dendrites is due both to cell division and cell advance).

The ask is to understand if these ingredients are enough to produce the formation of dendrites budding out from the mother colony with a correct shape knowing that the densities of cells in the mother colony, in the tip and in tail remain approximately constant. The mother colony is represented as 'frozen' cells with a density about three times as high as the tail of supporters. Moreover we know that the length of the active tip remains constant during the formation of dendrites. Finally, from experiments, we know that, once a dendrite of about $1.5\,cm$ is formed, we can cut it at the level of mother colony and it is able to move and to split again. We consider the surfactin, that is initially zero, to be released by the mother colony and either by supporters or swarmers or both (this is not clear neither at a biological level, so, for the moment, we are just making some suppositions). We denote by

- $n(x,t)$, the swarmers density, for which we consider a conservation equation (therefore no production of active cells). The swarmers move under the chemotactic effect of the surfactin $S$ and of a short range chemical substance $c$ which has the aim to hold together the cells forming tips and dendrites and to cooperate with $S$ in the splitting mechanism;
- $c(x,t)$, the chemical concentration of a short range attractant, which is itself produced by the swarmers, with a rate $\alpha_c$. It diffuses with a coefficient $D_c$ and decreases by a factor $\tau_c$;
- $S(x,t)$, the surfactin density that is released by both supporters and mother colony, with rates $\alpha_f$ and $\alpha_s$ respectively; it diffuses with a coefficient $D_s$ and it is degraded with a rate $\tau_s$;

- $D_m(x,t)$, the trace left by the swarmers, it is released by $n$ with a rate $d_m$;
- $m_{col}$, the population density of the mother colony of bacteria;
- finally $f(x,t)$, the supporters density that diffuses according to $D_m$ and is produced by $n$, with a birth rate $B_n$, and by $f$, with a rate $B_f(1-f)$.

The whole system has the following form

$$\begin{cases} \partial_t n + div\big(n(1-n)\nabla c - n\nabla S\big) = 0, \\ -D_c c + \tau_c c = \alpha_c n, \\ \partial_t S - D_s \Delta S + \tau_s S = \alpha_s m_{col} + \alpha_f f, \\ \partial_t D_m = d_m n, \\ \partial_t f - div(D_m \nabla f) = B_f f(1-f) + B_n n, \end{cases} \tag{4.3}$$

where all the quantities are adimensionalized. This system is considered in a bounded domain $\Omega \subset \mathbb{R}^2$ and it is completed with Neumann boundary conditions (N.b.c.) for $c$ and $S$, with no-flux boundary condition for the swarmer concentration $n$. We have performed some simulations for $x = (x_1, x_2) \in \Omega = [0, L]\text{x}[0, L]$. The parameters chosen are $D_c = 0.001$, $\tau_c = 1$, $\alpha_c = 1$, $D_s = 0.5$, $\tau_s = 10$, $\alpha_s = 2$, $\alpha_f = 30$, $d_m = 50$, $B_f = 0$, $B_n = 1$. We observe that the main branching features are kept putting $B_f \neq 0$.

For the initial guess we take $n(0,x) = n_0(x) = 1$ on the set $I = \{x = (x_1, x_2) : 0.16 < x_1^2 + x_2^2 < 0.25\}$ and 0 elsewhere. The initial concentration of $S$, $S(0,x) = S_0(x)$, is given by the solution to problem

$$-D_s \Delta S_0 + \tau_s S_0 = \alpha_s m_{col}.$$

This avoids initial layers. We also take $D_m(0,x) = 0$, $f(0,x) = 0$ and $m_{col}(x_1, x_2) = 3$ on the set $\{x = (x_1, x_2) : x_1^2 + x_2^2 < 0.16\}$ and 0 elsewhere.

The results are shown in Figure 4.4 where we depict five steps of the simulation. The left column represents the supporters plus the swarmers densities. The right part represents the surfactin concentration. The system presented above allows to obtain numerical branching which is compatible with the observations. Moreover, from a mathematical view point, the system presents a very complex structure whose study is really difficult. Therefore in the following we will focus on simplified versions that are more amenable to analysis.

**Numerical scheme.** We assume all quantities are known at time $t$ and we want to compute the solution of (4.3) at time $t + dt$. We discretize $c$ and $S$ by piecewise linear approximation on each element of the mesh.

- We compute $c$ thanks to a straightforward finite element method. And we compute $S$ by an implicit discretization of the parabolic equation.
- With the updated values for $c$ and $S$, we discretize the scalar conservation law for $n$ using a finite volume Engquist-Osher-type scheme. From there we need to impose the CFL condition $dt < dx/(max|\nabla S| + max|\nabla c|)$.
- The computation of the trace $D_m$ at time $t + dt$ relies on an explicit Euler scheme.
- The supporters concentration $f$ is updated with an implicit discretization of the parabolic equation for $f$ and a finite element method.

In other words we used an explicit scheme for the hyperbolic part and an implicit one for the parabolic part.

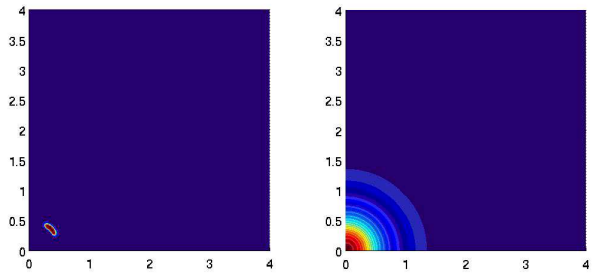
0 0.5 1 1.5 2 2.5 3 3.5 4
0 1 2 3 4

a)

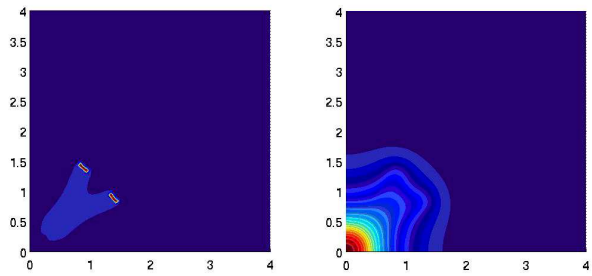
0 0.5 1 1.5 2 2.5 3 3.5 4
0 1 2 3 4

b)

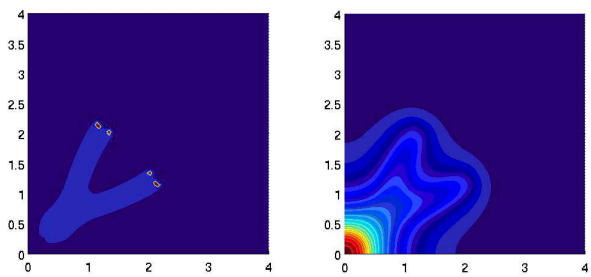
0 0.5 1 1.5 2 2.5 3 3.5 4
0 1 2 3 4

c)

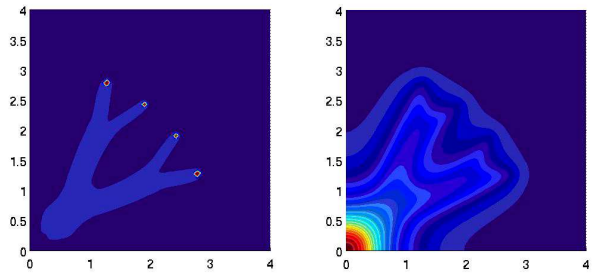


d)

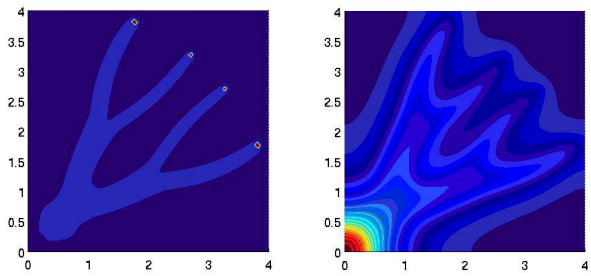


e)

FIGURE 4.4. Time dynamic of swarmers plus supporters density (left) and of the surfactin concentration (right) computed with the model (4.3).a) Initial guess b-d) intermediate steps e) final step

## 4.4. Analysis of reduced models

In this section we discuss some results on a reduced version of model (4.3) in which we do not consider the presence of any supporters, focusing explicitly on the role of the chemical substances $S$ and $c$ in the

equation for the density of swarmers $n$. In this way we are essentially studying the dynamics of the tip of dendrites.

**The Dolak-Schmeiser model.** Our model (4.3) is based on an hyperbolic Keller-Segel system proposed by Dolak and Schmeiser [**52**]

$$\begin{cases} \partial_t n + \partial_x(n(1-n)\partial_x c) = 0, \\ -D_c\partial_x^2 c + \tau_c c = \alpha_c n, \end{cases} \tag{4.4}$$

with N.b.c. on $c$ in a bounded domain $\Omega \subset \mathbb{R}$ and with no-flux boundary condition for the swarmer concentration $n$. This model, eventually with a small diffusivity for the swarmer concentration, has been studied in [**52, 49, 50, 68**]. The term $n(1-n)$ takes into account the prevention of overcrowding effect, sometimes also referred as "volume filling" effect. The long-time asymptotics of equation (4.4) have been studied in [**52**]. The observed behaviour is a coarsening process reminescent of phase change models, where plateau-like peaks of the cell density form after a short transient period and then merge exponentially slow. In [**52**] it is shown that constant solutions $\bar{n} = \bar{c} = const$ with $const \in (0,1)$ are unstable. If $\bar{n}$ gets sufficiently small then $\bar{n} = 0$ is attractive and a similar argument holds for $\bar{n} = 1$. Solutions approach, as $t \to \infty$, plateaus $\bar{n}_\infty = 1$ alternate with vacuum regions $\bar{n}_\infty = 0$. The study of stationary solutions is treated in [**49, 50**].

In order to single out the role of $S$, we consider the system

$$\begin{cases} \partial_t n - \partial_x(n\partial_x S) = 0, \\ \partial_t S - \varepsilon\partial_x^2 S + \tau_s S = \alpha_s n, \end{cases} \tag{4.5}$$

with N.b.c. for $S$ in a bounded domain $\Omega \subset \mathbb{R}$ and with no-flux boundary condition for the swarmer concentration $n$. In this case it is known that for $\varepsilon = 0$ there are traveling wave solutions (see also [**64**], where

is considered the case with a small diffusivity for the swarmer concentration). So, in this case, the effect of $S$ is to push forward plateau-like intial states.

**A reduced model explaining the traveling front.** The next step is therefore to couple the two chemical substances $c$ and $S$ to see their cumulative effect. Up to now we know that the presence of $c$ causes splitting, maintaining stable $0-1$ plateau-like solutions, while an appropriate shape of $S$ let them be traveling waves.

In order to combine both effects, we consider the following model in which the surfactin is released by the swarmers themselves

$$\begin{cases} \partial_t n + \partial_x(n(1-n)\partial_x c - n\partial_x S) = 0, \\ -D_c\partial_x^2 c + \tau_c c = n, \qquad\qquad x \in \mathbb{R} \\ \partial_t S = \alpha n. \end{cases} \tag{4.6}$$

In this case we study the existence and stability, under certain conditions, of traveling waves which are $0-1$ plateau-like peaks. Let $v = -\partial_x S$, we rewrite the system (4.6) as

$$\partial_t \begin{pmatrix} n \\ v \end{pmatrix} + \partial_x f(n, v; \partial_x c) = 0, \quad f = \begin{pmatrix} n(1-n)\partial_x c + nv \\ \alpha n \end{pmatrix}, \tag{4.7}$$

$$-D_c\partial_x^2 c + \tau_c c = n. \tag{4.8}$$

***1. Existence of pulse wave.*** Traveling waves are solutions under the form $n(x-\sigma t)$, $v(x-\sigma t)$ and are given by the reduced system

$$\begin{cases} -\sigma\partial_x n + \partial_x(n(1-n)\partial_x c - n\partial_x S) = 0, \\ -\sigma\partial_x S = \alpha n. \end{cases}$$

It is easy to build a traveling pulse solution (i.e. that vanishes out of an interval) and we have the

THEOREM 4.1 (Existence of traveling pulse solutions). *There exists a* $0-1$ *plateau like traveling pulse solution to Equation* (4.7) *given by*

$$n(x,t)=\begin{cases}1, & \sigma t\le x\le L+\sigma t,\\ 0 & otherwise,\end{cases}\qquad v(x,t)=\begin{cases}\sqrt{\alpha}, & \sigma t\le x\le L+\sigma t,\\ 0 & otherwise,\end{cases}$$

*with the shock speed* $\sigma=\sqrt{\alpha}$.

PROOF. The traveling pulse system is reduced to ($y=x-\sigma t$)

$$\begin{cases}-\sigma n+n(1-n)\partial_y c-n\partial_y S=0,\\ -\sigma\partial_y S=\alpha n.\end{cases}$$

Therefore

$$n(y,t)=\begin{cases}1, & 0\le y\le L,\\ 0 & otherwise,\end{cases}$$

is a solution if and only if

$$\begin{cases}\sigma=-\partial_y S=\frac{\alpha}{\sigma},\\ \partial_y S=-\frac{\alpha}{\sigma}n.\end{cases}$$

This gives the formula for $v=\partial_y S$. □

***2. Stability***. The stability of these pulse solution depends on the stability of the two shocks waves that form the pulse. This means that we have to check if these are entropic shocks. To this end we first compute the Jacobian.

Consider now that $\partial_x c$ is given as an external input. The Jacobian of the flux with respect to $(n,v)$ is given by

$$f'(n,v;\partial_x c)=\begin{pmatrix}(1-2n)\partial_x c+v & n\\ \alpha & 0\end{pmatrix},\tag{4.9}$$

leading to the equation

$$\lambda^2-\lambda\big((1-2n)\partial_x c+v\big)-\alpha n=0,\tag{4.10}$$

for its eigenvalues. The eigenvalues are

$$\lambda_\pm(n,v)=\frac{1}{2}\Big((1-2n)\partial_x c+v\pm\sqrt{((1-2n)\partial_x c+v)^2+4\alpha n}\Big).\tag{4.11}$$

Thus, for given smooth $c$, when $n$ is positive, (4.7) is a strictly hyperbolic system as long as $(n, v) \neq (0, -\partial_x c)$ and $\lambda_+ > 0$, $\lambda_- < 0$. An eigenvector corresponding to eigenvalue $\lambda$ is given by $r = (\lambda, \alpha)$. Differentiation of (4.10) gives

$$\begin{aligned}(2\lambda - (1-2n)\partial_x c - v)\partial_n \lambda &= \alpha - 2\lambda\partial_x c,\\ (2\lambda - (1-2n)\partial_x c - v)\partial_v \lambda &= \lambda,\end{aligned}$$

and therefore,

$$r\cdot \nabla_{(n,v)}\lambda = \pm 2\big(((1-2n)\partial_x c + v)^2 + 4\alpha n\big)^{-1}\lambda(\alpha - \lambda\partial_x c). \tag{4.12}$$

The $\lambda$-field is genuinely nonlinear as long as $\lambda(\alpha - \lambda\partial_x c) \neq 0$, which motivates looking for shock waves solutions.

THEOREM 4.2 (Stability of traveling pulse solutions). *The traveling pulse solution in Theorem 4.1 consists of two shocks. The first shock at the location $x - \sigma t = 0$ is*

$$\begin{cases} \textit{stable} & \textit{if} \quad \partial_x c(-\sigma t) > \sqrt{\alpha} \\ \textit{linearly degenerate} & \textit{if} \quad \partial_x c(-\sigma t) = \sqrt{\alpha} \\ \textit{unstable} & \textit{if} \quad \partial_x c(-\sigma t) < \sqrt{\alpha} \end{cases}.$$

*The second shock at $x - \sigma t = L$ is unconditionally stable.*

PROOF. We first study the shock connecting the left state $(n_l, v_l) = (0, 0)$ to the right state $(n_r, v_r) = (1, \sqrt{\alpha})$. As stated earlier, the Rankine-Hugoniot conditions are

$$n_r(\sigma - (1-n_r)\partial_x c - v_r) = 0, \quad \sigma v_r - \alpha n_r = 0.$$

The Hugoniot locus of the point $(0, 0)$ consists of two curves, one is the $v$-axis $\{(0, v_r),\ v_r \in \mathbb{R}\}$ with $\sigma = 0$ (which is linearly degenerate), and the other is determined by

$$\alpha n_r - v_r(1-n_r)\partial_x c - v_r^2 = 0. \tag{4.13}$$

When the shock speed is $\sigma = \sqrt{\alpha}$, $(n_r, v_r) = (1, \sqrt{\alpha})$ is indeed on the Hugoniot locus. At point $(0,0)$ the $\lambda_-$-field in (4.12) is linearly degenerate, therefore the shock belongs to the field where the $+$-sign is chosen. Assuming $\partial_x c > 0$ at the location of the shock, therefore

$$\begin{aligned} \lambda_l &= \lambda_+(0,0) = \partial_x c, \\ \lambda_r &= \lambda_+(1,\sqrt{\alpha}) = \frac{1}{2}\big(\sqrt{\alpha} - \partial_x c + \sqrt{(\sqrt{\alpha} - \partial_x c)^2 + 4\alpha}\big). \end{aligned}$$

The Lax entropy condition $\lambda_r < \sigma < \lambda_l$ is satisfied iff $\partial_x c > \sqrt{\alpha}$, so that this shock is stable when $\partial_x c(-\sigma t) > \sqrt{\alpha}$.

When $\partial_x c(-\sigma t) = \sqrt{\alpha}$, $\lambda_+(n_r, v_r) = \sqrt{\alpha}$ holds along the whole *plus*-curve (4.12) of the Hugoniot locus, which means that the *plus*-field is linearly degenerate in this case and, in particular, $\lambda_r = \sigma = \lambda_l$ holds. In the case $\partial_x c(-\sigma t) < \sqrt{\alpha}$, the entropy condition is not satisfied and the shock is unstable; we expect to observe a rarefaction wave (and numerically we do observe it).

We now study the stability of the second shock connecting $(n_l, v_l) = (1, \sqrt{\alpha})$ to $(n_r, v_r) = (0,0)$. Assume the second shock keeps large distance to the first one, we now expect $\partial_x c < 0$ at the shock location. This shock again belongs to the *plus*-field, and we obtain

$$\begin{aligned} \lambda_l &= \lambda_+(1,\sqrt{\alpha}) = \frac{1}{2}\big(\sqrt{\alpha} - \partial_x c + \sqrt{(\sqrt{\alpha} - \partial_x c)^2 + 4\alpha}\big), \\ \lambda_r &= \lambda_+(0,0) = \partial_x c. \end{aligned}$$

Since $\alpha$ is positive, the Lax entropy condition $\lambda_r < \sigma < \lambda_l$ is now satisfied unconditionally. □

***3. Small diffusion on S***. Consider now the model

$$\begin{cases} \partial_t n + \partial_x(n(1-n)\partial_x c - n\partial_x S) = 0, \\ -D_c\partial_x^2 c + \tau_c c = n, \qquad\qquad x \in \mathbb{R}, \\ \partial_t S - \varepsilon\partial_x^2 S = \alpha n. \end{cases} \tag{4.14}$$

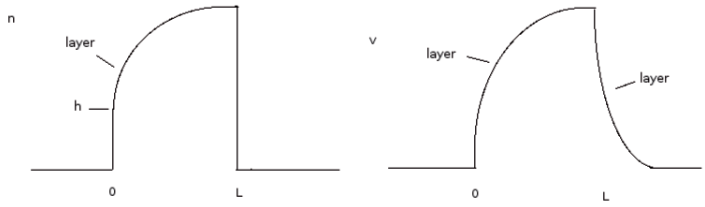


FIGURE 4.5. Qualitative representation of traveling pulse solutions to equation (4.14). The left figure represents the swarmers density $n$ where $h = 1 - \frac{\sigma}{\partial_x c(0)}$ is the hight of the jump on the left side of the front. The right one is the velocity $v$ of the front.

Inspired from the case $\varepsilon = 0$, (4.6), we look for a traveling pulse for the swarmers density composed by two layers in place of the shocks at $y_1 = 0$ and at $y_2 = L$ with possible layers at the shocks. We do this by formal analysis.

**Claim** *For model* (4.14) *there are traveling pulse solutions as depicted in Figure 4.5.*

- **Step 1: Reduction.**
  Here again we set in (4.14)

$$v = -\partial_x S.$$

  The smoothness of $c$ implying that its variations are small on the interval of variations of $n$ and $v$ (for $\varepsilon = 0$ these are points), therefore we assume that the chemical concentration $c$ is given and drop the second equation of (4.14).

  We rescale the system (4.14) by the change of variable $\xi = (x - \sigma t)/\varepsilon$ ($\sigma = \sqrt{\alpha}$) is the velocity of the shock waves when $\varepsilon = 0$) and we still denote by $(n, v)$ functions which now depend on the variable $\xi$. For $\varepsilon > 0$, the equation for $S$ is parabolic and then we are looking for a solution $v \in \mathcal{C}(\mathbb{R})$.

The rescaled system, after integration of the first equation of (4.14), is, denoting $\dot{f} = \partial_\xi f$,

$$\begin{cases} n(1-n)\partial_x c + vn - \sigma n = 0, \\ -\sigma v + \alpha n = \dot{v}. \end{cases} \tag{4.15}$$

- **Step 2: Analysis around $y_1 = 0$.**

  There could be two types of layers in this case. The first one is when $n = 0$ and $\xi < 0$. We have from the second equation of (4.15) that $v(\xi) = ce^{-\sigma\xi}$ and, since $v$ should stay bounded for large negative $\xi$, we have $c = 0$, therefore $v(\xi) = 0$. There is no boundary layer on the bottom part of the left side of the plateau.

  The second one is when $n > 0$ and $\xi > 0$ the first equation in (4.15) gives $n = 1 + (v - \sigma)/\partial_x c$. By inserting the first into the second equation of (4.15) we have

$$\begin{aligned} \dot{v} &= -\sigma v + \alpha n = -\sigma v + \alpha(1 + \frac{v-\sigma}{\partial_x c}) \\ &= (\frac{\alpha}{\partial_x c} - \sigma)v + \alpha(1 - \frac{\sigma}{\partial_x c}). \end{aligned} \tag{4.16}$$

  For $v$ to stay bounded, we have that $(\frac{\alpha}{\partial_x c} - \sigma)$ has to be negative. Then, by continuity of $v$,

$$v(\xi) = \frac{\alpha(\partial_x c - \sigma)}{\sigma\partial_x c - \alpha}(1 - e^{(\frac{\alpha}{\partial_x c} - \sigma)\xi}).$$

  Thus the boundary layer starts from $(v(0), n(0)) = (0, 1 - \sigma/\partial_x c(0))$ and reaches $(\sigma, 1)$ with a velocity given by (4.16). The system presents a jump from $(0, 0)$ to $(0, 1 - \sigma/\partial_x c(0))$ and a subsequent shock layer. If $(\frac{\alpha}{\partial_x c} - \sigma) > 0$ there is no bounded solution for (4.15) and therefore we have no traveling waves as we already know from the stability analysis.

- **Step 3: Analysis around $y_2 = L$.**

  For the analysis of the right side of the plateau we have to

shift $\xi$ to $y_2 = L$. We perform a similar analysis as for $n > 0$ above, imposing that $v$ goes to $\sigma$ and $n$ to 1 for large negative $\xi$, because $\partial_x c$ is always negative, $v$ has no boundary layer since it is always increasing to infinity. While studying $n = 0$ for $\xi$ very large, the system presents the only solution $(n, v) = (0, exp(-\sigma\xi))$. Therefore we have a jump in $y_2$, on $n$, from 1 to 0 and a smooth layer for $v$.

- **Step 4: Numerical results.**
  Finally we performed numerical simulation with $x \in [0, 7]$ setting $\epsilon = 0.01$, $\alpha = 0.5$, $\tau_c = 1$, $D_c = 0.01$ and the result is shown in Figure 4.6 in which we can clearly see Figure 4.6b the formation of the boundary layer on the left side of the traveling wave and the jump on the right one. We present in Figure 4.6b numerical simulations when the condition $\frac{\alpha}{\partial_x c} - \sigma < 0$ is not satisfied. We observe that there is no shock at the left part of the profile but a rarefaction wave appears.

## 4.5. Numerical branching in the reduced models

In this section we explain, based on numerical solutions, how the reduced model is able to produce branching. In particular the source term for $S$ is crucial and we explore several possible forms of this term.

**Splitting in one dimension with $S$ given.** In this section we want to emphasize the origin of the splitting. Let be $x \in [0, L]$, we take a given $\partial_x S$, not depending on time, forcing it to have the right shape to push away the swarmers,

$$\begin{cases} \partial_t n + \partial_x(n(1-n)\partial_x c - n\partial_x S) = 0, \\ -D_c\partial_x^2 c + \tau_c c = \alpha_c n, \\ \partial_x S = -\alpha_s x, \end{cases} \tag{4.17}$$

a)

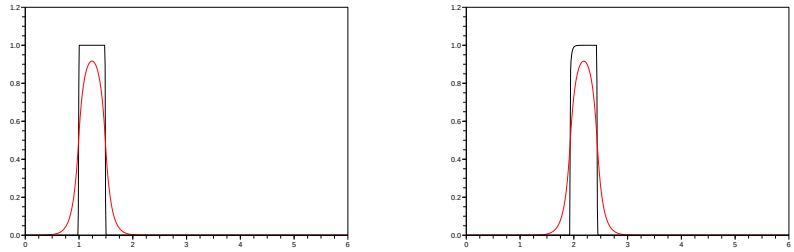

b)

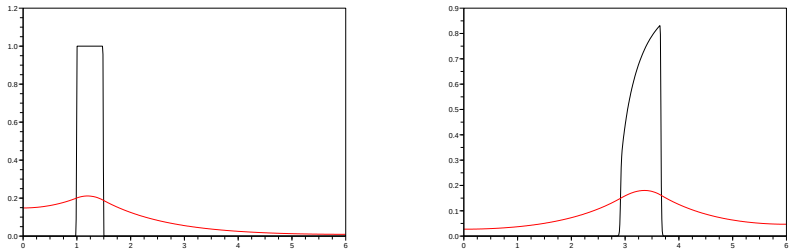

FIGURE 4.6. Numerical results of Eq. (4.14) with a) $\varepsilon = 0.01$, $\alpha_s = 0$, $\alpha = 0.5$, $\tau_s = 0$, $\tau_c = 1$ and $D_c = 0.01$. On the left column we show the initial guess for swarmers density (continuous black line) plus the chemical substance $c$ (dashed red line). In the right there is an intermediate shape with boundary layer on the left side for $n$ but not for $v$. b) The same of a) but with $\varepsilon = 0.01$, $\alpha_s = 0$, $\alpha = 0.01$, $\tau_s = 0$, $\tau_c = 1$ and $D_c = .01$, therefore the condition $(\frac{\alpha}{\partial_x c} - \sigma) < 0$ is not satisfied. In this case the shock becomes a rarefaction wave.

with N.b.c for $c$ and with no-flux boundary condition for the swarmer concentration $n$. In this way it is easy to obtain traveling front plus the splitting of the wave. A main ingredient is the effect of the mother colony which is replaced here by the term $-\alpha_s x$.

The initial guess for $n$ is a plateau-like function (in Figure 4.7) we use $n(0,x) = \chi_{[0.5,1.5]}$, where $\chi_I$ is the characteristic function on the interval $I$).

With this choice of $S$ we have that $-\partial_x S$ is greater on the right side of the plateau than in the left one, therefore it stretches the plateau diminishing it and widening the interval $I$ on which it is different from 0; this trend is in contrast with the conservation of mass and the action of $n(1-n)\partial_x c$, which, as we know from Section 4.4, leads to stable $0-1$ plateaus-like states. We notice that the term $\partial_x c$, to be strong enough to counteract $-\partial_x S$, has to be very strong on the sides of the plateau and very small on its center (as it can be seen on Figure 4.7), this is obtained by diminishing the diffusion coefficient $D_c$.

Actually, the smaller it is, more numerous are the splittings. For the numerical simulations represented in Figure 4.7 we take $\alpha_c = 1$, $\alpha_s = 0.1$, $D_c = 0.009$ and $\tau_c = 1$. With this choice of the parameters the splitting is really clear while the velocity of the front is low.

**Reduced $1-d$ model without supporters keeping the main features for the tips.** The system (4.17) can be made closer to the full model for the colony, setting

$$\begin{cases} \partial_t n + \partial_x(n(1-n)\partial_x c - n\partial_x S) = 0, \\ -D_c\partial_x^2 c + \tau_c c = n, \\ \partial_t S - D_s\partial_x^2 S + \tau_s S = \alpha_s m_{col} + \alpha n, \end{cases} \tag{4.18}$$

which is model (4.14) with $\varepsilon = D_s$, a degradation term for $S$ and the term $\alpha_s m_{col}$ in order to obtain both splitting and traveling front.
We investigate the numerical results in the case $\varepsilon = D_s$ and $\alpha \neq 0$. We set $x \in [0,9]$, $\alpha_c = 1$, $\alpha_s = 6$, $\alpha = 3$, $D_c = 0.002$, $D_s = 7$ and $\tau_c = \tau_s = 1$, with $m_{col} = 3\chi_{[0,1]}$. The initial guess is $n_0 = \chi_{[1.5,2]}$. The results are shown in Figure 4.8, where in the right column are shown

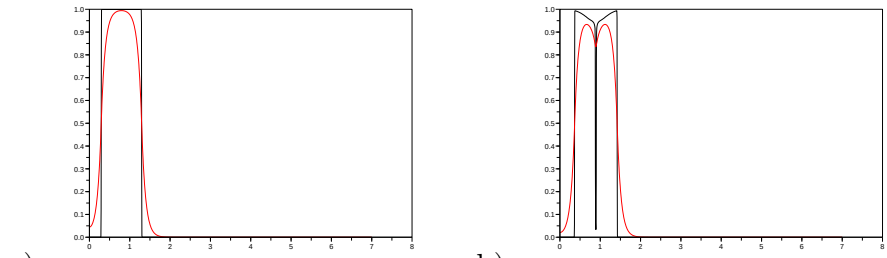

a) b)

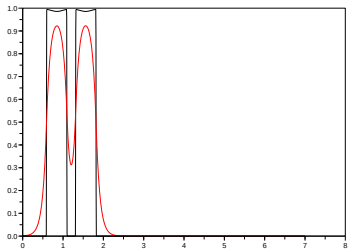

c)

FIGURE 4.7. Swarmers density (continuous black line) and chemical concentration $c$ (dashed red line) for the solution to equation (4.17). a) The initial state. b) Intermediate shape. c) Splitted state.

the initial, an intermediate and the final density of $n + m_{col}$, while in the left column there are the corresponding shapes of $S$.

We note that without production of surfactin from $n$, in one dimension, we are not able to reproduce the splitting. In this case, actually, the surfactin would just cause transport of the plateau $n_0$. In fact, without the contribution $\alpha n$, $-\partial_x S$ would act in a completely opposite way than the one described in Eq. (4.17), since its shape is decreasing, therefore it contributes with $\partial_x c$ in packing the plateau instead of stretching it (no splitting could occur).

We have no evidence that there will be subsequent splitting from the two formed plateaus in Figure 4.8c.

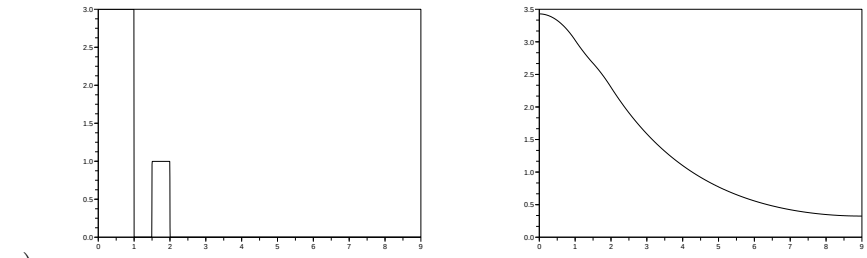

a)

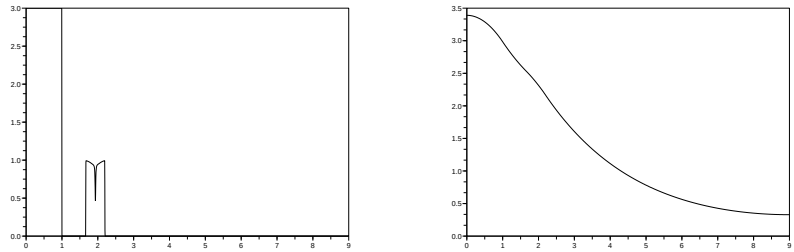

b)

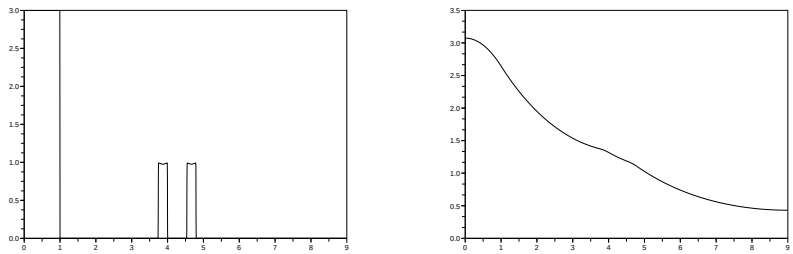

c)

FIGURE 4.8. Numerical solutions to Eq. (4.18) with $\varepsilon = D_s = 7$, $\alpha_s = 6$, $\alpha = 3$, $\tau_s = \tau_c = 1$, $\alpha_c = 1$ and $D_c = 0.002$. a) The initial contour of $n + m_{col}$, on the right, and of $S$ on the left b) Intermediate shape c) Splitted state.

**Reduced $2-d$ model without supporters keeping the main features for the tips.** In this section we present numerical results for the bidimensional version of (4.18), with $\varepsilon = D_s$ and $\alpha = 0$ i.e. the

following system

$$\begin{cases} \partial_t n + div(n(1-n)\nabla c - n\nabla S) = 0, \\ -D_c c + \tau_c c = \alpha_c n, \\ \partial_t S - D_s \nabla^2 S + \tau_s S = \alpha_s m_{col}, \end{cases} \tag{4.19}$$

completed by N.b.c. for $c$ and $S$ in a bounded domain $x = (x_1, x_2) \in \Omega \subset \mathbb{R}^2$ and with no-flux boundary condition for the swarmer concentration $n$. We emphasize the choice $\alpha = 0$: actually, in two dimensions, we do not need production of surfactin from $n$ to obtain the first splitting. This is shown in Figure 4.9. We have that $-\nabla S$ acts on radially stretching the initial plateau-like state (see Figure 4.9a) for the shape of $n(0, x)$). Once the stripe is too thin, the conservation of mass and the action of $\nabla c$ give rise to the splitting.

Here we set $x \in [0, 2]^2$, $\alpha = 0$, $D_s = 1$, $\tau_s = 10$, $\tau_c = 1$, $\alpha_c = 1$ and $D_c = 0.005$. The mother colony will occupy the left bottom corner of the computational domain. Let $m_{col} = 3$, in the set $\{x = (x_1, x_2) : (x_1^2 + x_2^2 < 0.2^2) \cap [0, 2]^2\}$, 0 elsewhere and the initial swarmers density is $n(0, x) = 1$, in the set $\{x = (x_1, x_2) : ((x_1 - 0.5)^2 + (x_2 - 0.5)^2 < 0.3^2) \cap (0.4^2 < x_1^2 + x_2^2 < 0.6^2)\}$ as displayed in Figure 4.9.

**Reduced $2 - d$ model with supporters keeping the whole main features.** The system now is like

$$\begin{cases} \partial_t n + \nabla(n(1-n)\nabla c - n\nabla S) = 0, \\ -D_c c + \tau_c c = n, \\ -D_s \Delta S + S = \alpha_s m_{col} + \alpha_f f, \\ \partial_t f = B_f f(\beta - f) + B_n n, \end{cases} \tag{4.20}$$

completed by N.b.c. for $c$ and $S$ in a bounded domain $x = (x_1, x_2) \in [0, L]^2$ and with no-flux boundary condition for the swarmer concentration $n$ and with $D_c, D_s$ small.

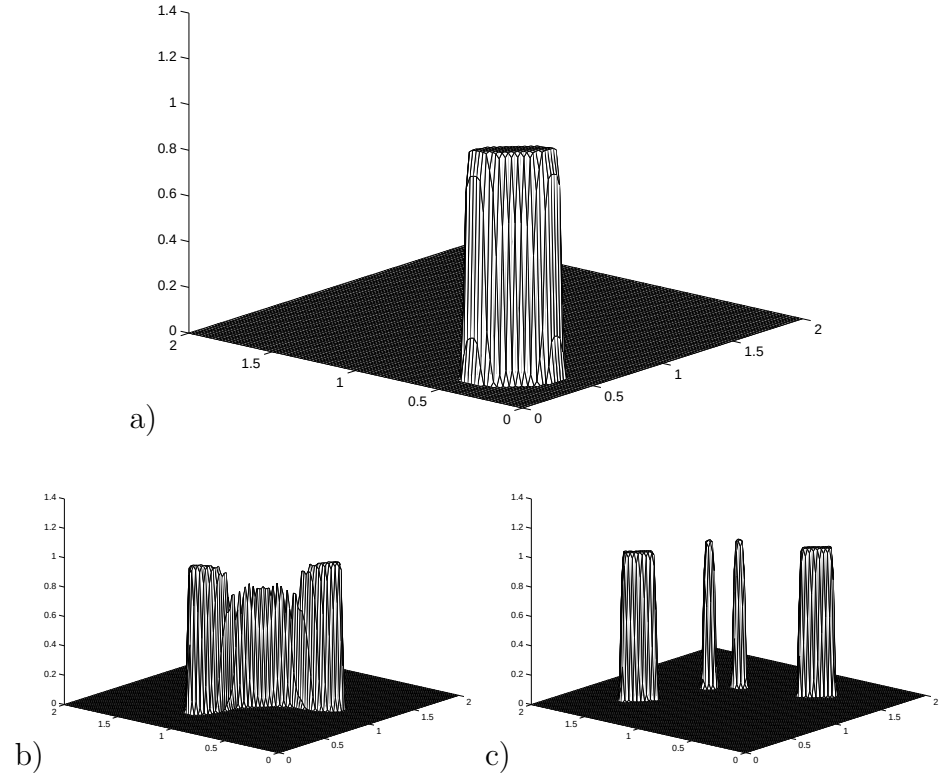


FIGURE 4.9. Numerical simulations of (4.19) with $x \in [0,2]^2$, $\alpha = 0$, $D_s = 1$, $\tau_s = 10$, $\tau_c = 1$, $\alpha_c = 1$, $D_c = 0.005$. a) The initial contour of $n(0,x)$. b) Intermediate shape. c) Splitted state.

Let us observe that there is a strong relation between model (4.20) and (4.3). Actually, the term $f(\beta - f)$ is used here to keep the swarmers to be constant and to avoid defining the trace $D_m$, while, as already observe, the term $B_f f(1-f)$ is not strictly necessary in (4.3), as it is shown in Figure 4.4, where $B_f = 0$. By this way, this last model is a mathematical simplification of the complete one and performs the same main features (see Figure 4.10).

Moreover, taking the time derivative for the equation for $S$, one gets

$$\partial_t S = D_s \partial_t \Delta S + \alpha_f \partial_t f = D_s \partial_t \Delta S + \alpha_f B_f f(\beta - f) + \alpha_f B_n n,$$

so that when $D_s$ small and $\mathbb{B}_f = 0$, (4.20) is a perturbation of the reduced traveling wave model (4.6). This guarantees us the presence of traveling wave solutions.

The numerical results are shown in Figure (4.10), here we set all the parameters as $L = 2$, $D_s = 0.05$, $D_c = 0.0005$, $\alpha_c = 2$, $\alpha_m = 1$, $\alpha_f = 2$, $B_f = 12$, $B_n = 4$, $\beta = 1/3$, $m_{col} = 3$ in the set $\{x = (x_1, x_2) : x_1^2 + x_2^2 < 0.2^2\}$ and 0 elsewhere. The initial conditions are chosen as $f(0, x) = 0$ initially $n(0, x) = 1$ in the set$\{x = (x_1, x_2) : 0.2^2 < x_1^2 + x_2^2 < 0.3^2\} \cap \{x = (x_1, x_2) : (x_1 - 0.2)^2 + (x_2 - 0.2)^2 < 0.1^2\}$ and 0 elsewhere.

As it can seen, this simplified model reproduces a good branching, with a constant density of swarmers and supporters respectively in the tip and along the dendrite.

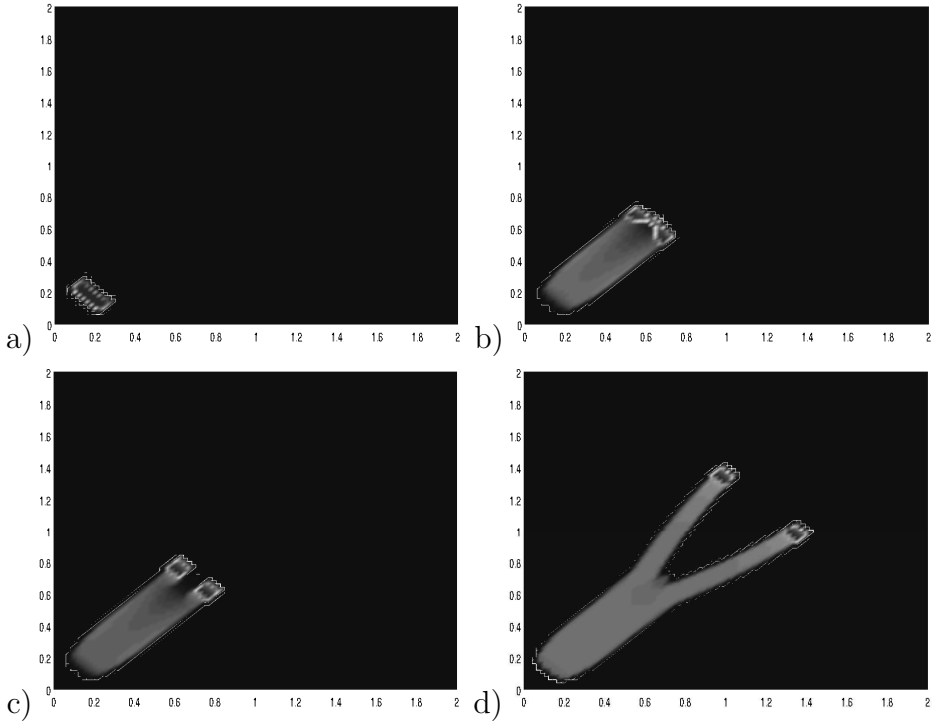


FIGURE 4.10. Time dynamic of swarmers plus supporters density computed with the model (4.20).

# Bibliography


[1] S. Allen, J. Cahn: A microscopic theory for antiphase boundary motion and its application to antiphase domain coarsening. Acta Metall. **27**, 1084-1095 (1979).

[2] A. Ajdari, J. Prost: Mouvement induit par un potential périodique de basse symétrie: diélectrophorèse pulsée. C. R. Acad. Sci. Paris, t. **315**, Série II, 1635-1639 (1992).

[3] L. Bertini, S. Brassesco, P. Buttà, E. Presutti: Front fluctuations in one dimesional stochastic phase field equation. Ann. Henri Poincareé **3**, 29-86 (2002).

[4] L. Bertini, S. Brassesco, P. Buttà: Soft and hard wall in a stochastic reaction diffusion equation. Arch. Rational Mech. Anal. **190**, 307-345 (2008).

[5] P. Billingsley. *Convergence of Probability Measures.* New York, Wiley (1968).

[6] S. Brassesco: Stability of the instanton under small random perturbations. Stoch. Proc. Appl. **54**, 309-330 (1994).

[7] S. Brassesco, P. Buttà: Interface fluctuations for the D=1 Stochastic Ginzburg-Landau equation with non-symmetric reaction term. J. Statist. Phys. **93**, 1111-1142 (1998).

[8] S. Brassesco, P. Buttà, A. De Masi, E. Presutti: Interface fluctuations and couplings in the d=1 Ginzburg-Landau equation with noise. J. Theoret. Probab. **11**, 25-80 (1998).

[9] S. Brassesco, A. De Masi, E. Presutti: Brownian fluctuations of the interface in the d=1 Ginzburg-Landau equation with noise. Annal. Inst. Henri Poincaré. **31**, 81-118 (1995).

[10] J. Carr, B. Pego: Metastable patterns in solution of $u_t = \varepsilon^2 u_{xx} + u(1-u^2)$. Commun. Pure Applied Math. **42**, 523-576 (1989).

[11] P. Collet, S. Martinez: Asymptotic velocity of one dimensional diffusions with periodic drift. Math. Biol. **56**, 765-792 (2008)

[12] C. R. Doering: Nonlinear parabolic stochastic differential equations with additive colored noise on $\mathbb{R}^d \times \mathbb{R}_+$. Commun. Math. Phys. **109**, 537-561 (1987).

[13] W. G. Faris, G. Jona-Lasinio: Large fluctuations for a nonlinear heat equation with noise. J. Phys. A **15**, 3025-3055 (1982).

[14] JP. C. Fife, J. B. McLeod: The approach of solutions of nonlinear diffusion equations to traveling front solutions. Arch. Ration. Mech. Anal. **65**, 335-361 (1977).

[15] G. Fusco, J. Hale: Slow-motion manifolds, dormant instability and singular perturbations. J. Dynamics Differential Equations **1**, 75-94 (1989).

[16] I. Karatzas, S. E. Shreve: *Brownian motion and stochastic calculus. Second edition* New York: Springer (1991).

[17] M. O. Magnasco: Forced thermal ratchets. Phys. Rev. Lett. **71**, 1477 (1993).

[18] P. Reimann: Brownian motors: noisy transport far from equilibrium. Physics Reports **361**, 57-265 (2002).

[19] A. N. Shiryaev: *Probability. Second edition*. New York: Springer (2006).

[20] J. B. Walsh: *An introduction to stochastic partial differential equations*. Lecture Notes in Mathematics **1180**, 265-437. New York: Springer (1984).

[21] Buttà P. Cerreti F. Servedio V. D. P. Triolo L. J. Stat. Mech., P05013 (2009)

[22] Ambrosi D. Bussolino F. Preziosi L. J. Theor. Medic. **6**, 1 (2005)

[23] Keller E. F. Segel L. A. J. Theor. Biol. **26**, 399 (1970)

[24] Othmer H. G. Stevens A. SIAM J. Appl. Math. **57**, 1044 (1997)

[25] Murray J. Oster G. J. Math. Biol. **19**, 265 (1984)

[26] Friedl P. Hegerfeldt Y. Tusch M. Int. J. Dev. Biol. **48**, 441-449 (2004)

[27] Friedl P. Curr. Op. Cell. Biol. **16**, 14-23 (2004)

[28] Manoussaki D. Lubkin S. R. Vernon R. B. Murray J. Acta Biotheor. **44**, 271 (1996)

[29] Gamba A. Ambrosi D. Coniglio A. de Candia A. Di Talia S. Giraudo E. Serini G. Preziosi L. Bussolino F. Phys. Rev. Lett. **90**, 118101 (2003)

[30] Serini G. Ambrosi D. Giraudo E. Gamba A. Preziosi L. Bussolino F. The Embo Journal **22**, 1771 (2003)

[31] Ambrosi D. Gamba A. Serini G. Bull. Math. Biol. **66**, 1851 (2004)

[32] Ambrosi D. Gamba A. Giraudo E. Serini G. Preziosi L. Bussolino F. Internal Report, (2001)

[33] Manoussaki D. ESAIM: M2AN **37**, 581 (2003)

[34] Tosin A. Ambrosi D. Preziosi L. Bull. Math. Biol. **68**, 1819 (2006)

[35] Plank M. J. Sleeman B. D. J. Theor. Medic. **5**, 137 (2003)

[36] Dye J. F. Lawrence L. Firth J. A. Linge C. Endothelium - J. Endoth. Cell. Res. **11**, 151 (2004)

[37] Levine H. A. Sleeman B. D. in *Cancer Modeling and Simulations*, L. Preziosi ed. (Chapman Hall/CRC Press), ISBN 9781584883616. (2003)

[38] Turner H. E. Harris A. L. Melmed S. Wass J. A. H. Endocrine Reviews **24**, 600 (2003)

[39] Serini G. *et al.*, Nature **424**, 391 (2003)

[40] Di Talia S. Gamba A. Lamberti F. Phys. Rev. E **73**, 041917 (2006)

[41] Preziosi L. Astanin S. in *Integration of complex Systems in Biomedicine*, A. Quarteroni ed. (Springer-Verlag Press). (2005)

[42] Merks R. M. H. Glazier J. A. Nonlinearity **19**, C1 (2006)

[43] Allen M. P. Tildesley D. J. *Computer simulation of liquids*, (Clarendon Press, New York, NY, USA), ISBN 0-19-855645-4. (1989)

[44] Press W. H. Teukolsky S. A. Vetterling W. T. Flannery B. P. *Numerical Recipes in C: The Art of Scientific Computing*, (Clarendon Press, New York, NY, USA), ISBN 0521437148. (1992)

[45] Gamba A. private communication

[46] Merks R. M. H. Brodsky S. V. Goligorksy M. S. Newman S. A. Glazier J. A. Developmental Biology **289**, 44 (2006)

[47] Serini G. private communication (2007)

[48] M. Banaha, A. Daerr, L. Limat, Spreading of liquid drops on agar gels. Eur. Phys. J. Special Topics, **166**, 185-188 (2009).

[49] M. Burger, M. Di Francesco, Y. Dolak-Strauss, The Keller-Segel model for is with prevention of overcrowding: linear vs. nonlinear diffusion. SIAM J. Math. Anal. **38** No. 4, 1288-1315 (2006).

[50] M. Burger, Y. Dolak-Strauss, C. Schmeiser, Asymptotic analysis of an advection-dominated chemotaxis model in multiple spatial dimensions. Commun. Math. Sci. **6** No. 1, 1-28 (2008).

[51] F. A. C. C. Chalub, P. A. Markowich, B. Perthame, C. Schmeiser, Kinetic models for chemotaxis and their drift-diffusion limits. Monatsh. Math. **142**, 123-141 (2004).

[52] Y. Dolak-Strauss, C. Schmeiser, The Keller-Segel model with logistic sensitivity function and small diffusivity. SIAM J. Appl. Math., **66** No. 1, 286-308 (2005).

[53] R. Erban, H. G. Othmer, From individual to collective behavior in bacterial chemotaxis. SIAM J. A. M. **65**, 361-391 (2004).

[54] I. Golding, Y. Kozlovsky, I. Cohen, E. Ben-Jacob, Studies of bacterial branching growth using reaction-diffusion models for colonial development. Physica A **260**, 510-554 (1998).

[55] P. Gray, S. K. Scott, Autocatalytic reactions in the isothermal continuous stirred tank reactor: isolas and other forms of multistability. Chem. Eng. Sci. **38**, no. 1, 29-43 (1983)

[56] K. Hamze, D. Julkowska, S. Autret, K. Hinc et al., Identification of genes required for different stages of dentritic swarming in *Bacillus subtilis*, with a role for *phrC*. Microbiology **155**, 398-412 (2009).

[57] D. Horstmann, From 1970 until present: The Keller-Segel model in chemotaxis and its conse quences, Part I. Jahresbericht der DMV **105**, no. 3, 103165, (2003).

[58] D. Horstmann, From 1970 until present: The Keller-Segel model in chemotaxis and its conse quences, Part II. Jahresbericht der DMV **106**, no. 2, 5169, (2004).

[59] D. Julkowska, M. Obuchowski, I. B. Holland, S. J. Seror, Branched swarming patterns on a synthetic medium formed by wild type Bacillus subtilis strain 3610. Microbiology **150**, 1839-1849 (2004).

[60] D. Julkowska, M. Obuchowski, I. B. Holland, S. J. Seror, Comparative analysis of the development of swarming communities Bacillus subtilis 168 anda a natural wild type: critical effect of the surfactin and the composition of the medium. J. Bacteriol. **187**, 65-74 (2005).

[61] Y. Kozlovsky, I. Cohen, I. Golding, E. Ben-Jacob, Lubricating bacteria model for branching growth of bacterial colony. Phys. Rev. E, Phys. plasmas fluids Relat. Interdisciplinary Topics, **50**, 7025-7035 (1999).

[62] D. A. Kessler, H. Levine, Fluctuation induced diffusive instabilities. Nature, **394**, 556-558 (1998).

[63] K. Kawasaki, A. Mochizuki, M. Matsushita, T. Umeda, N. Shigesada, modeling spatio-temporal patterns created by Bacillus-subtilis. J. Theor. Biol., **188**, 177-185 (1997).

[64] T. Li, Z. Wang, Nonlinear stability of traveling waves to a hyperbolic-parabolic system modeling chemotaxis. Accepted for publication by SIAM J. Appl. Math. (2009).

[65] A. Marrocco, H. Henry, I. B. Holland, M. Plapp, S. J. Séror, B. Perthame, Models of self-organizing bacterial communuities and comparisons with experimental observations. Submitted to Math. Model. Nat. Phenom.

[66] M. Mimura, H. Sakaguchi, M. Matsushita, Reaction diffusion modeling of bacterial colony patterns. Physica A, **282**, 283-303 (2000).

[67] B. Perthame, *Transport equations in Biology* (LN Series Frontiers in Mathematics), Birkhauser, (2007).

[68] B. Perthame, A. L. Dalibart, Existence of solutions of the hyperbolic Keller-Segel model. Trans. Amer. Math. Soc. **361** No. 5, 2319-2335 (2009).

[69] A. Sokolov, I. S. Aranson, J. O. Kessler, R. E. Goldstein, Concentration dependence of the collective dynamics of swimming bacteria. PRL **98**, 158102 (2007).

[70] S. M. Troian, X. L. Wu, S. A. Safran, Fingering instabilities in thin wetting films. Phys. Rev. Lett., **62**, 1496-1499 (1989).